Research supported by NOAA under grant number NA67RJ0152 and by NASA under grant number NAG5-9665 as well as a graduate fellowship from the American Meteorological Society.

INTRASEASONAL OSCILLATIONS AND THE SOUTHEAST ASIAN MONSOON ONSET

by

Erica M. Loechl

Richard H. Johnson, P.I.

Colorado State University

DEPARTMENT OF ATMOSPHERIC SCIENCE

PAPER NO. 703

INTRASEASONAL OSCILLATIONS AND THE SOUTHEAST ASIAN MONSOON ONSET

Erica M. Loechl

Department of Atmospheric Science
Colorado State University
Fort Collins, Colorado 80523-1371

Spring 2001

Atmospheric Science Paper No. 703

ABSTRACT

INTRASEASONAL OSCILLATIONS AND THE SOUTHEAST ASIAN MONSOON ONSET

The role of intraseasonal oscillations as a triggering mechanism for the Southeast Asian monsoon (SEAM) is investigated through a detailed study of the 1998 SEAM and expanded analysis to include the 20 years from 1979–1998. Spectral analysis of outgoing longwave radiation (OLR) at each gridpoint over the South China Sea (SCS) (10–20° N, 110–120° E) revealed the presence of intraseasonal oscillations with periods of 12–24 days and 30–60 days during the monsoon season. The SCS is an area of maximum variability for both of these oscillations during the SEAM onset.

The monsoon onset was defined as the first day of sustained convection (based on analysis of OLR) and the commencement of southerly and westerly winds over the SCS. The range of SEAM onset dates for the 20 year period was from 10 May – 15 June. The onset timing was considered normal if it occurred between 11 May – 31 May.

Analysis of band-pass filtered OLR, 850 and 200 mb winds suggest the 1998 SEAM onset was triggered by the nearly simultaneous arrival of the 12–24 day and 30–60 day oscillations into the SCS. The main component of the 12–24 day oscillation developed in the northwest Pacific near Japan and propagated southwestward into the SCS. The 30–60 day oscillation is comprised of the eastward-moving Madden-Julian oscillation (MJO) and the northward-moving monsoon trough.

Lag regression analysis revealed circulation and convection patterns of the intraseasonal oscillations for the 20 years to be similar to the patterns seen in 1998. However, the oscillations appeared to be stronger during the monsoon onsets compared to the entire monsoon seasons. Significant midlatitude influence on the SCS during the onset was observed in the regressions in the form of an upper and lower level wave train that extended from the SCS into the northern Pacific. The northern part of the SCS (15–20° N) served as a "transition zone" between midlatitudes and the tropics. Regressions based on this area displayed characteristics of both midlatitude and tropical influence during the SEAM onset.

The interannual variability of the onset timing and intraseasonal oscillations was assessed by catagorizing each year according to the onset timing, presence of intraseasonal oscillations at the onset, and ENSO phase. Years where both the 12–24 day and 30–60 day oscillation were present at the onset tended to have normal onsets. Years where only the 30–60 day mode was present at the SEAM onset had the earliest onsets and years where neither oscillation was present at the SEAM onset had the latest onsets. It appears that the existence of intraseasonal oscillations assists the monsoon onset and can cause it to happen earlier than it would otherwise occur. However, monsoon onsets will occur despite the absence of such oscillations — they simply will occur later. A direct link between the onset timing and ENSO events was not obvious from this study.

Erica M. Loechl
Department of Atmospheric Science
Colorado State University
Fort Collins, Colorado 80523-1371
Spring 2001

ACKNOWLEDGEMENTS

This research was supported by the National Oceanic and Atmospheric Administration under Grant NA67RJ0152 and the National Aeronautics and Space Administration/Tropical Rainfall Measuring Mission under Grant NAG5-9665 as well as a one year graduate fellowship from the American Meteorological Society and ITT Aerospace / Communications Division.

I would like to thank my advisor, Dr. Richard Johnson, for his patience and counsel throughout the completion of this work. I thank Dr. George Kiladis, Dr. Michael Montgomery and Dr. Gerald Taylor for serving on my graduate committee. I am especially greatful to Dr. Kiladis for providing insight and direction into this research, not to mention the OLR and NCEP data and analysis tools. I am indebted to Kathy Straub for her help in understanding the data analysis tools. I am obliged to the Johnson research group staff: Paul Ciesielski, Gail Cordova and Rick Taft, for their time and effort spent answering my many questions and keeping things running smoothly. I also appreciate the other members of the Johnson research group, past and present, whose experience saved me a lot of time and trouble throughout the completion of this work.

CONTENTS

FIGURES

TABLES

Chapter 1

INTRODUCTION

The Asian monsoon system can be divided into three components: the Indian (South Asian), East Asian (Meiyu-Baiu) and Southeast Asian monsoons (SEAM). Though these individual monsoons represent distinct parts of the Asian monsoon system, they are not entirely separate from one another. Many prior studies of the Asian monsoon system have focused primarily on the Indian component of the monsoon. While many scientists agree on the mechanisms which trigger the onset and drive the Indian monsoon, the same cannot be said for the SEAM. There has been much less study of this component of the Asian monsoon system, and it appears to be a much more complex phenomena than the other two components of the Asian monsoon (Lau et al 2000a). The SEAM appears to draw influence from both midlatitudes and the tropics (Johnson and Ciesielski 1999) in contrast to the Indian monsoon which is driven primarily by the heating of the Tibetan Plateau (Webster 1987b).

Several different theories or hypotheses for what triggers the onset of the SEAM have been proposed in previous studies. These theories suggest the cause of the monsoon onset could be from Tibetan Plateau forcing, the influence of midlatitude frontal systems or due to intraseasonal oscillations (disturbances on weekly to monthly timescales). These ideas will be discussed in more detail in Chapter 2. The diversity of current ideas to explain the triggering of the monsoon onset lends support to its complexity. It is clear that more study is needed to better understand the mechanisms which trigger the onset of the Southeast Asian monsoon. The goal of this study is to explore aspects of the SEAM, namely, the role of intraseasonal oscillations in its onset.

The SEAM onset is indeed a complex event, drawing influence from many different atmospheric processes. One mechanism for describing the onset that has been proposed is the forcing by intraseasonal or low-frequency oscillations, particularly by those on 12–24 and 30–60 day timescales. As will be discussed in Chapter 2, entire studies are dedicated to unearthing the mystery behind the influence of intraseasonal oscillations (e.g., Chen and Chen 1995). Even studies which propose an alternate forcing as the primary mechanism that triggers the SEAM must concede that intraseasonal oscillations play a role in the triggering of the monsoon (e.g., Wu and Zhang 1998). Either way, exactly what role intraseasonal oscillations play in the onset of the SEAM is not totally clear.

It is important for many reasons to unlock the mystery of what forces the onset of the SEAM. Understanding this has implications for future predictiblility and possible forecasting. The accuracy of seasonal-to-interannual rainfall forecasts in East Asia depends mostly on correctly tracking convection over the SCS (Lau and Yang 1997). There are also regional and global social and economic impacts to consider. The geographical region of the Southeast Asian monsoon includes Indo-China, southern China, the South China Sea (SCS) and the Philippines. This region contains over a third of the total population of the Asian monsoon area. Additionally, these regions have been a major supplier of raw materials, agricultural products and industrial outputs both globally and throughout the monsoon region (Lau and Yang 1997). The South China Sea Monsoon Experiment (SCSMEX) was an important step toward understanding the SEAM. It was an international field experiment which took place from 1 May–30 June 1998. Its objective was to better understand the key physical processes for the onset and evolution of the SEAM with the aim of improving monsoon predictions (Lau et al. 2000b).

The goal of this study is also to contribute toward a better understanding of the processes which force the onset of the Southeast Asian monsoon. To help in the understanding, a background of the Asian monsoon system, the climatology of the SEAM and discussion of the different ideas for the triggering of the onset are presented in Chapter 2. The data sets and methods of analysis used for this study are described in Chapter 3. Chapter 4 discusses the SEAM onset characteristics and definitions. It also provides a detailed analysis of the 1998 SEAM onset and an analysis of the intraseasonal oscillations within the 1998 monsoon and monsoons from 1979–1998. Additionally, the interannual variability of the intraseasonal oscillations with respect to the SEAM onset can be found in Chapter 4. Finally, a summary, conclusions and suggestions for future study are given in Chapter 5.

Chapter 2

BACKGROUND

Through a review of literature related to the South China Sea (SCS) monsoon onset, this chapter will describe the background for this study. It will include general background of monsoons, regional interactions, a brief comparison between the Southeast Asian Monsoon (SEAM) and the Indian monsoon, climatology of the SEAM, and ideas for onset mechanisms.

2.1 The Asian monsoon system

A monsoon is generally regarded simply as a seasonal change in wind direction. However, many definitions (with varying complexity) exist. Ramage (1971) offers very specific criteria based on wind direction and speed for which he defines the monsoon. His definition includes only the major monsoon regions of Asia, Australia and Africa. Other common definitions use annual variations of wind and rainfall. To be considered part of a monsoon system, the wind must reverse in direction between summer and winter. Additionally, the summer season is typically wet and the winter season is typically dry (Webster 1987a). These definitions basically yield the same monsoon regions (Fig. 2.1) as defined by Ramage (1971). The wind reversals which constitute the monsoons are a result of the atmosphere's response to the contrast in heating between land and ocean. For example, in the Indian monsoon system, the elevated heating of the Tibetan Plateau is responsible for this heating contrast and the resulting reversal of the winds (e.g., Wu and Zhang 1998). In this sense, it may be considered a "classical" monsoon (Lau et al. 2000a).

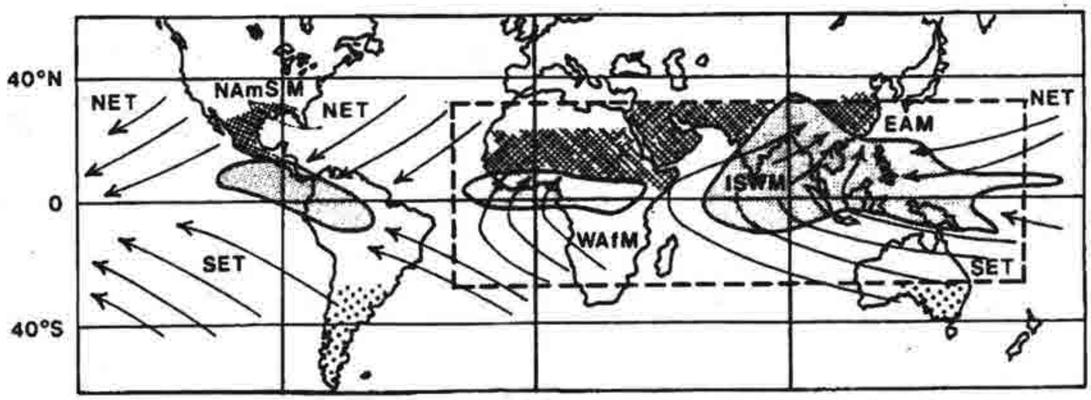

Figure 2.1: Northern Hemisphere summer monsoon regions from Webster (1987a). Arrows and shaded areas indicate main surface winds and areas of maximum seasonal precipitation. The cross-hatching indicates land areas with maximum surface temperatures, and stippling is the coldest land areas.

The Asian summer monsoon is a huge system in which the Indian monsoon, SEAM and East Asian monsoon are the principle elements. While each of these monsoon systems have their own respective components, they are closely related (Tao and Chen 1987). Even in their relations and interactions with one another, there is a principle difference between the Indian monsoon and SEAM systems. Viewing the Indian monsoon as the "classical" monsoon system, the principle driver and trigger for its onset is the annual march of solar insolation and the resulting heating of the Tibetan Plateau. Additional forcing of the Indian monsoon is solely from the tropics. For instance, the Madden-Julian oscillation (MJO) affects the onset as well as active and break periods of the monsoon (Webster 1987b). The Tibetan Plateau prohibits midlatitude influence on the Indian region. In a study of the 1998 summer monsoon, there was no evidence of southward propagating signals from the Tibetan Plateau. Only evidence of northward propagation of convection and wind anomalies was found (Johnson and Ciesielski 1999). This is an obvious difference from the SEAM. Lau et al. (2000a) describe the SEAM as a "hybrid" monsoon, noting influence from both midlatitudes and the Tropics. Johnson and Ciesielski (1999) found evidence of both northward-propagating and southward-propagating convection in association with the onset of the 1998 SEAM. With the increased areas of influence on the SEAM, it appears to be more complicated and difficult to understand than the Indian monsoon.

As different as these two components of the Asian monsoon appear to be, there are some similarities as well. Both the Indian monsoon and the SEAM appear to be influenced by intraseasonal oscillations (e.g., Webster 1987b; Chen and Chen 1995). They are also no longer regarded as simply a local or regional phenomenon, but rather considered players in the global (planetary) climate system. They can be considered part of a global circulation evolution from a winter regime to summer regime (e.g., Webster and Yang 1992; Li and Qu 1999). There are many components of the SEAM which reflect its areas of influence from the midlatitudes to the tropics (Fig. 2.2). These components include: the monsoon trough (or ITCZ) and associated convection in the SCS and western Pacific, the cross-equatorial flow to the east of 100° E, the cold anticyclone in Australia, the subtropical high in the western Pacific, upper-level northeasterly flow, the Mei-Yu and Baiu frontal zones and midlatitude disturbances. The Indian monsoon has similar components, although they are limited to a more tropical extent (Tao and Chen 1987).

2.2 Climatology

The onset of the SEAM occurs around mid-May, and is one of the earliest of the entire Asian summer monsoon system (Lau and Yang 1997). The climatological onset dates of the Asian monsoon (Fig. 2.3) range from 10 May in the SCS to mid-June over India and July as far north as Korea. This progression of the onset follows the northward shift of monsoon convection from the equator to midlatitudes. Both the intensity and the onset date vary from year to year. The transition of the atmosphere surrounding the onset tends to be very abrupt. This is illustrated in the global precipitation index (GPI) pentad climatology for May (Fig. 2.4) from Lau and Yang (1997). The SCS contains little to no precipitation in the 11–15 May pentad, and convection develops very rapidly during the 16–20 May pentad.

Rainfall tends to be heaviest over the southern SCS (5° N) for most of the year except

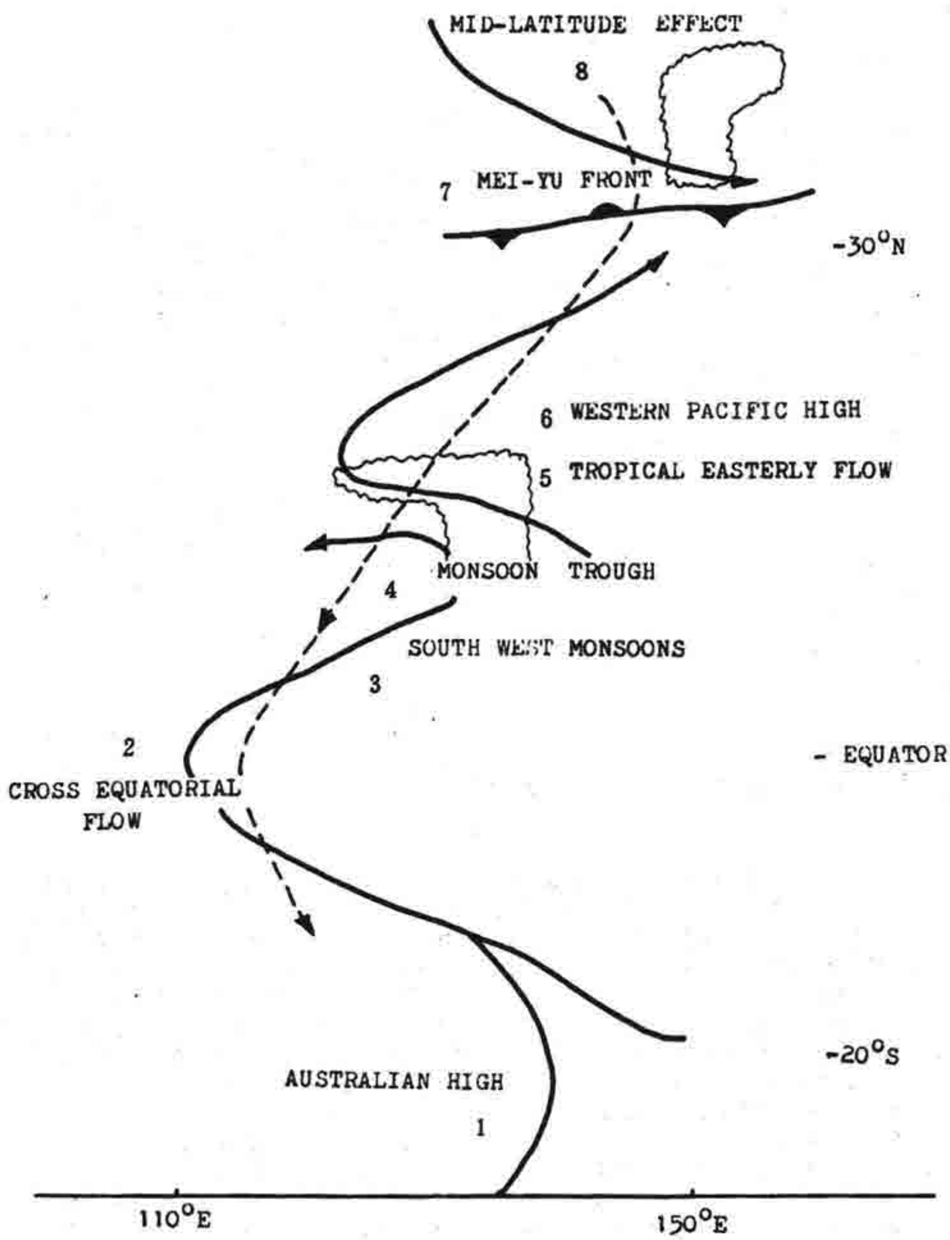

Figure 2.2: Schematic of the summer SEAM system from Tao and Chen (1987).

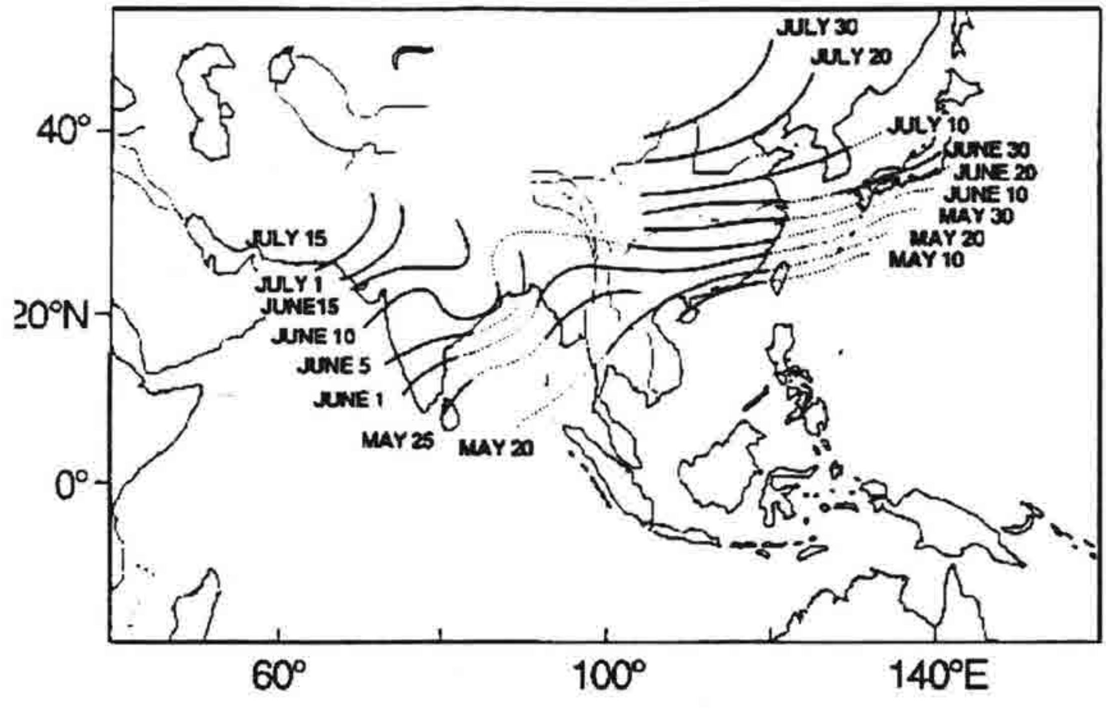

Figure 2.3: Climatological onset dates of the Asian summer monsoon from Lau and Yang (1997).

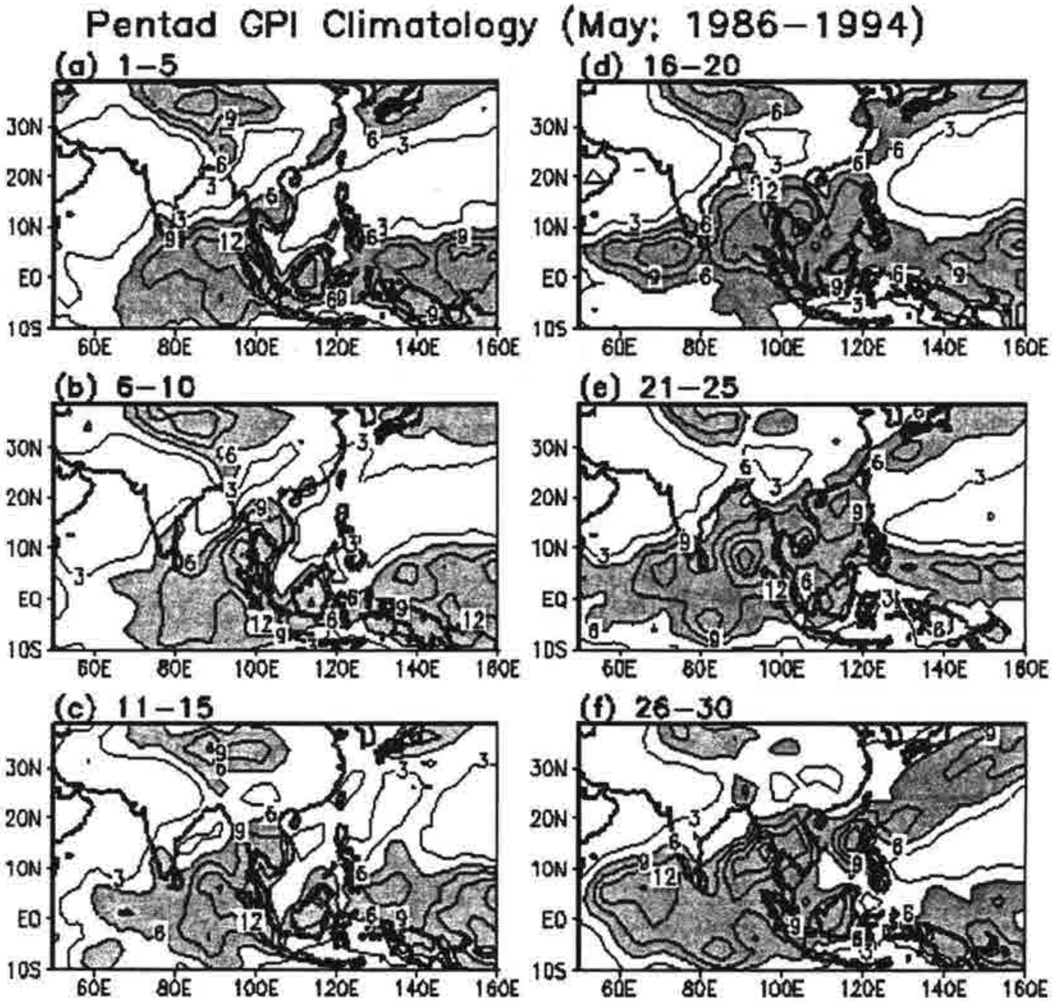

Figure 2.4: GPI climatology for May pentads from Lau and Yang (1997).

from June through August when the band of heavy rainfall shifts northward to the central SCS (10–15° N). The rainfall in the northern SCS just off the coast is typically lighter than either of these two regions throughout the entire year (Lau and Yang 1997). The SEAM also has significant variability on a subseasonal time scale. This manifests itself in the form of onsets and breaks (e.g., Webster 1987a). These transitions tend to be very abrupt, much like the initial onset.

Rainfall is not the only factor that characterizes the SEAM. One of the most important large scale atmospheric circulation features that control the SEAM is the western Pacific subtropical high (WPSH) (Lau and Yang 1997). Prior to onset, the WPSH affects the SCS and low-level easterlies are present. With onset, the WPSH retreats eastward and allows low-level westerly flow to be present over the SCS. This is illustrated in Fig. 2.5 which shows the 850 mb wind climatology. Lau and Yang (1997) point out that the difference between the pentads before and after the onset (Fig. 2.5c) depicts the anomalous cyclonic circulation associated with forcing by enhanced convection over the SCS during onset (Fig. 2.4e).

2.3 Mechanisms of the SEAM onset

As previously mentioned, the complexity of the SEAM has lead to multiple theories about what controls or triggers the SEAM onset. Several of the main ideas are presented in the following sections. At this point we make no judgement as to the correctness or feasibility of these ideas, but merely present them as background on which further study is based.

2.3.1 Tibetan Plateau forcing

The heating of the Tibetan Plateau during the late spring and summer months has long been accepted as the forcing mechanism which drives the Indian monsoon. It has been suggested that forcing from the Tibetan Plateau may have a role in the onset of the SCS

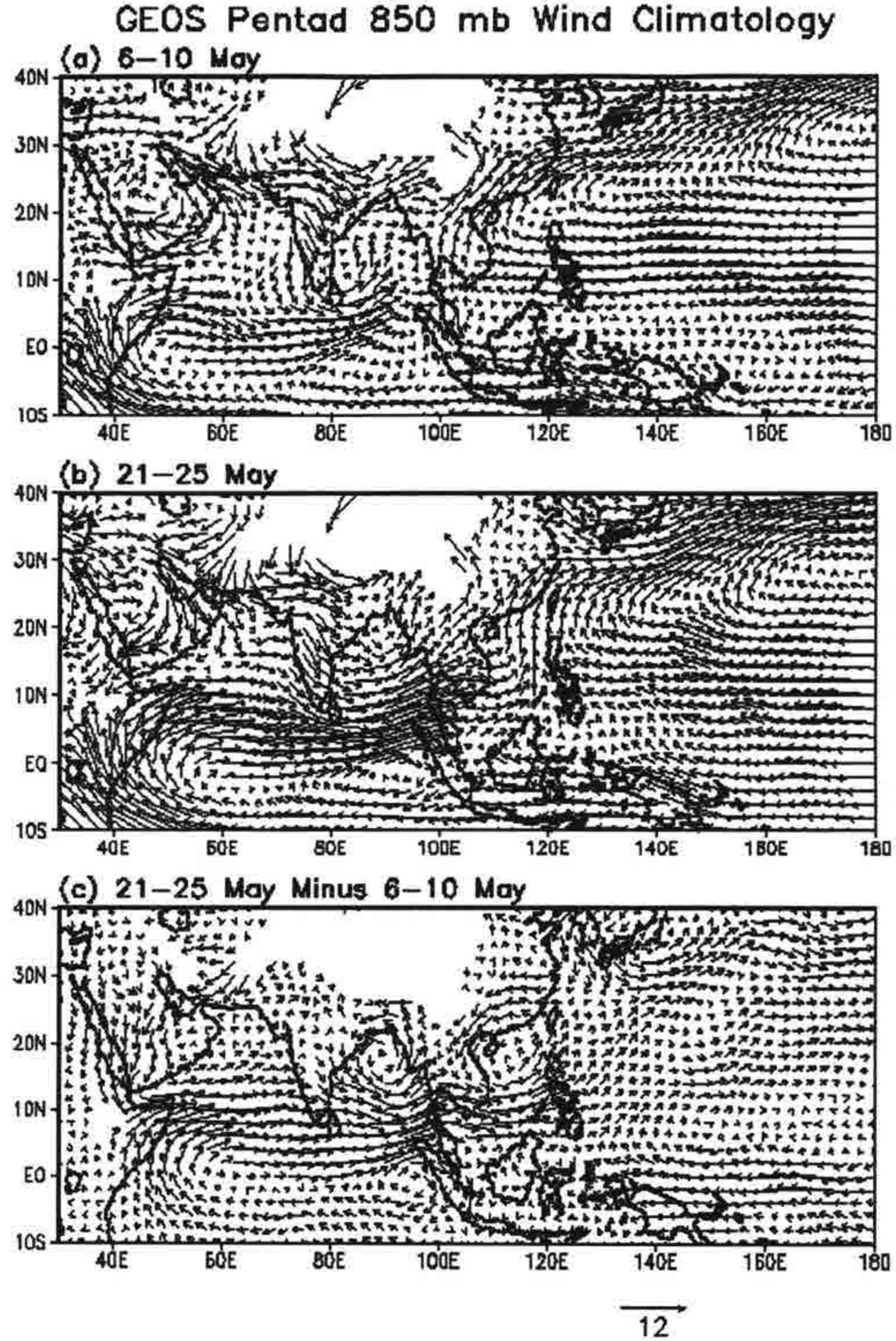

Figure 2.5: 850 mb wind climatology from Lau and Yang (1997).

monsoon as well (Ueda and Yasunari 1997; Wu and Zhang 1998). It seems that the primary difference between the Tibetan Plateau's influence over the Indian monsoon and the SEAM is that its forcing on the Indian monsoon is direct, whereas it has only an indirect affect on the SEAM. In a study of the 1989 monsoon over South Asia and the SCS by Wu and Zhang (1998), the monsoon onset occurred first over the Bay of Bengal (BOB) in early May and was followed by the onset in the SCS by 20 May. The onset of the BOB monsoon is directly linked to the forcing of the Tibetan Plateau, which then sets up a favorable environment for the onset of the SCS monsoon (Wu and Zhang 1998). However, Wu and Zhang (1998) also acknowledge that when considering the onset timing, it is important to take into account atmospheric motions with different frequencies in addition to plateau forcing.

Tibetan plateau forcing has also been suggested to be linked to the early onset of the SEAM. It is again assumed that the onset of the BOB monsoon and the SCS are interlinked. According to Ueda and Yasunari (1998), the early onset of these two monsoons is induced by an eastward extension of low-level monsoon westerlies up to 120° E during mid-May, which is driven by the continent-ocean thermal contrast enhanced by warming over the Tibetan Plateau. The warming over the Tibetan plateau begins in early spring and increases up to mid-June (Wu and Zhang 1998; Ueda and Yasunari 1998). The start of the SEAM coincides with an abrupt increase in warming over the plateau, which implies that the onset of the SEAM is associated with the meridional temperature gradient between the Tibetan plateau and surrounding regions (Ueda and Yasunari 1998).

2.3.2 Midlatitude frontal systems

The approach of a midlatitude trough-front system is another possibility to explain the onset of the SEAM. This mechanism may also explain why the SCS onset occurs prior to other regions of the Asian monsoon system (Chang and Chen 1995). Using data for May-June from 1981–1986, and their westerly index, by Chang and Chen (1995) showed that monsoon onsets are associated with a midlatitude trough/front moving equatorward and increased southwesterlies, moisture and rising motion moving poleward to meet the front. The front that is associated with the pre-monsoon rainy period is the triggering mechanism of the SCS summer monsoon onset (Chang and Chen 1995). This region of the monsoon is the only one which is open to midlatitude frontal influence. Topographic barriers prevent fronts from influencing areas such as the Arabian Sea, India and the Bay of Bengal during the spring.

Additionally, Lau et al. (2000b) reported that midlatitude disturbances strongly impacted the northern SCS during the 1998 SEAM onset with an active frontal convective system which developed over the northern SCS, and Chan et al. (2000) also cite a midlatitude front as the triggering mechanism for the 1998 monsoon. However, arguments have been made to the effect that for determining onset, the origin of the rains and southwesterly winds matters as much as the presence of those winds and rains (Li and Wu 2000). Li and Wu (2000) make a distinction between monsoon rains and frontal rains based on northward or southward propagation, respectively, and argue that the frontal rains and associated southwesterlies do not constitute the onset of the SCS monsoon.

2.3.3 Intraseasonal oscillations

The presence of intraseasonal oscillations in the SEAM region has received much attention in the literature (e.g., Nitta 1987; Wang and Wu 1997; Hartmann et al. 1992; Fukutomi and Yasunari 1999). These intraseasonal oscillations are present with both the Indian monsoon and the SCS monsoon, and have been seen in both the summer and winter regimes. Whether they are the main forcing mechanism, or just a portion of the onset trigger is still a matter of debate. However, that they have an effect on the onset seems to be a common idea. Two oscillations that appear to have a significant effect on the monsoon onset occur in a 30–60 day period and an approximately 12–24 day period. Through methods discussed in chapter 3, it is possible to recognize and isolate these two modes. However, it is not such an easy task to distinguish what they represent physically.

There are multiple oscillations represented by a 30–60 day period. The Madden-Julian Oscillation (Madden and Julian 1971) is an eastward moving equatorial wave which has a period of around 30–70 days. There have been suggestions that the MJO has influence over the SEAM onset (e.g., Fukutomi and Yasunari 1999). Another 30–60 day oscillation which has influence over the onset of the monsoon is the 30–60 day monsoon trough/ridge (Chen and Chen 1995). This oscillation is a seperate entity from the MJO. It is a northward moving mode which is argued to be responsible for the initial onset of the SEAM and its active and break periods. For instance during the 1998 SCS monsoon, after the initial onset, convection fluctuated with a timescale of 20–30 days (Lau et al. 2000b). This is shown to couple with the eastward-propagating 30–60 day global divergent circulation (another name for the MJO) over the SCS (Chen and Chen 1995).

Compared to the 30–60 day mode, the 12–24 day mode has not been very well observed. This mode is seen as a primarily westward moving system which originates in the tropical western Pacific (Chen and Weng 1997; Fukutomi and Yasunari 1999). For example, during the 1979 monsoon, this mode originated in the open sea southeast of the Philippines. It moved northwestward to the Philippines and then straight westward into Indochina (Chen and Chen 1995). Chen and coauthors (1995, 1997, 2000) found the 12–24 mode to exhibit a double-cell structure with one cell centered at $15° - 20°$ N and the other on the equator (Fig. 2.6). Though clearly identifiable, a clear physical explanation of this mode has not yet been presented in the literature. Chen and Chen (1995) simply call it a 12–24 day monsoon low, and offer no explanation as to what causes it. This is true for subsequent studies as well (e.g., Chen and Weng 1997,1999; Chen et al. 2000). Other studies interpret this mode as a Rossby wave response to tropical heating over the South China Sea (Fukutomi and Yasunari 1999; Nitta 1987).

The onset of the SCS monsoon is suggested to be triggered by the simultaneous arrival of the 30–60 day monsoon trough and the 12–24 day monsoon low in the northern SCS for the 1979 SEAM (Chen and Chen 1995; Chen and Weng 1999). Chen and Weng (1997)

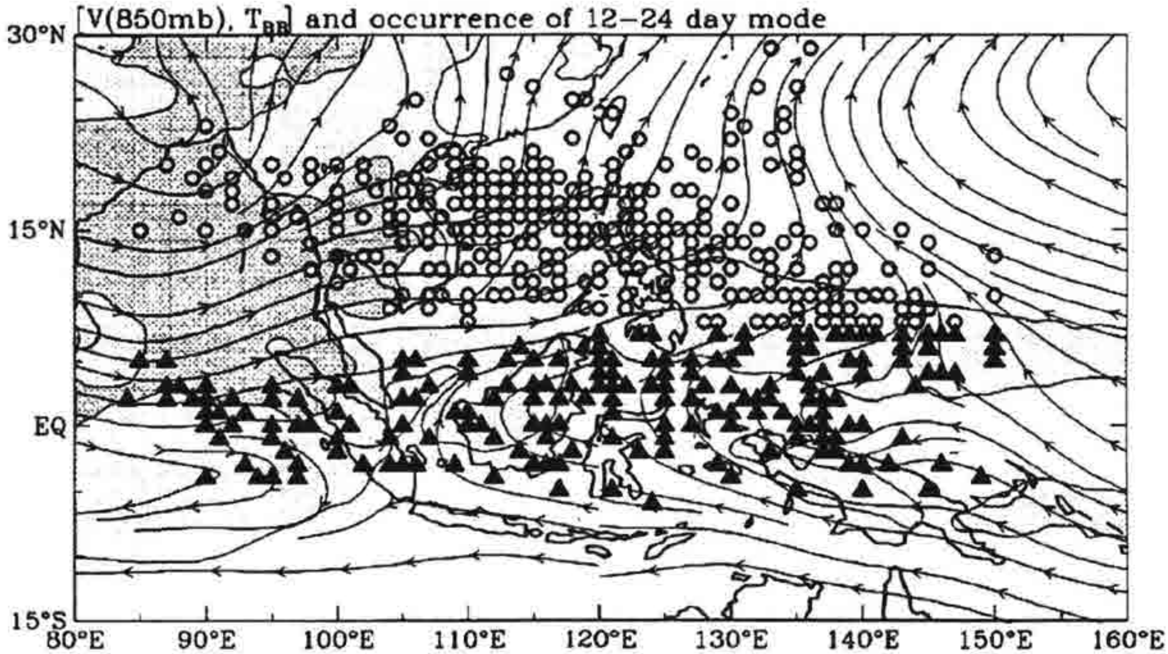

Figure 2.6: Occurrences of 12–24 day monsoon modes (as identified from closed lows) with the May-Aug. mean 850 mb streamlines and equivalent blackbody temperature (shaded) for 1979–1993 from Chen et al. 2000. Open circles (triangles) represent the northern (southern) track of the 12–24 day mode.

tested this idea by extending the analysis to include the years 1979–1993. Similar results were found. However, one intraseasonal mode may be more significant that the other during one monsoon season, and the opposite may be true for another monsoon season (Chen et al. 2000).

2.3.4 Summary

The complexity of interactions between the SEAM and the global and regional climate has led to many different ideas for what mechanism may be the onset trigger. Some of the main ideas include Tibetan Plateau forcing, midlatitude frontal system influence, and the effects of intraseasonal oscillations on a 30–60 day and 12–24 day timescale. Though each of these mechanisms were suggested separately, it is possible that no one mechanism is exclusively responsible for triggering the onset. For example, Wu and Zhang (1998) proposed that Tibetan plateau forcing was the primary mechanism behind the SEAM onset. However, they also suggested that the timing of the 1989 monsoon onset was influenced by the concurrent arrival of the MJO and a two-to-three week oscillation in the SEAM area. Chang and Chen (1995) also acknowledge the possibility of multiple influences. They promote the idea of midlatitude fronts triggering the monsoon. However, they acknowledge a possible relationship between intraseasonal oscillations and monsoon onset. They suggest that a midlatitude-triggered event may locally amplify the intraseasonal oscillations resulting in the appearance of an onset triggered by those oscillations. It seems the question of what triggers the SEAM onset is far from answered. Hopefully this study will provide some basis for moving toward that answer.

Chapter 3

DATA AND METHODOLOGY

3.1 Data sets

Two primary datasets were used for this study. Daily values of zonal and meridional winds from the NCEP/NCAR reanalysis for 1979–1998 were used (Kalnay et al. 1996). These data are on a 2.5° x 2.5° lat/long grid. Daily-averaged values of outgoing longwave radiation (OLR) from 1979–1998 were also used. The estimates of OLR are averaged from the daytime and nighttime passes of the National Oceanic and Atmospheric Administration (NOAA) polar-orbiting satellite. These data are interpolated in space and time to remove missing values, and are archived on a 2.5° x 2.5° lat/long grid (Leibmann and Smith 1996). OLR is commonly used as an indicator of convection between 30° N and 30° S. For the unfiltered OLR, a threshold value of 240 W m^{-2} is used to infer convection. Data with values less than or equal to this threshold are considered representative of convection.

Figure 3.1 shows a representation of the domain used for data analysis. The red box highlights the SCS area. Smaller boxes labeled as SC (20–25° N, 115–120° E), NE (15–20° N, 115–120° E), SW (10–15° N, 110–115° E) and EQ (5–10° N, 110–115° E) are base areas used in analysis. These base areas were chosen because they represent the areas of greatest variability of filtered OLR as seen from the standard deviations. Choice of filtering bands will be discussed in section 3.2.2.

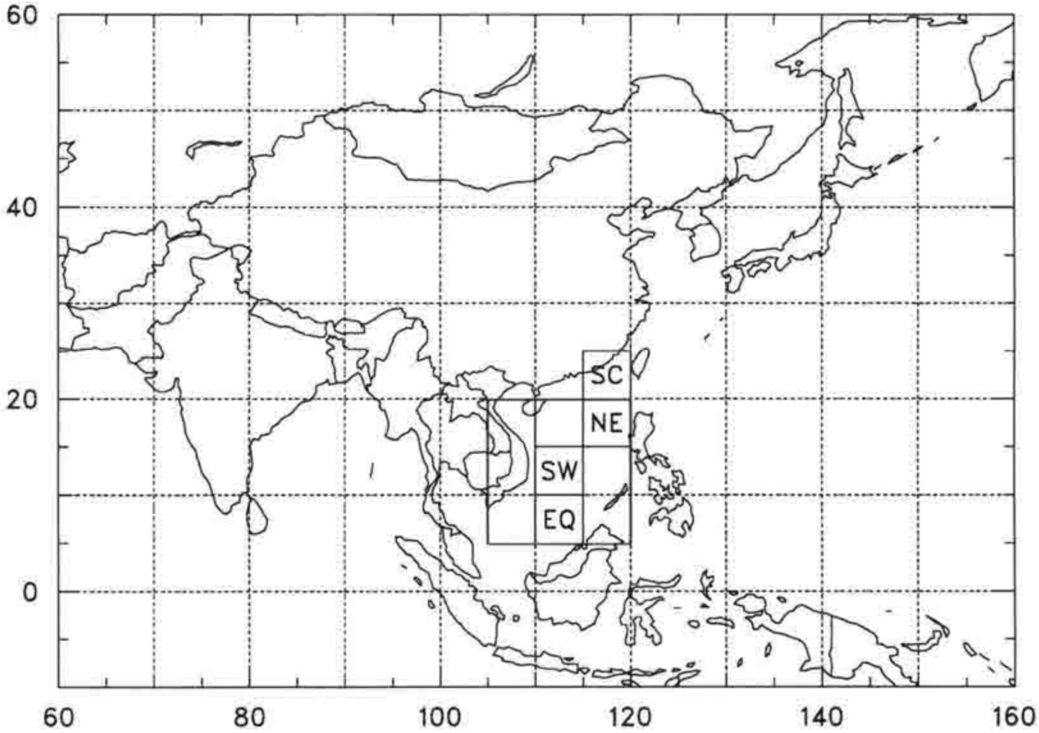

Figure 3.1: Areas of data analysis. The red box highlights the SCS area. Smaller boxes labeled as SC (20–25° N, 115–120° E), NE (15–20° N, 115–120° E), SW (10–15° N, 110–115° E) and EQ (5–10° N, 110–115° E) are base areas used in analysis.

3.2 Analysis techniques

3.2.1 Spectral Analysis

Spectral analysis was performed on daily averaged OLR at 25 different 2.5° x 2.5° grid points in and around the SCS (10 - 20° N, 110 - 120° E) for the monsoon season. Separate spectra were calculated for May through September (MJJAS) of each year from 1979–1998. Additionally, the ensemble spectra for all the years were calculated at each grid point. The resulting spectra give an estimate of the amount of variance that is contributed to the total variance by oscillations at different frequencies. This estimate is called the spectral density. The analyzed spectrum is used to discern the dominant time scales of variability within the analyzed region over the timeframe in which the data were analyzed. Even though the principal concern of this study is the onset of the monsoon which occurs most commonly in May, it is necessary to use a large range of months such as MJJAS to more accurately capture the low-frequency oscillations which occur on a 30–60 timescale.

The spectral densities were computed using fast fourier transforms closely following the method presented in Ciesielski (1980). There are several steps to the calculation process. To start, the input is one full year of data. These data are then transformed into spectral space where the lowest three harmonics are calculated and removed from the data. This is to remove the annual cycle and other strong spectral peaks which may contaminate the spectral density estimates at low frequencies (Ciesielski 1980). Once the first three harmonics are removed from the full year of data, the monsoon season (MJJAS) is extracted from the original data to make a new, shorter timeseries. The data are then detrended. Again, this eliminates low frequency components which cannot be resolved within the length of the timeseries. A cosine tapering is performed at each end of the time series to suppress leakage in the spectral density estimates as a result of finite sample length (Ciesielski 1980). The power spectral density estimates, $\hat{G}(f)$, are then calculated,

$$\hat{G}(f) = 2 \times (A^2 + B^2)N^{-1} \tag{3.1}$$

where f is frequency, A is the real Fourier component, B is the imaginary Fourier component and N is the number of points in the data series (Ciesielski 1980). The calculated spectrum is then smoothed over three adjacent spectral estimates.

Once the spectral densities are calculated, their significance must be tested. This is done by comparing them to a null hypothesis, usually a red noise spectrum (Gilman et. al 1963), and then testing whether the estimated spectrum falls within accepted confidence limits of the hypothetical spectrum. As is commonplace in studies of the atmosphere, the hypothetical spectrum is represented by a two parameter, aliased Markov spectrum given in Ciesielski (1980) as:

$$G(f) = \frac{2V}{1 + \alpha^2 - 2\alpha\cos(2\pi f)} \tag{3.2}$$

where V is the variance of the forcing, α is the lag-1 autocorrelation, and f is the frequency. The confidence intervals express at a given confidence level (i.e. 90% or 95%) how close to the values of the hypothetical spectrum one would expect to find sample estimates for given degrees of freedom (Ciesielski 1980). In other words, given that the red noise spectrum is the null hypothesis, the confidence intervals represent boundaries which are used to accept or reject the null hypothesis. If an estimated spectral peak exceeds the 95% confidence limit, there is only a 5% probability that this peak has occurred by chance. In other words, we can be 95% confident that this spectral peak with its excess power (i.e. amplitude) represents "true" variability above that contained in the hypothetical spectrum. The confidence levels are based on the Chi-squared value such that the probability that the chi-squared value of the sample estimate is less than the chi-squared value of the confidence level is represented by the given confidence level. The number of degrees of freedom (DOF) affect the width of the confidence interval, and are calculated based on the number of adjacent spectral estimates over which the spectra were smoothed. The number of DOF are also adjusted because of the cosine tapering (Ciesielski 1980). For smoothing over three adjacent spectral estimates, the DOF is 5. There was no smoothing done to the ensemble spectra because smoothing is inherent when averaging all 20 years together. For only one year of data to be used in the ensemble, an unsmoothed spectrum would have only 2 DOF. However, the number of DOF will increase when the averaging of many independent spectra is taken into account. The new DOF is given by the following equation from Ciesielski (1980):

$$DOF = (DOF^{\star}) \times \overline{ns} \tag{3.3}$$

where $DOF^{\star}$ is the original number of degrees of freedom and $\overline{ns}$ is the number of independent spectra over which the averaging is done. Given this formula, the DOF for an ensemble of 20 years would be 40. For this analysis, however, a more conservative estimate of 25 DOF was used for the ensemble spectra.

An example of the spectral analysis of the OLR is shown in Fig. 3.2. The top panel shows the spectrum for MJJAS 1998 at 10° N, 112.5° E. Among several distinct peaks, notice a peak centered around 18 days that eclipses the 95% confidence limit. Also there is an "enhancement" just beyond 30 days. The bottom panel is the ensemble of the individual spectra from 1979–1998 for the same point. This, too, has peaks centered near 18 days and just beyond 30 days which are significant at 95%. It is not always the case that the ensemble spectra have peaks that are statistically significant or as strong as those in the individual years. However, this does not preclude these peaks from being important. There is a large amount of variability in the spectra from year to year and point to point. The ensemble spectra tend to display "enhancements" rather than significant peaks, but the peaks show up in the individual years. This may indicate that variability in these frequency ranges are usually present, but can be stronger in some years than others. Spectral analysis done by Wang and Wu (1997) show similar results. They found peaks at various timescales including 15–20 days and 30 days in the individual years' analyses, but the 9-year average failed to display the same prominent features.

3.2.2 Band pass filter

A Lanczos band-pass filter was used to isolate intraseasonal oscillations with 12–24 and 30–60 day periods. The filter was applied to gridded OLR as well as zonal and

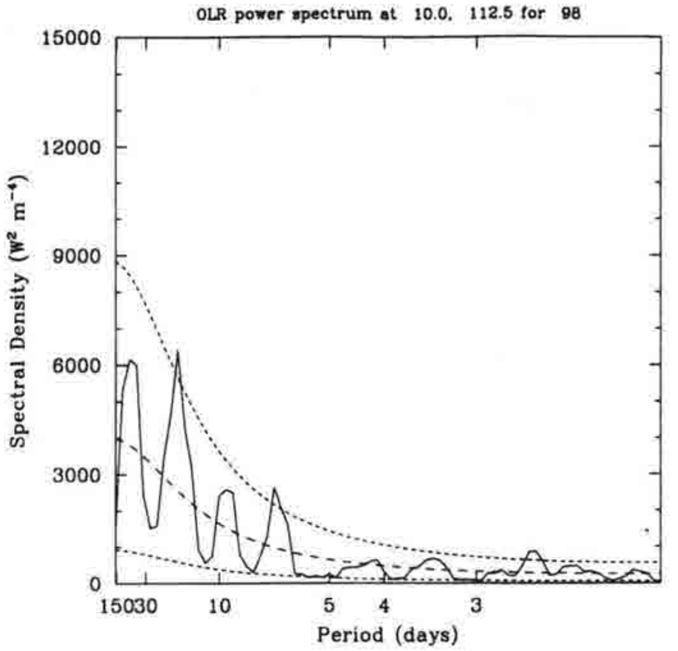

(a)

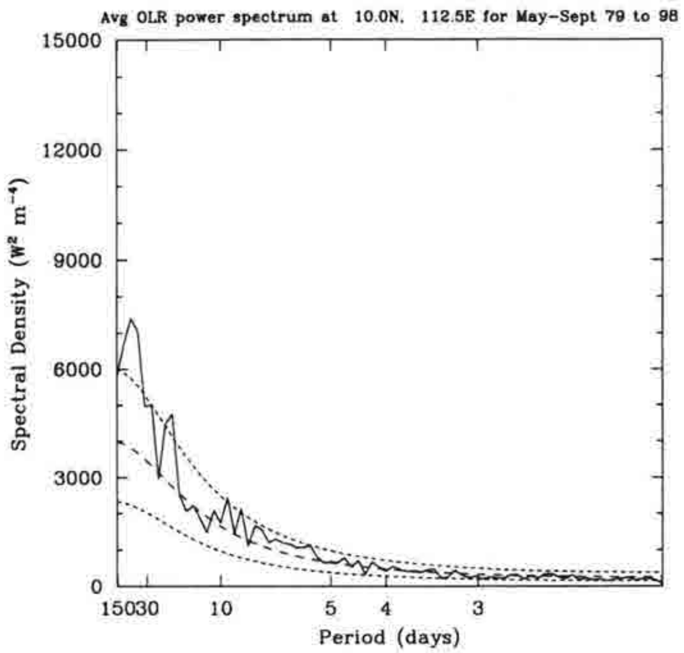

(b)

Figure 3.2: Spectral Density estimate at 10° N, 112.5° E in the SCS for MJJAS 1998 (a) and for MJJAS averaged from 1979–1998 (b). Solid line is the estimated spectrum (in W^2 m^{-4}). Long dashed line is the red noise background. Short dashed lines mark the 95% and 5% confidence intervals.

meridional winds at 850 mb and 200 mb. These two bands were chosen based on the peaks seen in spectral analysis. Additionally, there are many previous studies which found spectral peaks on a similar timescale (e.g., Wang and Wu 1997; Fukutomi and Yasunari 1999) and deemed these two periods to be integral to the onset of the SEAM (Chen and Chen 1995).

Lanczos filtering is a Fourier method of filtering digital data (Duchon 1979). The Lanczos band-pass filter takes a timeseries as input (x_t, t = time) and returns a new timeseries (y_t) which contains data with oscillations in the desired period. These oscillations are "extracted" from the data by way of a weighting function (w_k). This can be represented mathematically by the following equation from Duchon (1979):

$$y_t = \sum_{k=-\infty}^{\infty} w_k x_{t-k}. \tag{3.4}$$

The representation of the weight function in frequency space is called the response function, $R(f)$, which is just a Fourier transform of the weight function. An ideal response function could be represented by a step function where the response function is zero at frequencies less than the cut-in frequency, f_{c1}, and at frequencies greater than the cut-out frequency, f_{c2}, and one in between the two frequencies (Duchon 1979). The cut-in and cut-out frequencies represent the boundaries of the frequency band that the filter isolates. There are factors that prohibit the use of the ideal function, however. The main factor is the Gibbs phenomena. Simply put, the Gibbs phenomena is an overshoot and undershoot of the solution which is being approximated. It occurs when trying to approximate a discontinuous function (like a step function) with a finite Fourier transform. In general, there is a primary overshoot and undershoot of approximately 9% of the jump discontinuity. This is the case even for a very large number of terms in the Fourier series (Haberman 1987). To correct for this a smoothed version of $R(f)$ should be used. This smoothing helps to lessen the amplitude of the Gibbs oscillation (Duchon 1979). The truncated weight function for the smoothed response function is then determined by multiplying the original weight function by a function that Lanczos called the "sigma factor", which is of the form $\sin X/X$, where X here represents a general function (Duchon 1979).

The procedure used to band-pass filter the data was to first calculate the weight function using a finite number of weights. For filtering in both the 12–24 day band and the 30–60 day band, $n = 241$ weights were used. The more weights that are used, the more precise the filtering will be. It is important to note, however, that $n/2 + 1$ points are cut off at either end. So, the more weights, the less data are available after the filtering. This was not a problem in this study since only the monsoon season of each year was of concern and the only data which was cut off was the beginning of 1979 and the end of 1998. The smoothed weight function, $(\bar{w}_k)$, for a band-pass filter is

$$\bar{w}_k = \left(\frac{\sin 2\pi f_{c2} k}{\pi k} - \frac{\sin 2\pi f_{c1} k}{\pi k}\right)\sigma, \quad k = -n, \ldots, 0, \ldots n \tag{3.5}$$

where $\sigma = \frac{\sin \pi k/n}{\pi k/n}$ (Duchon 1979). Next, the truncated response function, $\bar{R}_n(f)$, is calculated from the weights, and represents the partial sum of the Fourier series obtained by replacing the infinite limits in the series with finite limits (Duchon 1979).

$$\bar{R}_n(f) = \bar{w}_0 + 2\sum_{k=1}^{n} \bar{w}_k \cos 2\pi f k \tag{3.6}$$

Figure 3.3 shows the response functions from the 12–24 day band and the 30–60 day band. Figure 3.4 shows a sample timeseries of OLR before and after the 12–24 day filter. Within the filtering, the weights were adjusted so that the mean of the output data is zero. Thus the filtered data represent anomalies of the input field. Figure 3.5 illustrates the same sample timeseries before and after the 30–60 day band pass.

3.2.3 Lag Correlation/regression

A lag correlation and regression analysis was used to establish relationships between deep convection and the circulation over the 12–24 day and 30–60 day timescales around the monsoon onset. These lagged regression relationships can be used to examine the evolution of the convection and circulation signals over time (Kiladis 1998). This analysis was used with the assumption that there is a linear, or nearly linear relationship between OLR and circulation. This assumption is valid to the extent that OLR anomalies are linearly related

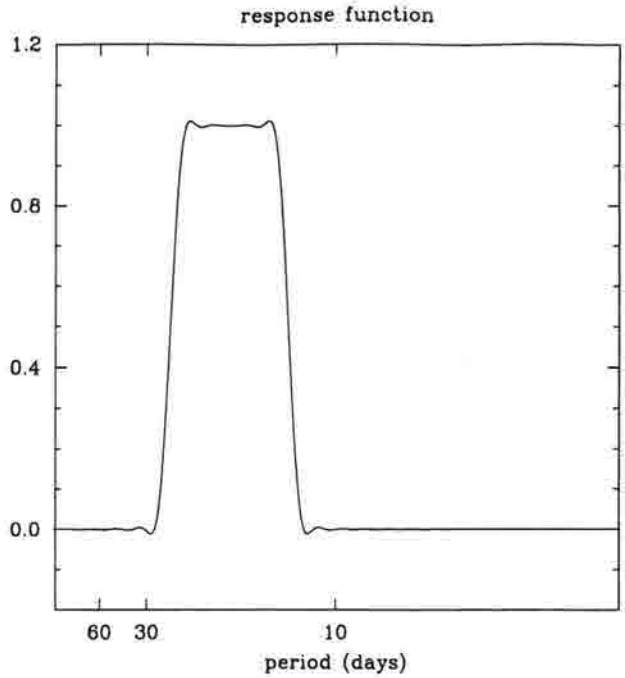

(a)

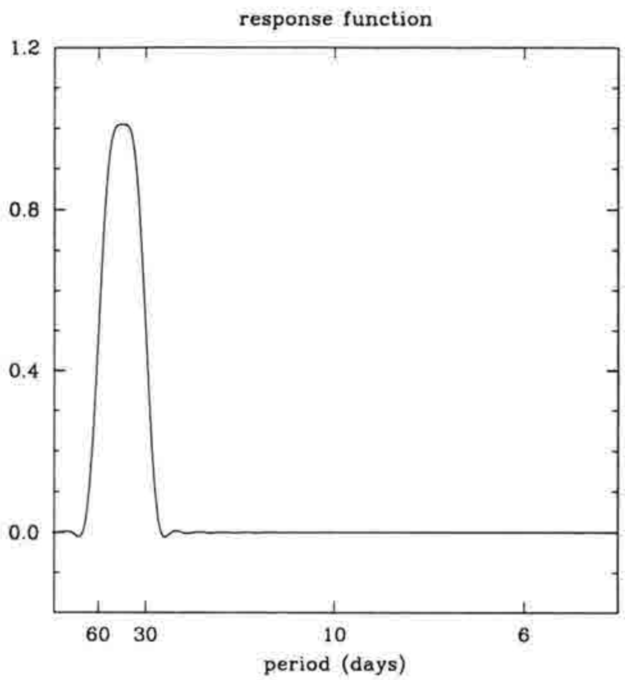

(b)

Figure 3.3: Response functions for 12–24 day band-pass filter (a) and the 30–60 day band-pass filter (b)

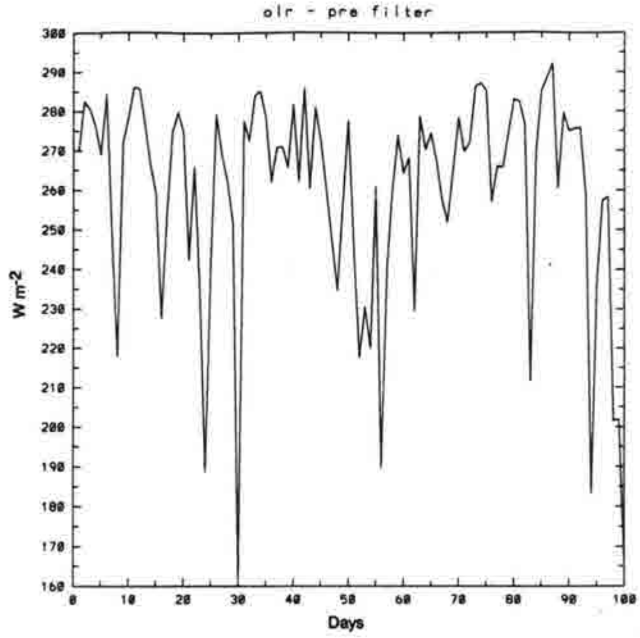

(a)

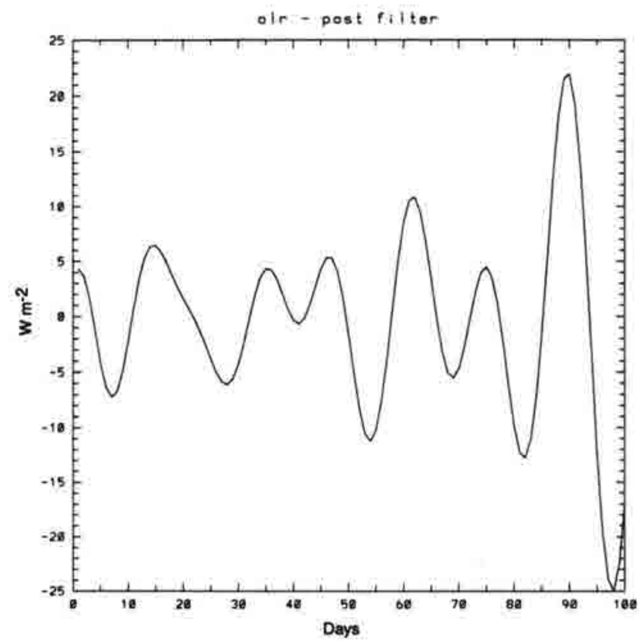

(b)

Figure 3.4: A sample OLR timeseries (a) before filtering and (b) after a 12–24 day band-pass filter.

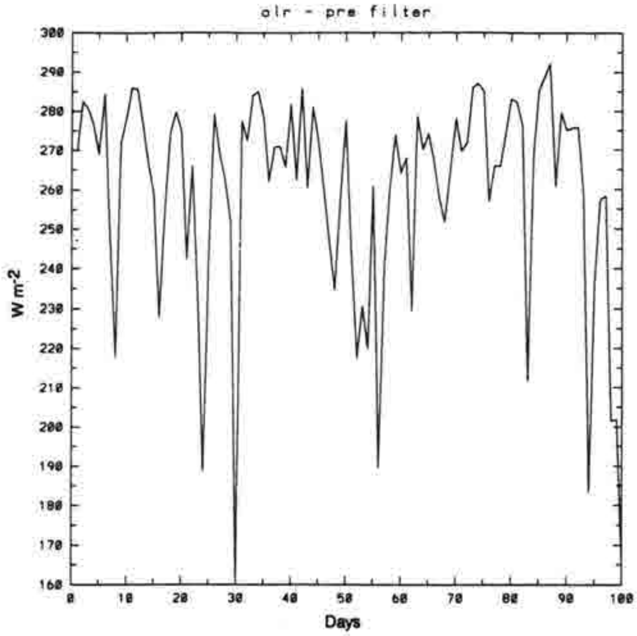

(a)

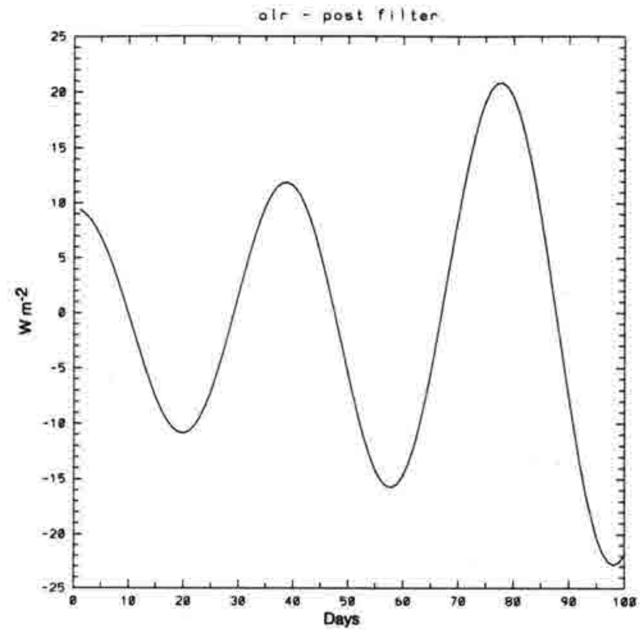

(b)

Figure 3.5: Same as figure 3.4 except (b) is for 30–60 day band-pass timeseries

to tropical heating anomalies and that linear dynamics can explain the response to tropical heating (Kiladis and Weickmann 1992).

For this study, 12–24 day and 30–60 day filtered OLR timeseries in the 5° base areas in and around the South China Sea were regressed against unfiltered OLR, 850 mb and 200 mb zonal and meridional winds at every gridpoint within the large domain shown in Fig. 3.1 for lags of ± 12 days and ± 30 days respectively. The base area timeseries were comprised of OLR averaged over the base area for the MJJA and MJ periods from the years 1979–1998.

The concept of a least-squares linear regression is a fairly simple one. For a given set of data in (x,y) pairs, the goal is to find a particular straight line

$$\hat{y} = a + bx \tag{3.7}$$

while minimizing the squared errors which are represented by a vertical distance (on the x-y plane) from the predicted line and the actual data point. The $\hat{y}$ indicates that the equation specifies a predicted value for y with a and b as the y-intercept and slope, repectively (Wilks 1995). There will be error for each data point. Taking these errors into account produces a regression equation such as that from Wilks (1995):

$$y_i = a + bx_i + e_i \tag{3.8}$$

where e is the error and i is simply an index to denote each point on the line. This equation is then solved for the minimum squared errors. Upon doing this, the regression coefficient, b, can be obtained and represented as

$$b = \frac{n\sum x_i y_i - \sum x_i \sum y_i}{n\sum(x_i)^2 - (\sum x_i)^2} \tag{3.9}$$

where $\sum$ represents $\sum_{i=1}^{n}$. With the y-intercept, represented by a in equations 3.7 and 3.8, set to zero the regression coefficient is all that is needed to get the straight line. Then for each lag, the linear dependence of the OLR, and circulation can be mapped by applying the regression equation, $y = bx$, for each grid point using an arbitrary value of OLR at the base region as the independent variable (Kiladis 1998). For this study, a value of -20 W m^{-2} was used because it represented a typical value for an OLR anomaly at the time of monsoon onset.

The correlation coefficient, r, for the same base areas and parameters is similarly calculated. Here $\sum$ is the same as in equation 3.9.

$$r = \frac{\sum x_i y_i - \frac{1}{n}(\sum x_i)(\sum y_i)}{\sqrt{\sum x_i^2 - \frac{1}{n}(\sum x_i)^2}\sqrt{\sum y_i^2 - \frac{1}{n}(\sum y_i)^2}} \tag{3.10}$$

The correlation coefficient enables the statistical significance of the local linear relationship between OLR in the base area and the dependent variable (OLR and winds) at any grid point to be assessed (Kiladis 1998). It is important to note that the computational forms of the regression and the correlation coefficient shown here are susceptible to roundoff errors. This is due to the large values that arise in the summations with the numerator generally the difference between two large numbers (Wilks 1995). To combat this effect, the climatological seasonal mean was subtracted from the unfiltered OLR and wind data before the calculations were made.

Given spatially correlated data, assessing the statistical significance of each point independently is not correct. Livezey and Chen (1983) address this problem. They assert that large spatial cross-correlations in a field as well as large lag autocorrelations reduce the number of effective samples, or degrees of freedom (DOF) in a timeseries. So, instead of a set of N individual samples, an interdependent field should be viewed as $n < N$ independent clusters of closely related samples. The key to correctly identifying statistically significant data is to estimate n accurately. This equates to a multi-step process as laid out by Livezey and Chen (1983). The first step is to obtain a measure of the effective time, τ, between independent samples. This can be estimated from the autoregressive properties of both timeseries (Livezey and Chen 1983).

$$\tau = [1 + 2\sum_{i=1}^{N} C_1(i\Delta t)C_2(i\Delta t)]\Delta t \tag{3.11}$$

In the equation for τ, Δt is the sampling time, N is the total number of samples, and C_1

and C_2 are the auto-correlations at lags $i\Delta t$ for the timeseries which are being used. The effective number of DOF (or independent samples) in the timeseries,

$$n = \frac{N\Delta t}{\tau} \tag{3.12}$$

is then calculated from τ (Livezey and Chen 1983). This formula for n is only used for $\tau > 1$. If $\tau < 1$, then $n = N$. Once the effective DOF is determined, the correlation coefficient for a chosen significance level can be calculated as

$$r_s = \frac{X}{\sqrt{n-3}} \tag{3.13}$$

where r_s is the absolute value of the correlation corresponding to the chosen significance level, X is the value for the area under a normal curve that corresponds to the chosen significance level (i.e. 1.96 for 95%) and n is the effective DOF (Wilks 1995). So, a calculated correlation value would have to be greater than (or equal to) r_s or less than (or equal to) $-r_s$ to be considered statistically significant. For this study, the 95% level of significance was used for all parameters.

Chapter 4

ANALYSIS

4.1 Onset characteristics and definition

As mentioned in Chapter 2, the climatological onset for the monsoon in the SCS is in mid-May. The exact dates for the onset of the SCS monsoon are not well defined and depend on the definition used. Onset definition is somewhat subjective and many different indices have been developed and used to try and quantify the timing of the onset and the strength of the monsoon. One simple indicator of onset is the shift from low-level southeasterlies and anticyclonic flow to southwesterly flow over the SCS. Explosive growth in convection in the central SCS also signals the onset (Lau and Yang 1997). The definition of onset used in this study is based upon these simple ideas.

4.1.1 Definition

In most years the monsoon onset in the northern and southern SCS differed by only a few days. In those years a single onset date for the entire SCS is assigned. Such was the case for the 1998 monsoon. During SCSMEX, the onset in the northern SCS (15–20° N, 110–120° E)(NSCS) occurred around 15 May, while the onset in the southern SCS (10–15° N, 110–120° E) (SSCS) occurred about 20 May (Johnson and Ciesielski 1999). In some years, however, (1981, 1982, 1983, and 1993) the onset dates between the NSCS and the SSCS differed by as much as several weeks. For these years, it is necessary to keep the northern and southern onset dates separate.

Onset dates were computed as a simple average of five dates determined by separate procedures. The first of these dates was chosen based on animations of unfiltered OLR and 850 mb winds over the entire domain shown in Fig. 3.1. Based on these plots, the onset date was chosen to be the first day of sustained convection and the commencement of a southerly and westerly component of the wind over the SCS (red outlined area in Fig. 3.1). These criteria were subjectively chosen and the first onset date was determined solely from inspection of the animations. The other four dates were chosen based on timeseries of unfiltered OLR, 850 mb zonal wind and 850 mb relative vorticity averaged over each of four 5° x 5° boxes over the SCS (from 10–20° N, 110–120° E). An example for the 1998 SEAM is shown in Figure 4.1. For each 5° box, the onset date was chosen as the date when the OLR dropped rapidly below 240 W m^{-2}, the zonal wind changed from easterly to westerly (negative to positive) and the relative vorticity switched from negative to positive. In each of the timeseries, the changes from the pre-onset to post-onset regime must be sustained for at least a week to consider the changeover date the onset. Once these 5 dates were determined, they were averaged together to produce the representative onset date for the SCS.

The onset dates for this study are shown in the first two columns of Table 4.1. Onset dates for previous studies are also shown. The criteria for determining the onset date in other studies will be discussed in the next section and details on onset timing for this study will be further discussed in section 4.1.3.

4.1.2 Indices and alternate definitions

As previously mentioned, many different definitions are used to signify the onset of the monsoon. Most of these are rather subjective. For the 1989 monsoon onset, Wu and Zhang (1998) used OLR values of less than 220 W m^{-2} and strong southerlies at 850 mb in the SCS region (10–20° N, 110–120° E) to determine onset. A westerly index was developed by Chang and Chen (1995) to help determine onset. This index is defined by the time series of area-averaged 850 mb zonal wind components over six grid points between 20–22.5° N

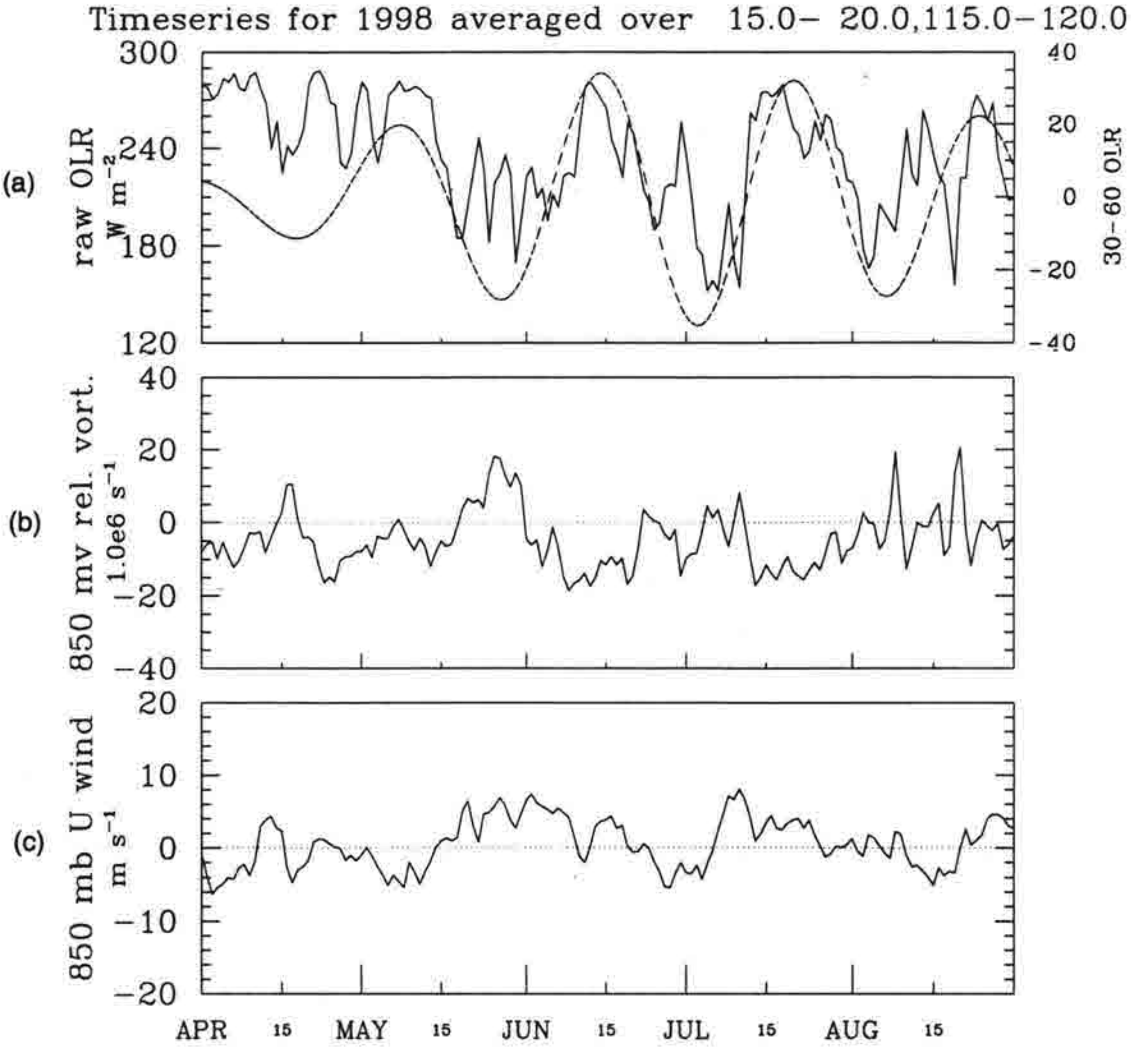

Figure 4.1: NE box timeseries of (a) unfiltered olr (solid) and 30–60 day filtered OLR (dashed), (b) unfiltered 850mb relative vorticity and (c) unfiltered 850mb zonal wind for the 1998 SEAM.

Table 4.1: South China Sea onset dates

Year	N SCS	S SCS	Wang and Wu 1997	Chen and Weng 1997	Xie et al. 1997	Lu and Chen 2000
1979	May 15	May 15	May 11-15	May 16	May 11-15	May 15
1980	May 15	May 15	May 16-20	May 19	May 16-20	May 15
1981	May 10	June 3	May 11-15	May 16	May 11-15	May 16
1982	May 29	May 17	May 16-20	May 17	June 1-5	June 8
1983	May 20	June 4	May 21-25	June 5	June 11-15	June 4
1984	May 21	May 21	Apr 26-30	May 23	May 1-5	June 6
1985	June 2	June 2	May 26-30	May 5	Apr 16-20	Apr 22
1986	May 14	May 14	May 11-15	May 15	May 6-10	May 14
1987	June 7	June 7	June 5-9	June 7	June 6-10	June 9
1988	May 22	May 22	May 21-25	May 20	May 21-25	May 22
1989	May 17	May 17	May 16-20	May 17	May 16-20	May 17
1990	May 16	May 16	May 16-20	May 15	May 11-15	May 21
1991	June 9	June 9	June 5-9	June 5	June 11-15	June 8
1992	May 26	May 26	May 21-25	May 16	June 1-5	June 18
1993	May 25	June 15		May 14	June 16-20	June 19
1994	May 24	May 24			May 16-20	June 1
1995	May 11	May 11			June 6-10	May 12
1996	May 17	May 17				Apr 20
1997	May 20	May 20				May 18
1998	May 20	May 20				May 21
mean	May 19	May 21	May 19	May 17	May 21	May 22

and 112.5–117.5° E. Monsoon onset is defined as the first event in May of each year in which the westerly index increases by at least 3 m s^{-1} over 24 hours and this strengthened westerly wind is sustained for at least 48 hours. In a study of the 1979 SEAM, the onset date was determined to be 16 May (Chen and Chen 1995). This determination was made using an 850 mb zonal wind index (u850) and a precipitation index (P). The indices were determined by an average of these parameters over a 5° x 5° grid inside the SCS. For the u850 index, the area used was from 115–120° E, 7.5–12.5° N. The P index was determined using a similar grid, from 115–120° E, 10–15° N. Both of these areas were determined for the 1979 monsoon only. The grid centers may not be the same for each monsoon due to interannual variability of the monsoon (Chen et al. 2000).

Several studies expanded their monsoon onset definitions beyond just one year and developed a list of onset dates for multiple years. It is with these lists that the onset dates of this study are compared (Table 4.1). Wang and Wu (1997) give onset dates from 1975-1992. They designate an onset pentad which must satisfy two conditions. First, the pentad-mean OLR averaged over 7.5–22.5° N, 110-120° E must be < 235 W m^{-2} and the subsequent 6 pentads must also meet that criteria. Second, the pentad-mean 850 mb zonal wind averaged over 2.5–12.5° N, 110–120° E, as well as the 6 subsequent pentads, must be > 0.5 m s^{-1}. The SCS monsoon onset is then the first pentad in which these criteria are met unless they differ by 2 or more pentads. In this case, the average of the two pentads is the onset.

A similar definition of onset was developed by Xie et al. (1997). Their onset dates are for the period 1979–1995. Onset is defined as the time when the area-average (0–20° N, 105–120° E) pentad OLR is < 235 W m^{-2} and the area-average pentad 850 mb zonal wind changes from easterly to westerly. These conditions must last for 3 pentads.

Lu and Chen (2000) define the onset of the SCS summer monsoon as the withdrawal of the subtropical high pressure system over the SCS. A vorticity index (VOR850) is used to quantify the onset time. The VOR850 index is based on the average of 850 mb vorticity over 10–20° N, 110–120° E. The date of onset is the date in which the following three criteria are satisfied. First, the date must be after 1 April. The onset date is then chosen as the first day of continuous 5 days of positive VOR850. This date is then valid only if within 45 days after the onset the VOR850 is not < 0 for more than 30 days. These numbers (5, 30, 45) were arbitrarily chosen.

Each of these definitions was based on similar ideas of what constitutes monsoon onset. Even with a few differences, Table 4.1 illustrates that subjective methods can yield similar onset dates and criteria. Eight out of the 14 years having onset dates for all methods exhibited onset dates within five days of each other. In addition to completely subjective definitions for the onset of the SEAM, several more objective measures, in the form of monsoon indices, have been used. These indices are used both to determine the onset date and also the strength of the monsoon. Even though these indices were not used directly in this study, they helped shape the criteria used to determine the onset and are therefore

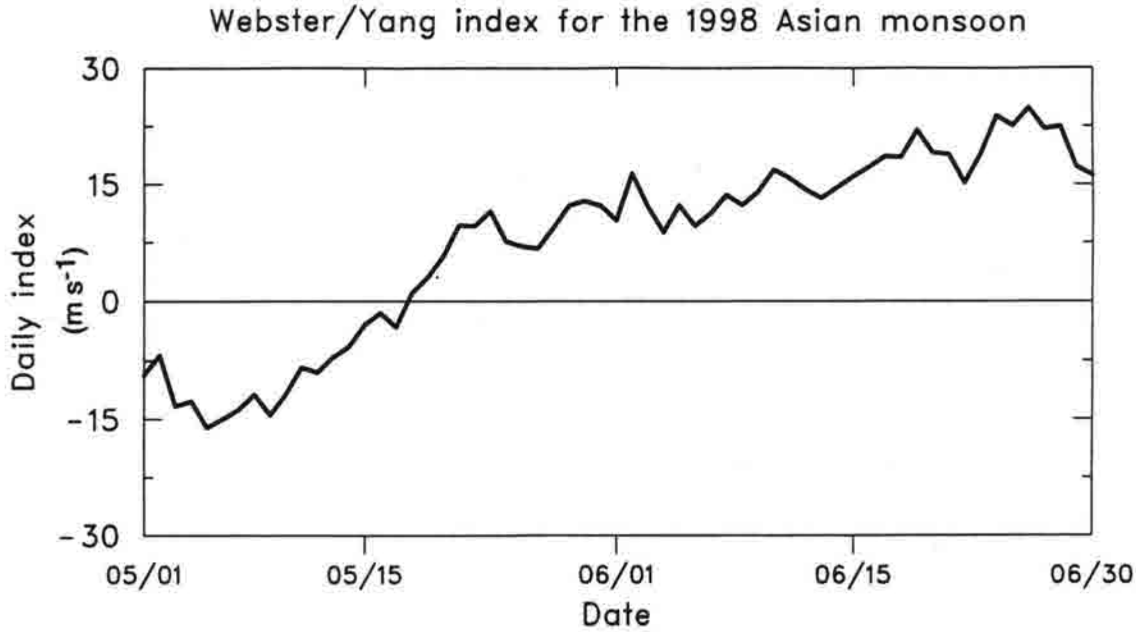

Figure 4.2: Time series of 1998 Webster and Yang (1992) monsoon index from Johnson and Ciesielski (1999).

worth mentioning.

One of the most widely used monsoon indices is that from Webster and Yang (1992) (WY). This index is typically used to assess the strength of the Indian monsoon. Through the thermal wind relationship, the strength of the north-south temperature gradient over South Asia is proportional to the magnitude of the regional vertical shear. This shear can be used as a measure of the strength of the monsoon. The index is the 850 to 200 mb shear of the zonal wind anomalies, $U_{850} - U_{200}$, calculated as an average over 0–20° N, 40–110° E. Johnson and Ciesielski (1999) used a modified form of this index to represent the onset of the 1998 SCS monsoon (Fig. 4.2). In their case, they averaged the shear from 0–20° N, 90–110° E and noted that the switch of the index from negative to positive corresponded to the onset date over the SCS as determined by wind and precipitation changes there. This event corresponds to the time when the N-S temperature gradient in the upper troposphere changes sign due to the heating of the Tibetan Plateau (Li and Yanai 1996). For 1998, the onset date as determined by the index corresponds well with the onset date as determined by previously described methods.

Other studies have indicated that indices used for the Indian monsoon are not necessarily applicable to the SEAM. The WY index does well to reflect broad-scale variations of the monsoon, but may not work well to represent more regional or local scale monsoon features (Wang and Fan 1999). This point is also brought up by Lau et al. (2000a). They define two regional monsoon indices, RM1 and RM2, which represent the Indian and Southeast Asian monsoon regions, respectively. These are circulation indices represented as: RM1 = $(v_{850mb} - v_{200mb})$ over the region 10–20° N, 70–110° E and RM2 = $(u_{200mb}$[40–50° N, 110–150° E] $-u_{200mb}$[25–35° N, 110–150° E] where the winds are averaged over the indicated regions (Lau et al. 2000a). The RM1 and RM2 indices correlate well with rainfall over the Indian and Southeast Asian monsoon areas, respectively. Also, the cross correlation between the indices and the rainfall over the alternate areas is small which emphasizes the idea that these indices represent distinct regional aspects of the monsoon.

4.1.3 Onset timing

When discussing the timing of the monsoon onset over many years, one cannot avoid mentioning the interannual variability of the onset. The onset date can vary significantly from year to year. It is necessary, then, to ascertain which years had abnormal (i.e. early or delayed) onsets and present the criteria by which these years were determined.

Like the definition of the onset, how one determines an abnormal onset is often subjective and can vary from study to study. For this study, the normal onset dates were chosen to be 11 May – 31 May. These dates were chosen based on histograms of the onset dates from Table 4.1. These histograms for the northern and southern portions of the SCS (Fig. 4.3) show skewed distributions with tails toward the latter part of May. The average onset date was around 19 May in the northern SCS and 21 May in the southern SCS. These dates fall toward the end of pentad 10 and beginning of pentad 11. So, to include some of the natural variability in the onset time, pentads 9 and 12 were also considered to fall into the normal onset time, thus giving the 11 May – 31 May timeframe. These dates are one standard deviation from the mean and are consistent with previous studies as well. Wang and Wu (1997) gave a range of 11 May–25 May for normal onsets and Xie et al. (1997) define delayed onset as those years when onset occurs in June. When necessary, distinction should be made between onset in the northern part of the SCS and the southern part. On average, the onset dates do not vary much between the two, but for any given year, the onset dates for the two regions may be up to several weeks apart.

For the aforementioned criteria, the following years were considered to have a late onset: 1981(S), 1983(S), 1985, 1987, 1991, and 1993(S). The years with (S) denote the southern SCS only; no designation is for both the northern and southern SCS. Given the differences in definitions of abnormal onset, and the differences in determining the onset date in general, these late onset dates also compare well with previous studies. Wang and Wu (1997) declared 1975, 1977, 1985, 1987 and 1991 to be late onset years, and 1982, 1983, 1987, 1991, 1992, 1993 and 1995 were deemed late onsets by Xie et al. (1997). The only early onset in this study came in the northern SCS in 1981. Having only one early onset year is not atypical. The majority of abnormal onset years are late onsets (Wang and Wu 1997). They found 5 of 6 abnormal onset years to be late.

4.2 1998 SEAM onset

Because of the SCSMEX experiment, there have been many studies focused on the 1998 SCS monsoon. In order to understand the monsoon and the role intraseasonal oscillations have on the SEAM onset, a detailed description of the monsoon onset for one year seemed to be a logical first step.

4.2.1 Determining onset date

Section 4.1 described how the monsoon onset was determined for this study and several previous works. The onset date for the 1998 SEAM was 20 May (Table 4.1). This is

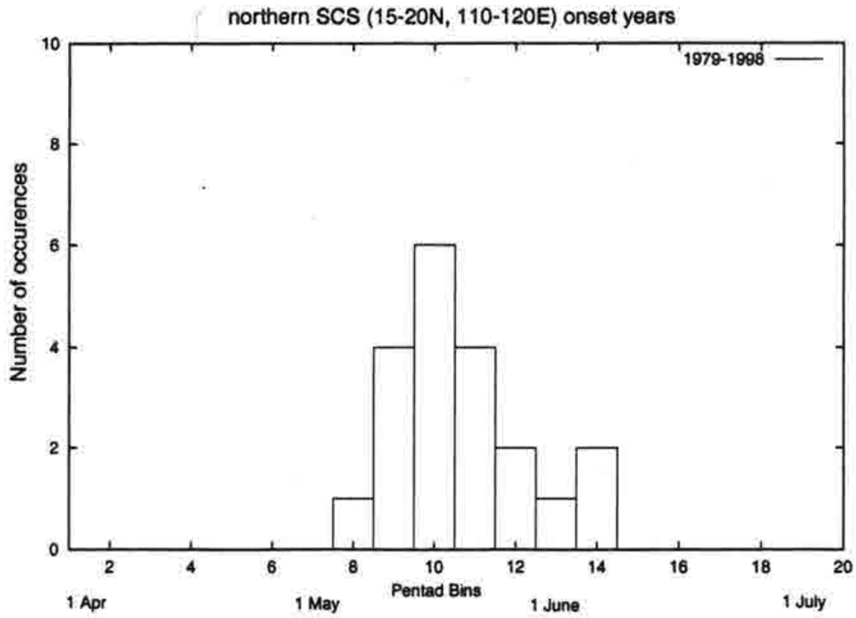

(a)

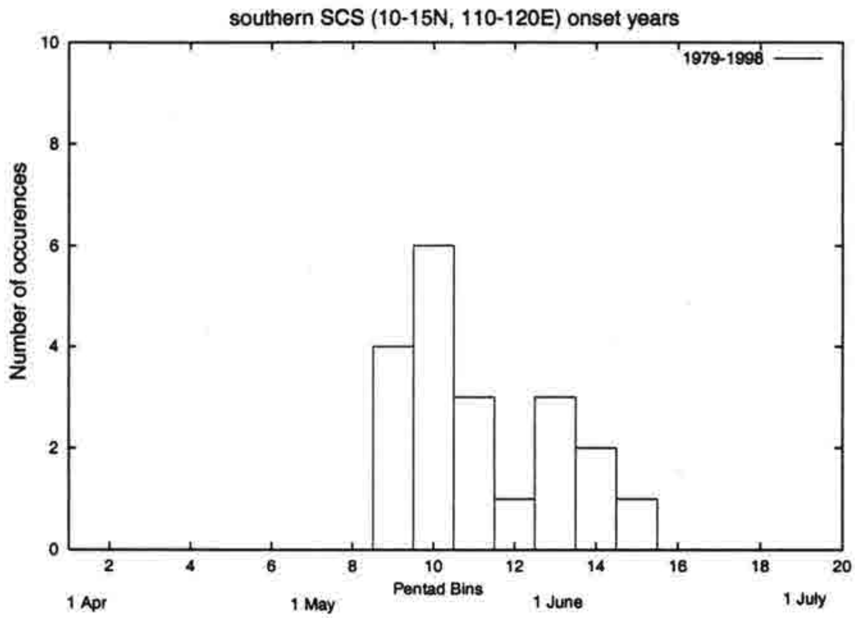

(b)

Figure 4.3: Distribution of monsoon onset dates in pentad bins for the northern SCS (a) and the southern SCS (b).

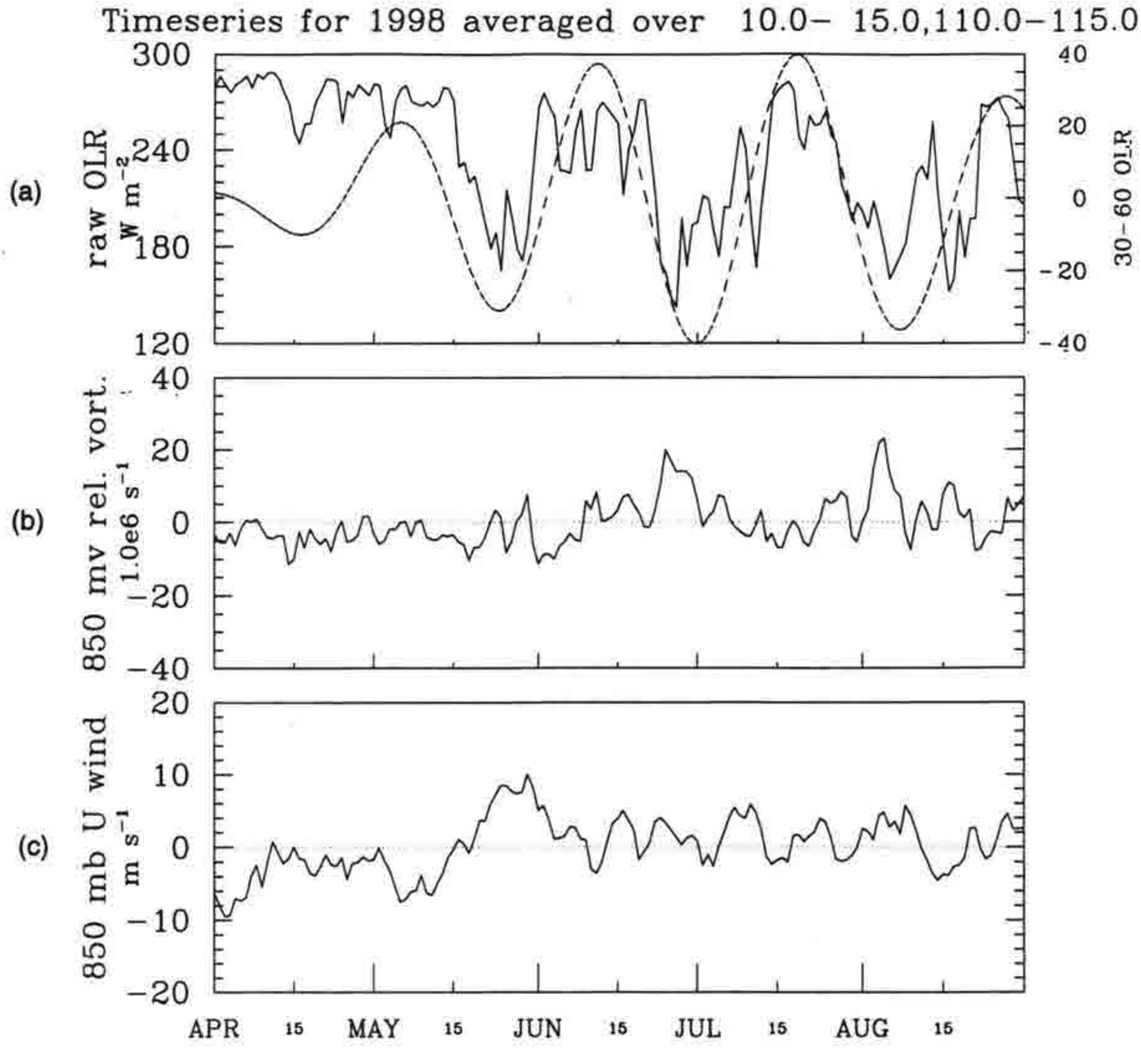

Figure 4.4: Same as in Figure 4.1 except for SW box.

in good agreement with Johnson and Ciecielski (1999) which gave 15 May (northern SCS) and 20 May (southern SCS) as the onset dates. Li and Wu (2000) gave 21 May as the onset date of the 1998 monsoon, which also agrees with this study. The timeseries shown in Fig. 4.1 and described in Section 4.1 clearly depicts the changes in OLR, 850 mb winds and vorticity associated with the onset in the northern SCS. Similar features can be seen for the southern part of the SCS (Fig. 4.4). The OLR (Fig. 4.4 a) drops rapidly below 240 W m^{-2} around 17 May. The 850 mb zonal wind (Fig. 4.4 b) shifts from easterly to westerly within the next day or two and the 850 mb vorticity (Fig. 4.4 c) switches from negative to positive shortly thereafter, around 22 May. In comparing the timeseries for the NE box and the SW box, one can see that all of these changes from a pre-onset to post-onset regime occur slightly later in the SW box than the NE box. The lag of the onset in the southern SCS is subtle, but it supports the idea that the onset time generally varies between the northern and southern SCS, even if only by a few days. Notice also that the zonal wind shift and the commencement of convection occur at roughly the same time while the change in vorticity clearly lags by several days. This is the case in both the NE box and the SW box.

4.2.2 Circulation with onset

Once the onset date is determined it is important to understand what is happening in the SCS region around the time of onset. The circulation in and around the SCS during the onset appears to be fairly typical of most monsoon onsets. The zonal wind at 850 mb averaged from 10–20° N switches from easterly to westerly just after 16 May (Fig. 4.5a) over the SCS (110–120° E). This shift happens slightly earlier west of the SCS (90–100° E). After the initial shift, the low-level zonal winds remain westerly and strengthen over the SCS area around 20 May with the onset of the monsoon. At 200 mb (Fig. 4.5b), an opposite shift over the SCS (from westerlies to easterlies) occurs about 20 May as well. Notice the zonal wind shift in both the upper and lower troposphere is earliest to the west of the SCS, and progresses eastward with time. This is inconsistent with the general notion of later onset dates shifting from southeast to northwest (Chapter 2). Recent studies (e.g., Wu and Zhang 1998) suggest a revision to this concept with earliest onset occurring over the Bay of Bengal. The upper-level winds north of 20° N are predominantly westerly. There is no distinct shift from westerlies to easterlies as in the lower latitudes. The westerlies set up a basic state which is favorable for influence on the SCS from midlatitudes.

Cross-equatorial flow is also a significant component of the monsoon onset. Variations in strength of the low-level cross-equatorial flow near 105° E have a close connection with the circulation features of the monsoon. Additionally, upper-level cross-equatorial flow is

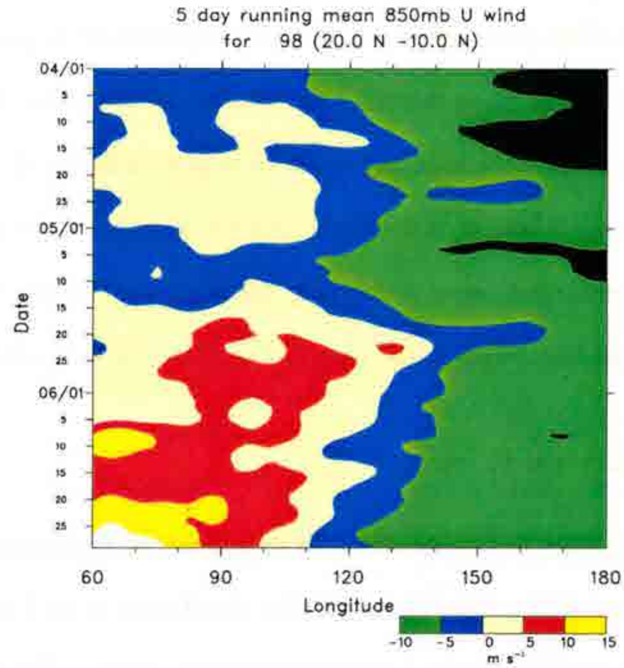

(a)

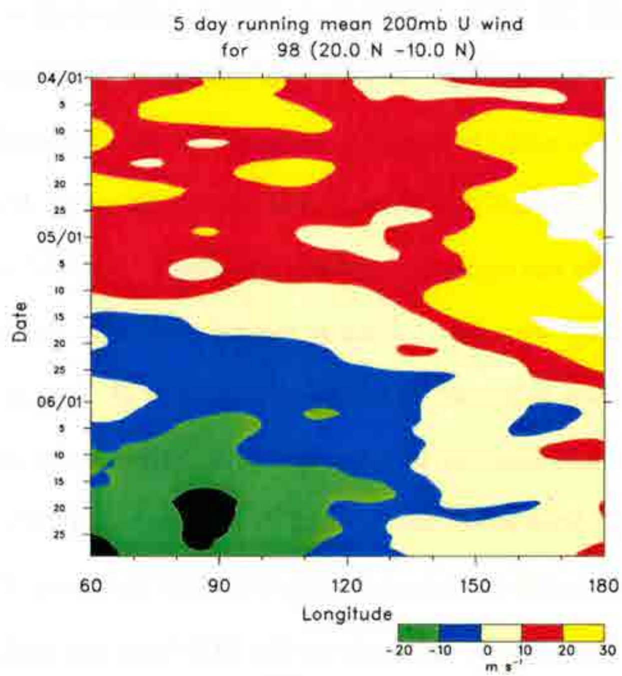

(b)

Figure 4.5: Hovmöller diagram of 850 mb zonal wind (a) and 200 mb zonal wind (b) averaged over the 10–20° N latitude band.

indicative of an active monsoon trough in the SCS (Tao and Chen 1987). However, Xie et al. (1998) argue that the cross-equatorial flow around 105° does not have a large impact on the timing of the SEAM onset. Nonetheless, at 850 mb, averaged between 12.5° N – 2.5° S, there was enhanced southerly flow around 105° E beginning about 20 May and continuing through the end of the month (Fig. 4.6a). Prior to that, the meridional winds were fairly weak throughout the equatorial Asian region. The one exception was a strong southerly flow around 90° E which persisted from about 13 May – 20 May. This is likely associated with a tropical cyclone that moved through the Bay of Bengal (BOB) and into the Indochina peninsula prior to the SEAM onset. At 200 mb, the cross-equatorial flow is primarily northerly throughout the SEAM region from around 10 May through the end of June (Fig. 4.6 b). There are periods of enhanced northerlies which move westward through the SCS area. One such band moved through just prior to the monsoon onset (approximately 17 May). These enhanced northerlies may be associated with periodic strengthening of the ITCZ which may have helped trigger the onset of the monsoon.

4.2.3 Convection with onset

The abrupt initiation of convection which is associated with the monsoon onset can be clearly seen in the OLR field averaged between 10–20° N (Fig. 4.7). The earliest convection starts around 10 May and is in confined areas over the BOB and Indochina peninsula. Convection becomes stronger and more widespread later on, closer to 17 May. Figure 4.7 also shows the evolution of the wind field and the slight delay between the initial outbreak of convection and the shift of the winds from southeasterly to southwesterly and westerly over the SCS. This delay can also be seen in the timeseries plots in Figs. 4.1 and 4.4. The earliest convection around the BOB is the strongest, and appears to be moving slightly eastward while later convection (around 20 May) is slightly weaker and appears to originate east of the SCS (around 130° E) and move slightly westward. Both the eastward and westward components of convection appear to be important in the SEAM onset. This point will be

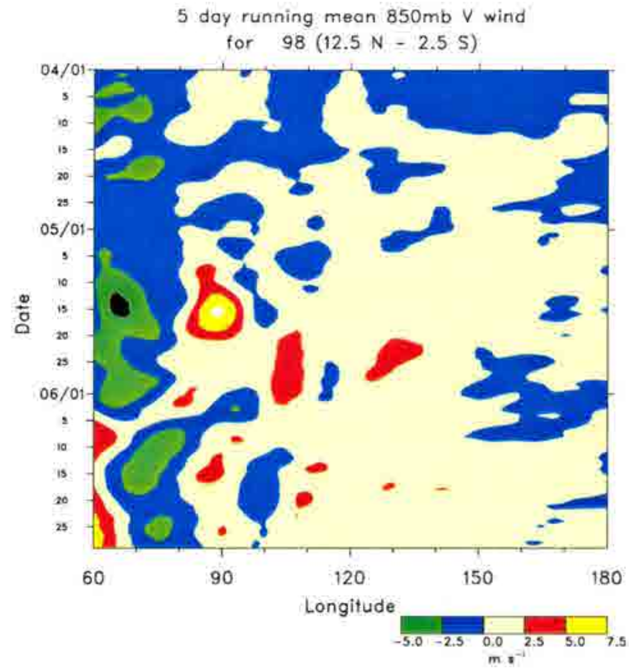

(a)

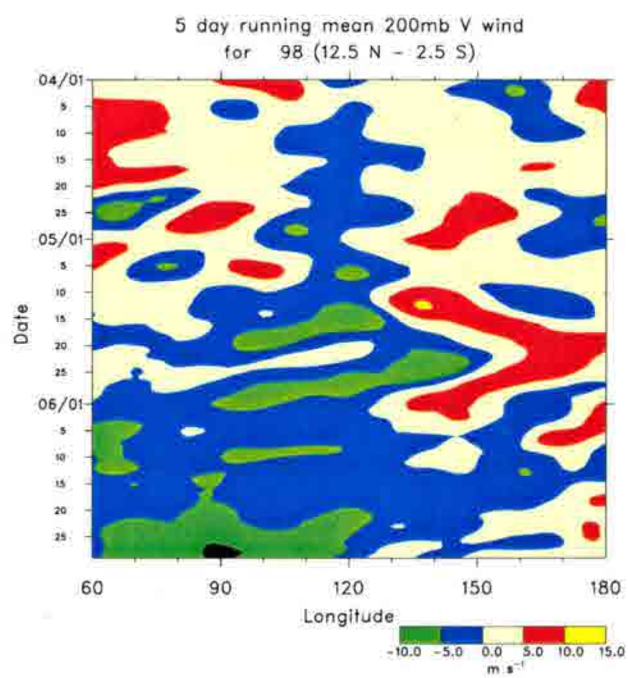

(b)

Figure 4.6: Hovmöller diagram of 850 mb meridional wind (a) and 200 mb zonal wind (b) averaged over the 12.5° N – 2.5° S latitude band.

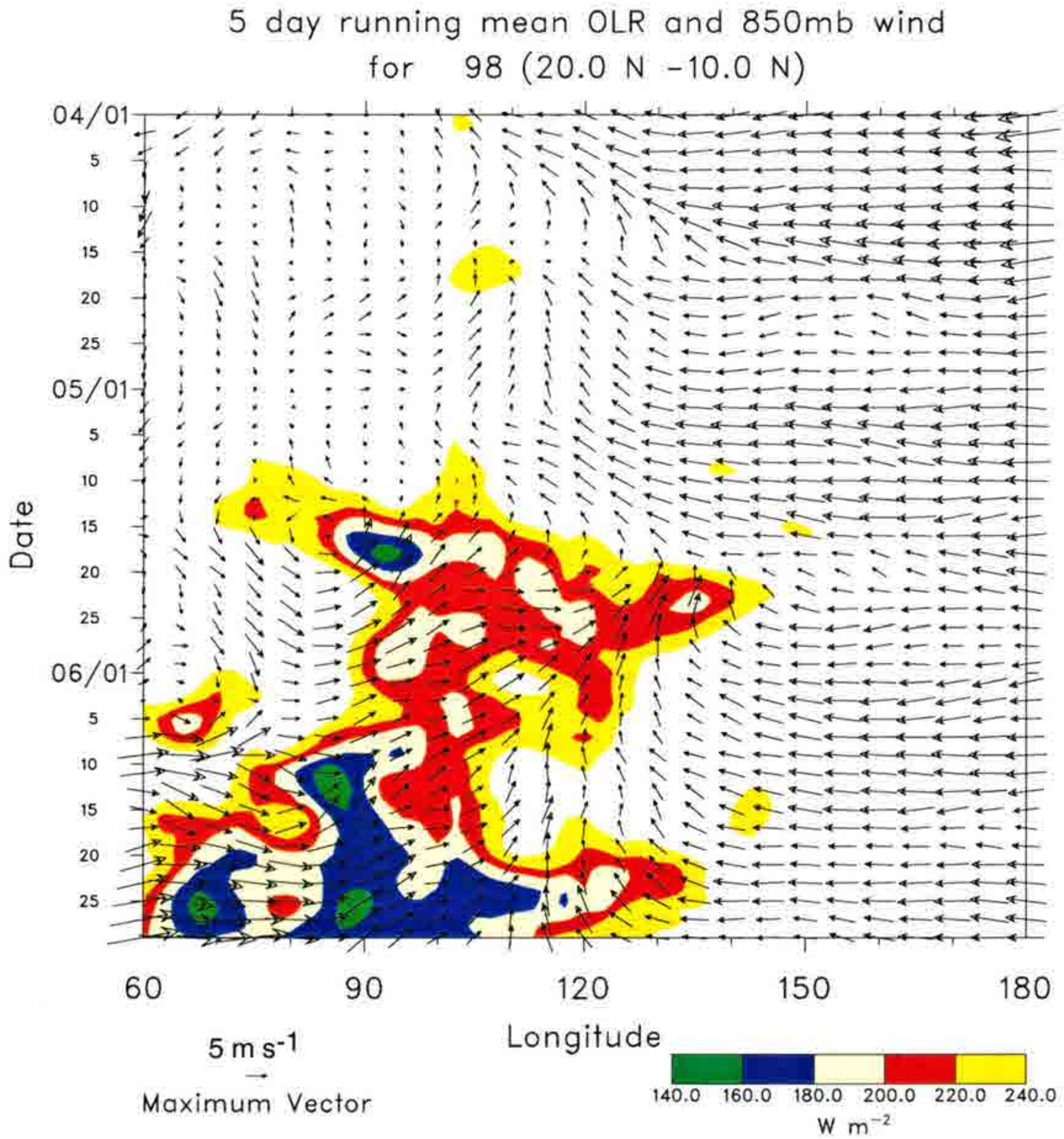

Figure 4.7: 5 day running mean OLR (solid) and 850 mb wind (vectors) averaged between 10–20° N for 1998.

elaborated in the next section.

Expanding the view of convection to a larger domain (Fig. 4.8) provides an even better picture of the convection and circulations surrounding the SEAM onset. Throughout the pre-monsoon period several midlatitude systems move eastward north of 30° N. On 14 May (Fig. 4.8 a) the monsoon trough (or ITCZ) can clearly be seen along the equator, and a tropical cyclone is positioned off the southern tip of India. The western Pacific subtropical high (WPSH) is located around 20° N, 140° E with a band of convection on its northern edge. By 17 May (Fig. 4.8 b), the WPSH has retreated to just northeast of 30° N, 150° E. Winds over the SCS have shifted from southeasterly to southerly with the movement of the WPSH. The tropical cyclone has moved eastward and is impinging on the Indochina peninsula. This tropical cyclone is the reason for the early, strong convection in the BOB and Indochina prior to the SCS monsoon onset. The ITCZ stays put along the equator with its convection shifting slightly eastward. A midlatitude front-type system has situated itself off the southern coast of mainland China. Convection stretches from Indochina northeast to Japan and is present only in the northern SCS at this point. This front is responsible for the earliest, slightly eastward moving convection over the SCS as seen in Fig. 4.7. By 20 May (Fig. 4.8 c), convection has moved southward and strengthened over the SCS. Winds are now westerly in the northern SCS and southwesterly in the southern SCS. The tropical cyclone has stalled over Indochina and the ITCZ has weakened. On 23 May (Fig. 4.8 d), convection is fairly widespread stretching from the southern SCS across the Philippines and into the western Pacific. Winds over the whole SCS are westerly. The tropical cyclone has weakened and another midlatitude disturbance is over mainland China.

The unfiltered OLR and winds show typical features of the SEAM (e.g., WPSH, ITCZ) and they provide a big-picture view of what is happening during the onset. The mid-latidude influence is prominent during the SEAM onset. However, the unfiltered fields cannot clearly show what is happening on the intraseasonal timescale.

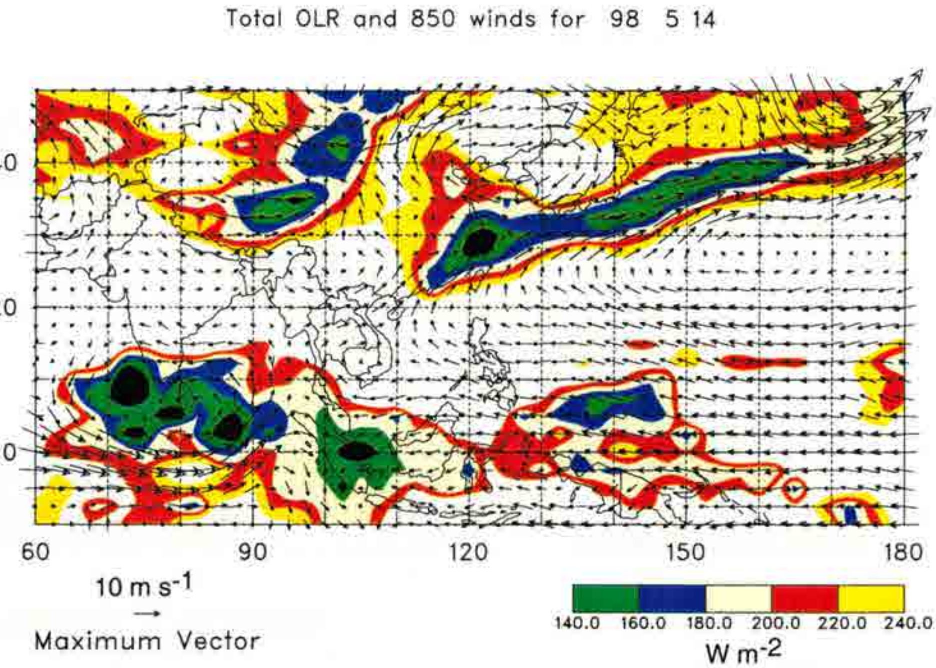

(a)

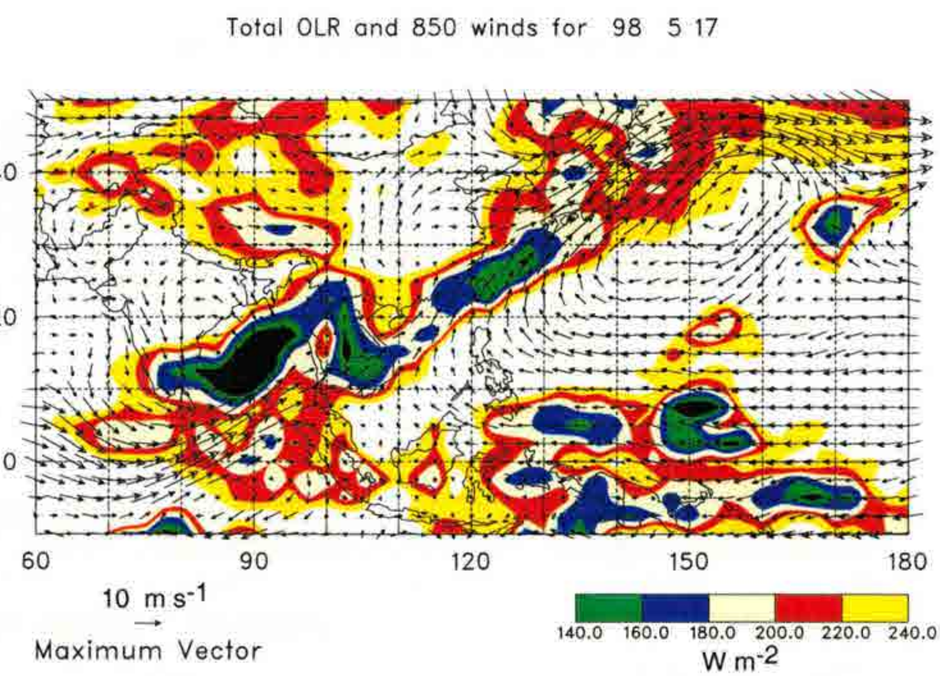

(b)

Figure 4.8: Total (unfiltered) OLR and 850 mb winds for May 14 (a), May 17 (b), May 20 (c) and May 23 (d) over the Asian monsoon region during the 1998 monsoon.

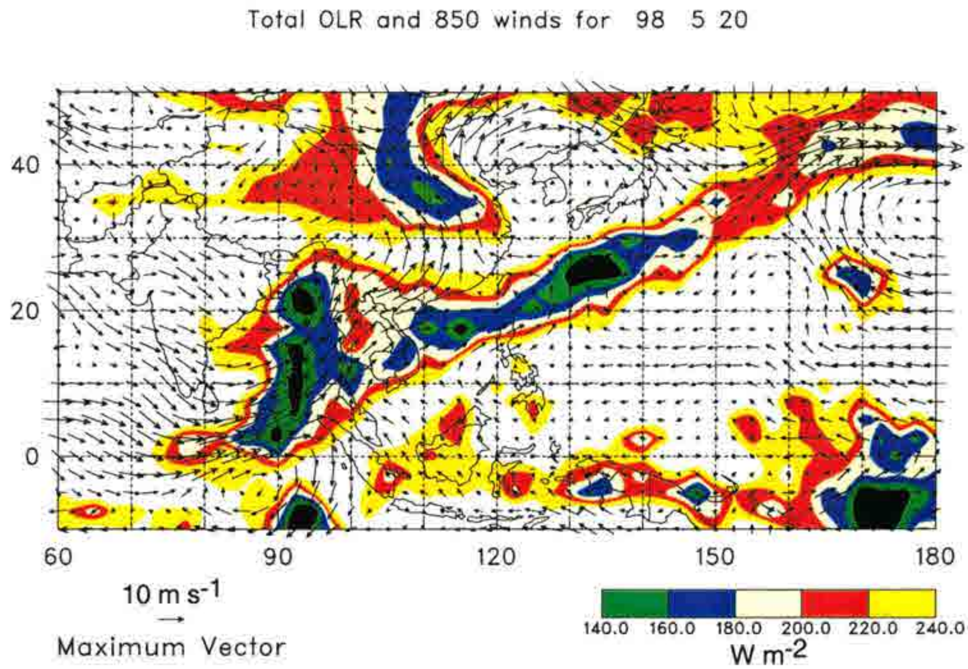

(c)

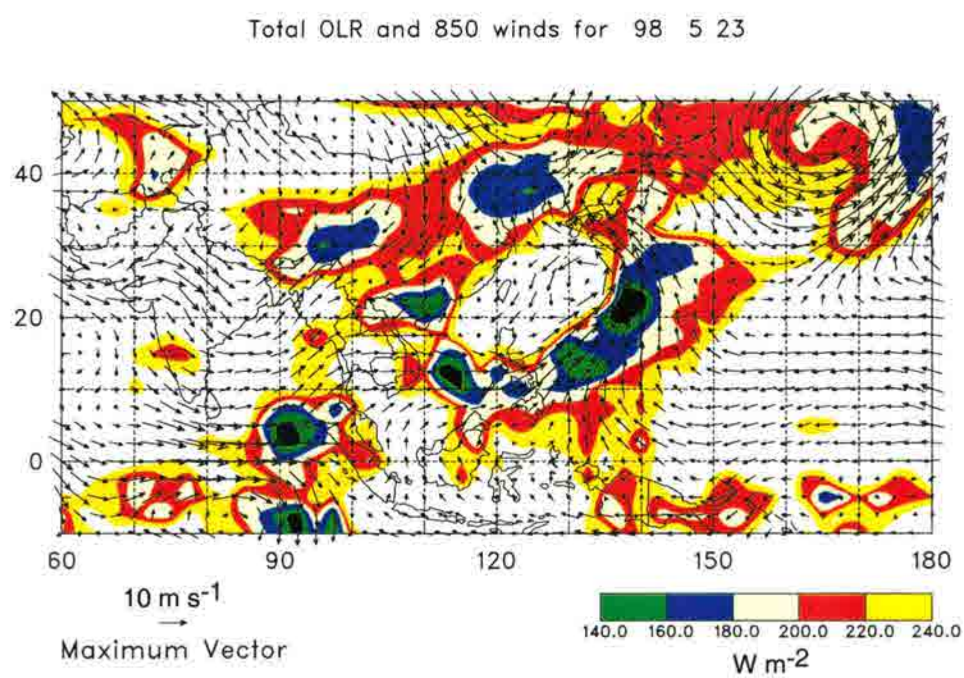

(d)

Figure 4.8: *continued*

4.3 Intraseasonal Oscillations

In past studies on the SEAM, a common question that keeps surfacing is: what role do intraseasonal oscillations play in the SEAM onset? The following analysis will establish that the 12–24 and 30–60 day modes actually play a part in the onset of the SEAM.

4.3.1 Intraseasonal oscillations during the 1998 monsoon

The total-field analysis described in the previous section is useful, but it only provides part of the picture. Every disturbance that is seen in the OLR or wind field is actually an aggregate of disturbances with many different frequencies. Spectral analysis (described in chapter 3) of the OLR is a way convective disturbances can be viewed to determine which periods of oscillation are dominant. Spectra can vary considerably between data points, even when they are close to one another. Because of this, the spectra for many points over a given area need to be taken into consideration when determining which are the dominant periods of oscillation. A sampling of spectra for four points in the SCS are shown in Fig. 4.9. Each of the spectra show a different structure, so to draw conclusions from just one of these gridpoints individually may be misleading. Fig. 4.9a shows a statistically significant peak with a period of 12–24 days, while the peak at 30–60 days is less prominent. The opposite is true in Fig. 4.9b. A peak in the 30–60 day range is clear as is a peak centered on 10 days. The spectra at 17.5° N, 115° E (Fig. 4.9c) has large peaks in both the 12–24 and 30–60 day periods, while the spectra in Fig. 4.9d shows a very significant peak near 10 days and a slightly significant peak at 12–24 days. The 30–60 day oscillation is very weak for this gridpoint. In looking at the OLR spectra over all the points in the SCS, the prominent modes are in the 12–24 day and 30–60 day periods, as discovered in many previous studies (e.g., Chen and Chen 1995).

To isolate these two modes from the total OLR and wind fields, the data were band-pass filtered. Since analysis at the individual gridpoints can vary, the standard deviations of the filtered OLR were calculated for May-June 1998 to get an idea of where the maximum

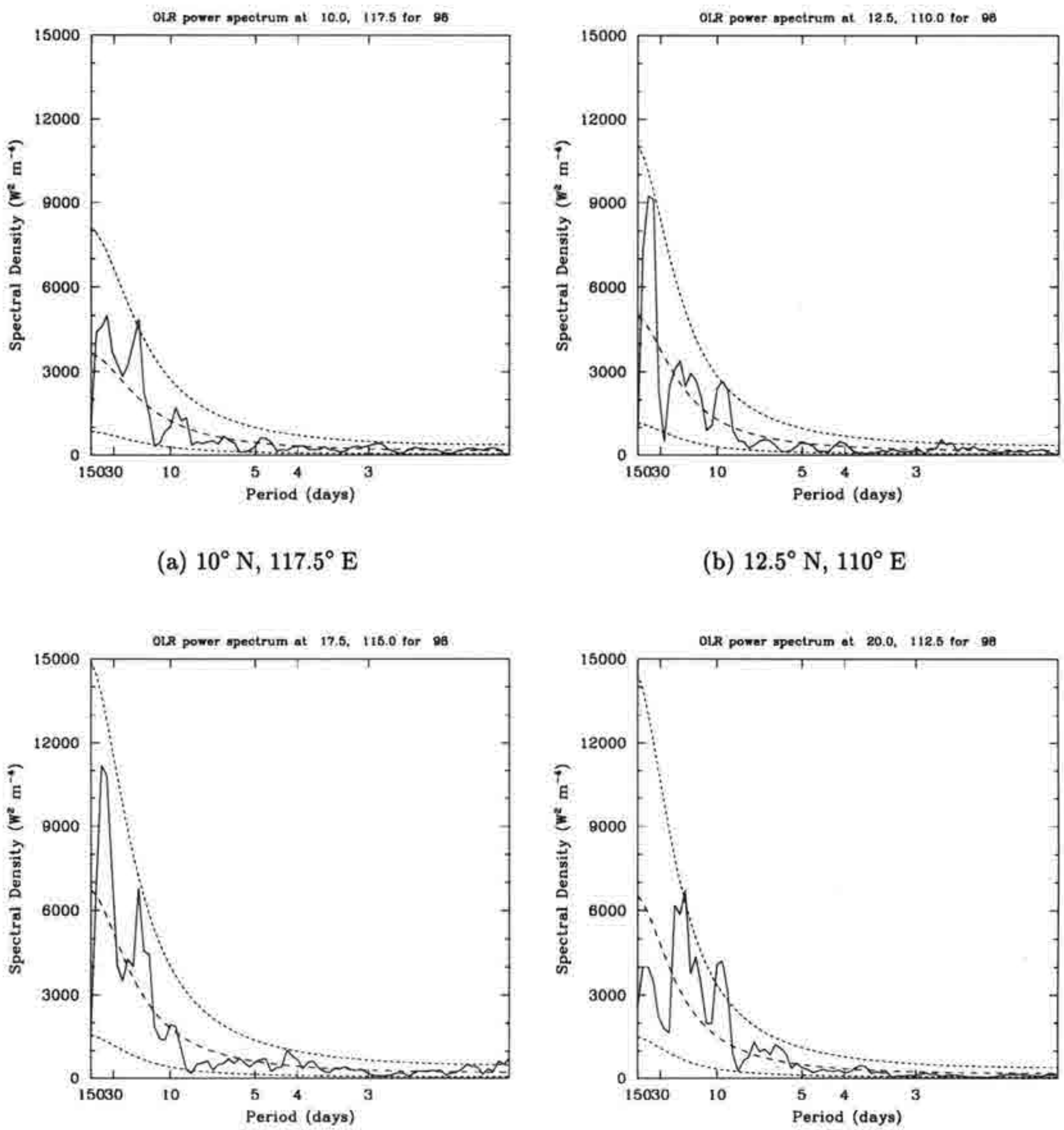

(a) 10° N, 117.5° E

(b) 12.5° N, 110° E

(c) 17.5° N, 115° E

(d) 20° N, 112.5° E

Figure 4.9: Spectral densities of OLR at points in the SCS for 1998. Lines are the same as Fig. 3.2

variability of OLR over the SCS was during the 1998 monsoon onset (Fig. 4.10). The 12–24 day mode shows three centers of maximum variability. One is in the northern SCS along 20° N, stretching from near 115° E into the west Pacific. Another maximum exists in the Indian Ocean between 70–80° E and 15° N to the equator. The third area is centered along the equator from 135–170° E. The 30–60 day mode has a swath of high variability between 10–20° N stretching from 80–140° E. There are centers of maximum variability in the Bay of Bengal (BOB) and the SCS. This area of variability coincides with the track of the MJO during the Northern Hemisphere summer (Wang and Rui 1990). The same calculations were made for the entire 1998 monsoon period from May-August (not shown). The areas of variability for May-August are very similar to those for just May-June.

With the SCS being a center of maximum variability in both the 12–24 day mode and 30–60 day mode during May and June, it is to be expected that these modes would be prominent features in the SCS during the monsoon onset. Such is the case during the 1998 monsoon. Figure 4.11 shows the evolution of the 12–24 day filtered OLR and 850 mb winds at 3 day intervals from 14 May to 23 May. On 14 May (Fig. 4.11a), there is a band of negative OLR anomalies (convection) which originated near Japan a few days prior situated from southwest to northeast. It stretches from just north of the SCS to Japan. This convection resides on the northwest edge of a similarly oriented anticyclone. Positive OLR anomalies are located on the southeast side of the anticyclone. There is a strong area of convection associated with a tropical cyclone located off the tip of India and a broad, weaker area of convection along the equator. The equatorial convection and the tropical cyclone both move eastward, and the tropical cyclone is located in the BOB by 17 May. The convection near the SCS has expanded, moved southwestward and strengthened so that by 17 May (Fig. 4.11b) it is influencing the northern SCS. Positive OLR anomalies remain over the southern SCS, and the anticyclonic circulation has weakened. By the onset date, 20 May (Fig. 4.11c), cyclonic circulation has become prominent over the west Pacific. The positive OLR anomalies over the southern SCS and east of the Philippines have weakened

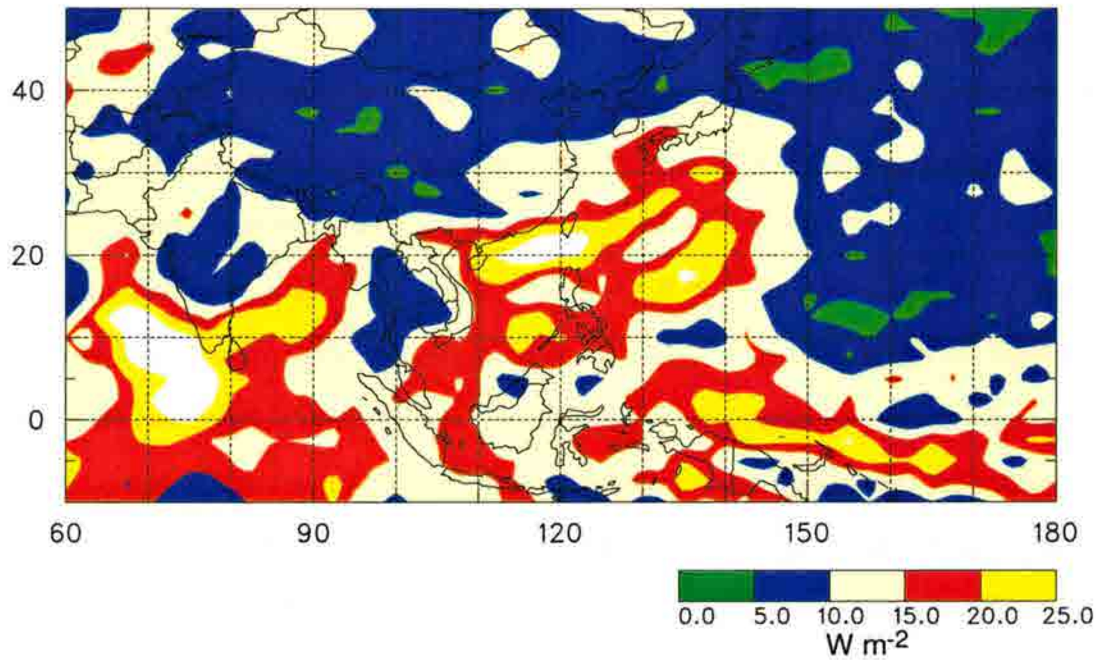

(a) 12–24 filtered OLR

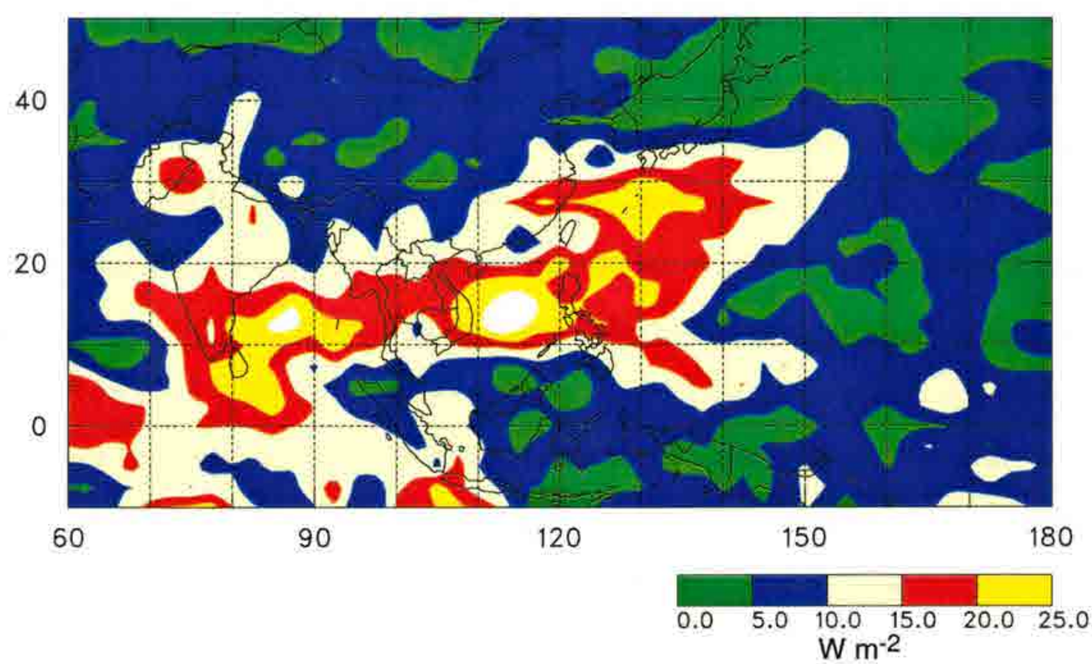

(b) 30–60 filtered OLR

Figure 4.10: Standard deviation of 12–24 day filtered OLR (a) and 30–60 day filtered OLR (b) for May-June 1998.

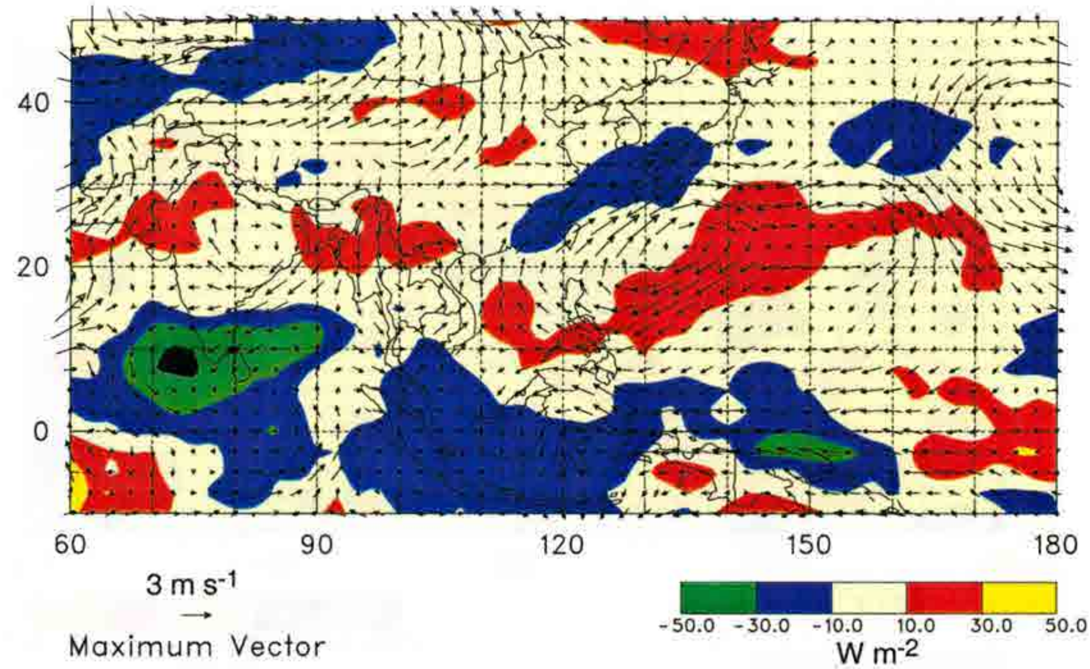

(a) 14 May 1998

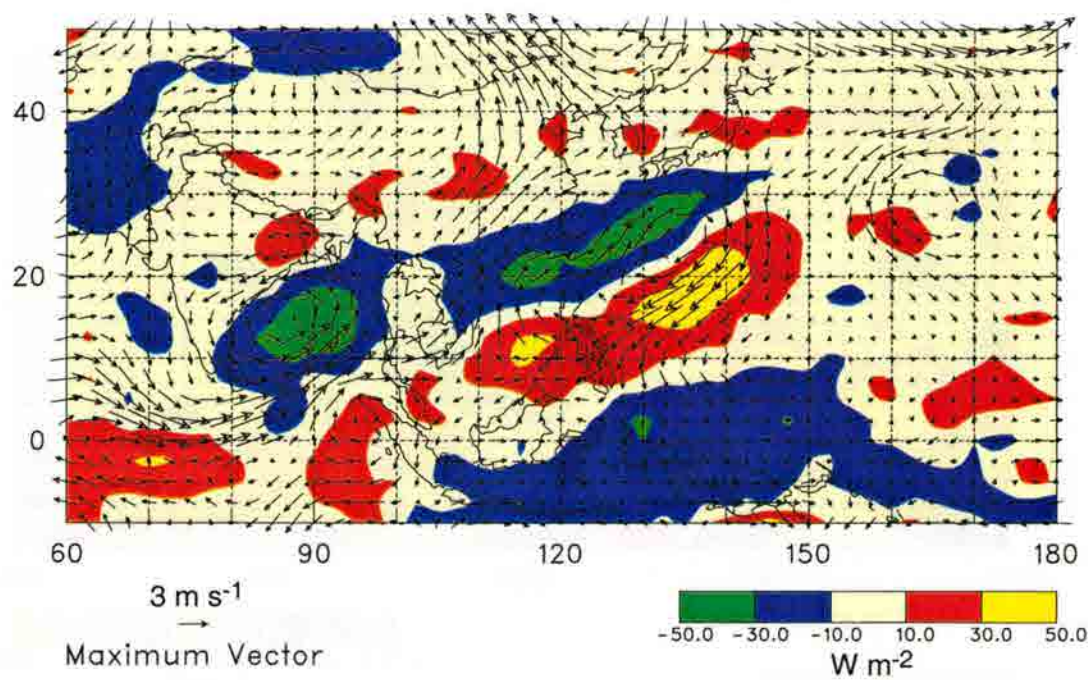

(b) 17 May 1998

Figure 4.11: 12–24 day filtered OLR and 850 mb winds for May 14 (a), May 17 (b), May 20 (c) and May 23 (d) over the Asian monsoon region during the 1998 monsoon.

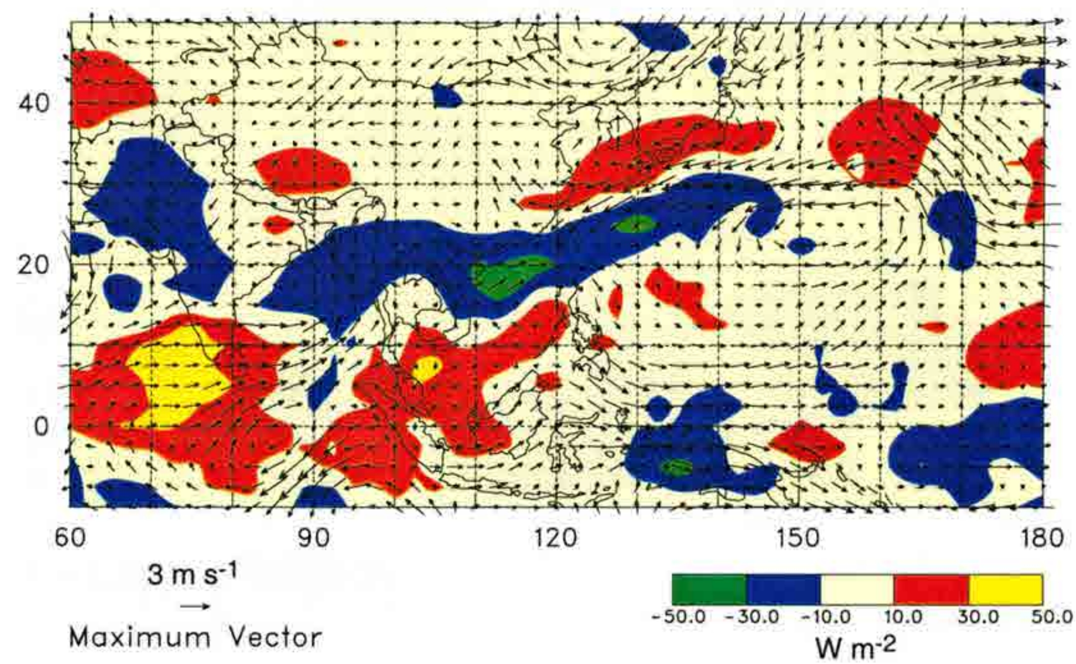

(c) 20 May 1998

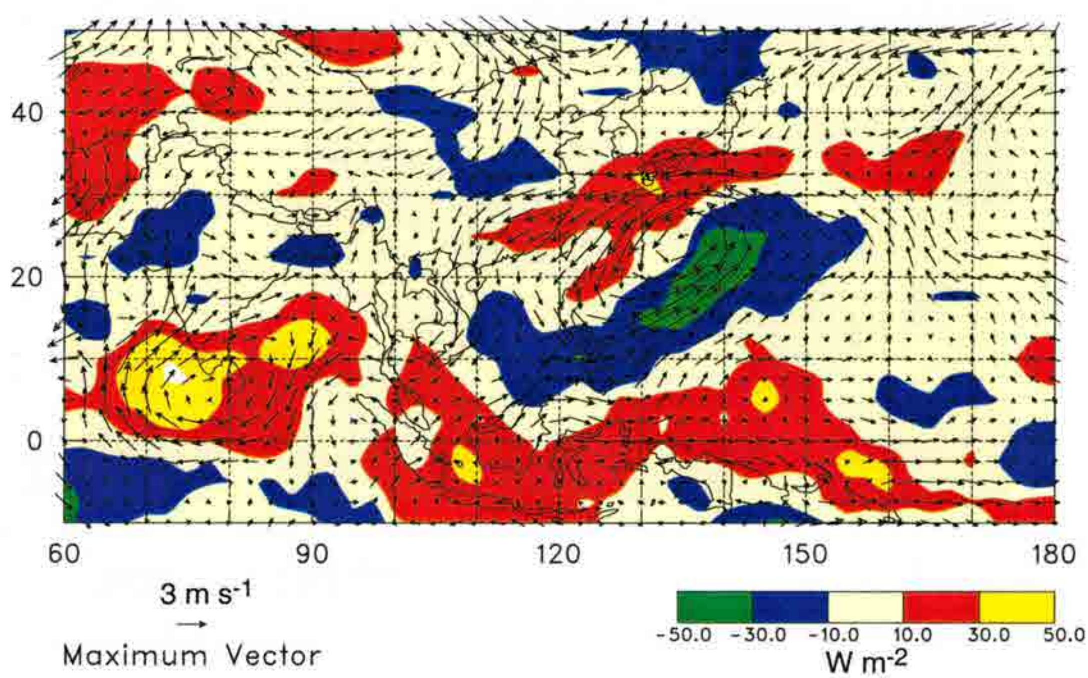

(d) 23 May 1998

Figure 4.11: *continued*

significantly as have the tropical cyclone in the BOB and the convection along the equator. The convection over the northern SCS continues to move slightly south-southwestward and positive OLR anomalies have developed near Japan in the same way as the convection did several days earlier. On 23 May (Fig. 4.11d), the OLR and wind pattern is nearly opposite of that seen on 14 May. Where there were negative OLR anomalies on 14 May, there are now positive anomalies. Anticyclonic circulation has been replaced by cyclonic circulation. This evolution of the 12–24 day mode shows its main influence on the 1998 SEAM monsoon onset came from convection which originated near Japan and propagated south-southwest into the northern SCS during the time of onset but there is a secondary contribution from convection propagating eastward from the BOB.

A similar evolution for 12-24 day filtered OLR and 200 mb flows is shown in Figure 4.12. An obvious relationship exists between the convection and upper level circulation on this timescale. In general, the negative OLR anomalies occur ahead of the upper level troughs, and positive OLR anomalies occur ahead of upper level ridges. On 14 May (Fig. 4.12a) a closed cyclonic circulation is located to the east of the southwest to northeast oriented band of convection which developed near Japan. By 17 May (Fig. 4.12b), the upper level trough has moved eastward and has taken on a southwest to northeast tilt similar to that of the band of negative OLR anomalies. Anticyclonic circulation is present over the SCS on the southern edge of the negative OLR anomalies and north of a band of positive OLR anomalies. The negative OLR is clearly located in a region of upper level divergence. The upper level trough continues to move east as the negative OLR anomalies begin to dissipate on 20 May (Fig. 4.12c). A ridge is present to the northeast of positive OLR anomalies which have developed near Japan. By 23 May (Fig. 4.12d) the upper level anticyclone has moved east as the positive OLR anomalies expand southwestward. Cyclonic circulation has developed over the SCS which places the positive OLR anomalies in a position of upper level convergence. This result is an example of convection forced by midlatitude circulations. Kiladis and Weickmann (1992) found similar connections between the circulation and convection for disturbances in the eastern Pacific during the boreal winter. These patterns are consistent with theory and modeling of Rossby waves in a westerly basic state extending from the midlatitudes into the tropics (Kiladis and Weickmann 1992).

An evolution of the 30–60 day mode similar to that of the 12–24 day mode is diplayed in Figure 4.13. On 14 May (Fig. 4.13a), there is a large area of convection between 70–90° E which stretches from south of the equator to 20° N. This system is propagating eastward and could first be seen in the analysis domain around 5 May. Because of its location and propagation characteristics, this system is likely an MJO event (Wang and Rui 1990). Also notable is a band of positive OLR anomalies in the northern SCS which extends northeastward into the northern west Pacific. This band retains its orientation as it moves northward and weakens. There is also a small band of convection just east of the Philippines along 10° N. The MJO convection continues eastward and by 17 May (Fig. 4.13b) it extends across the BOB and Indochina peninsula and into the extreme eastern SCS. By the onset (Fig. 4.13c), the convection has moved completely into the SCS and joined with the convection east of the Philippines (which has moved slightly northward like part of the ITCZ) to form a large band of convection across the SCS and into the west Pacific. This band of convection continues to move slowly north and east vacating the SCS area in June.

Though the direction of influence on the SCS was different for the 30–60 day mode than that of the 12–24 day mode, it also clearly had an impact on the onset of the SEAM. Convection in both modes propagated into the SCS around the same time as the onset of the monsoon. This can be seen more clearly from a hovmöller diagram of the filtered negative OLR anomalies (Fig. 4.14). The 30–60 day mode (blue dashed lines) moved eastward into the SCS area and was present at the same time as the westward moving 12–24 day mode (red, solid lines). It is also interesting to note from Fig. 4.14 that the onset is concurrent with the first major 30–60 day oscillation of the year in this latitude band. The onset of the SEAM marks a transition from a winter to summer regime. The track of the MJO during

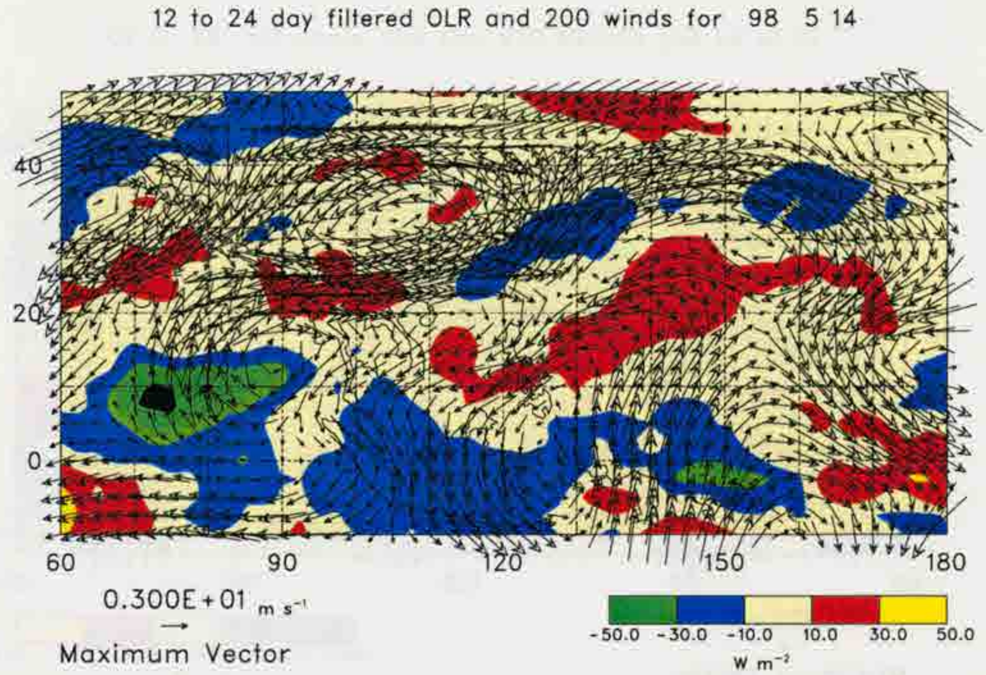

(a) 14 May 1998

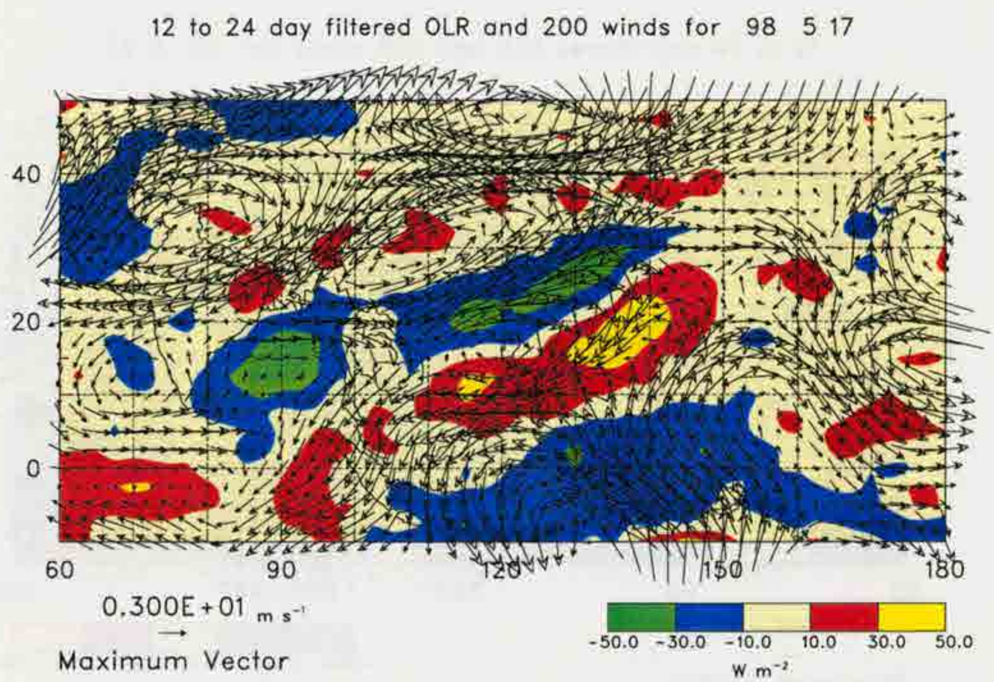

(b) 17 May 1998

Figure 4.12: 12–24 day filtered OLR and 200 mb winds for May 14 (a), May 17 (b), May 20 (c) and May 23 (d) over the Asian monsoon region during the 1998 monsoon.

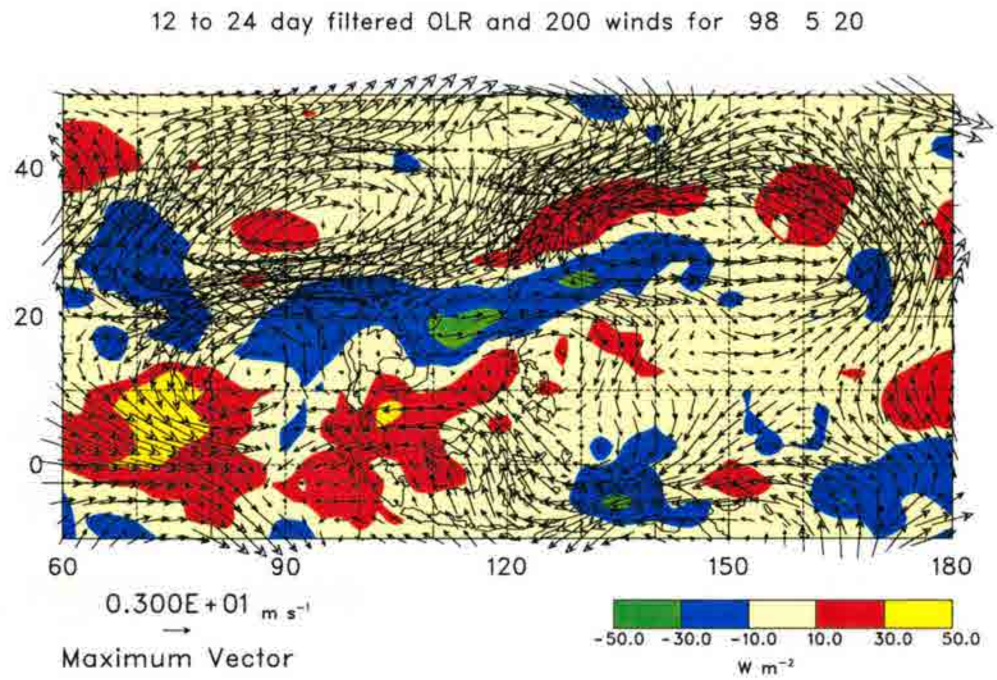

(c) 20 May 1998

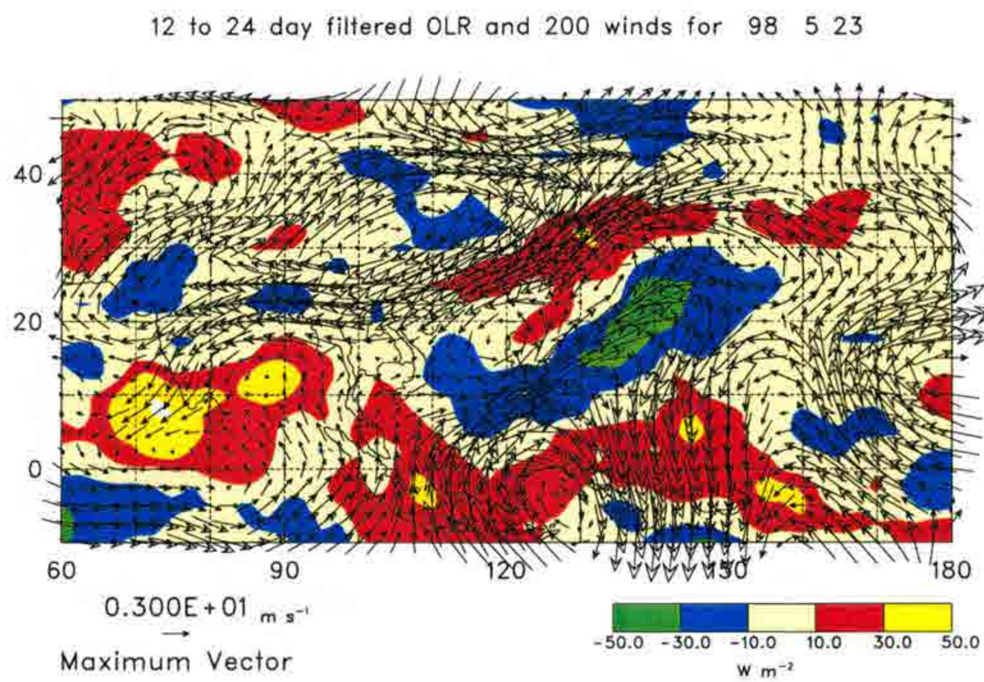

(d) 23 May 1998

Figure 4.12: *continued*

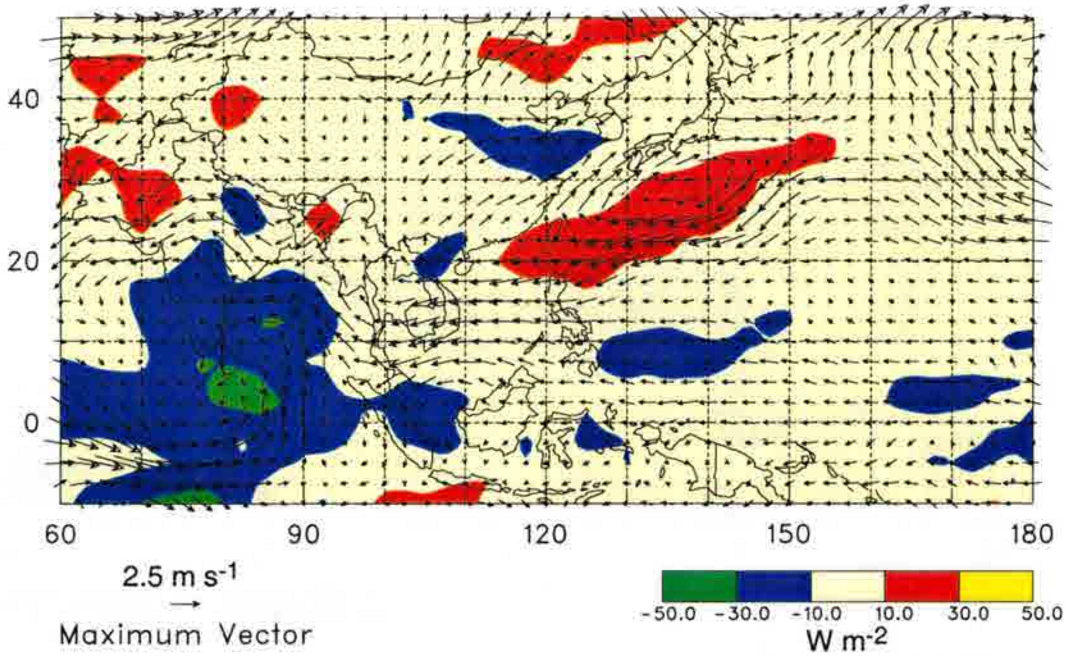

(a) 14 May 1998

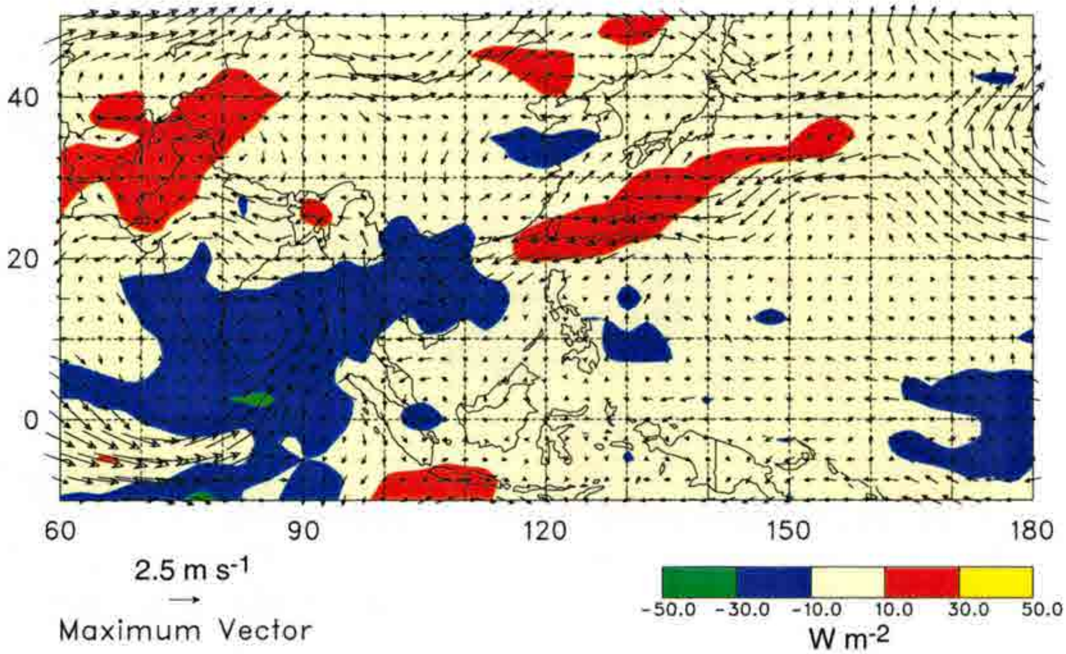

(b) 17 May 1998

Figure 4.13: 30–60 day filtered OLR and 850 mb winds for May 14 (a), May 17 (b), May 20 (c) and May 23 (d) over the Asian monsoon region during the 1998 monsoon.

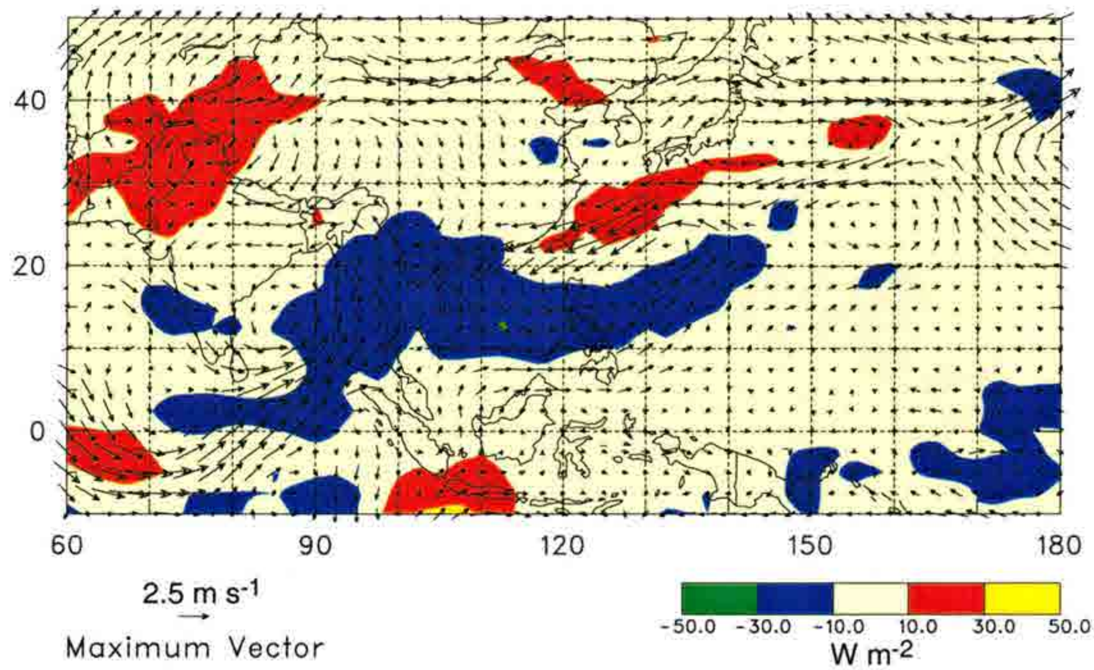

(c) 20 May 1998

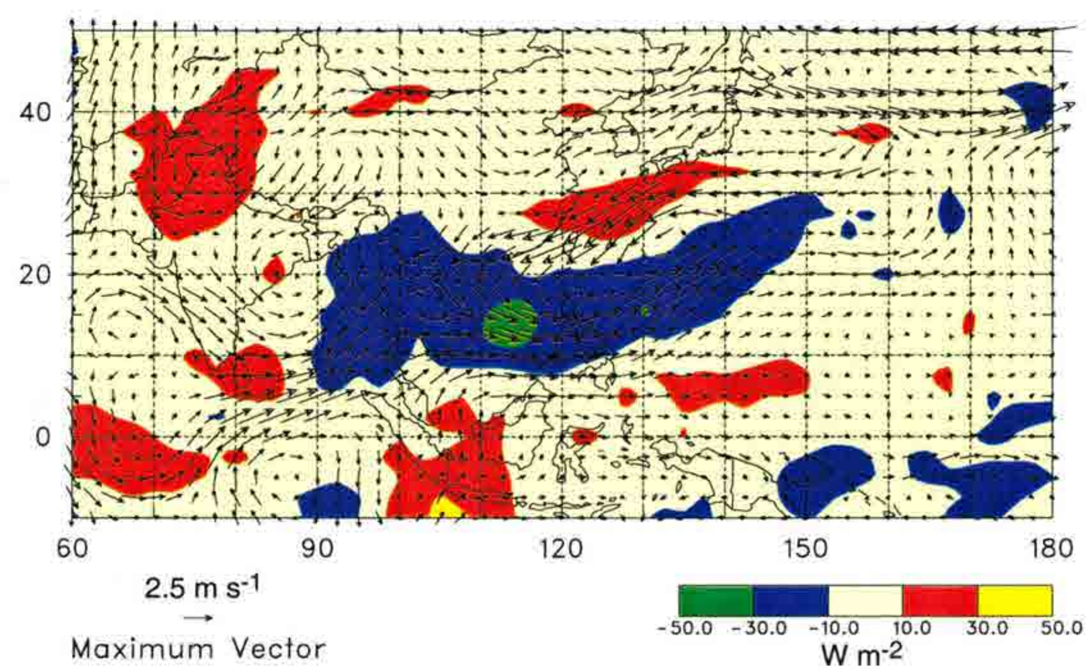

(d) 23 May 1998

Figure 4.13: *continued*

the winter lies primarily in the Southern Hemisphere and moves northward as the seasons progress where it makes it as far north as the 10–20° N latitude band during the summer. Thus it appears like the first summer MJO may be partly responsible for the triggering of the SEAM onset.

The latitude/longitude plots of the filtered OLR (Figs. 4.11 and 4.13) showed that the northern SCS was affected a bit earlier and influenced more by the 12–24 day mode while the southern SCS was impacted a few days later by the 30–60 day mode. This could be the reason for the slightly different onset dates in the northern and southern SCS. It is not clear at this point whether these modes act independently and happen to both be present during the onset or whether there is some phase-locking (e.g., Chen and Chen 1995) or modulation of one mode by the other required to trigger the onset. This question will be addressed further in section 4.3.3.

4.3.2 Twenty years of intraseasonal oscillations

The 30–60 day and 12–24 day intraseasonal oscillations both played a role in the onset of the 1998 SEAM. However, one cannot make definitive conclusions about the SEAM onset in general from looking at just one year. Analyses such as that shown in Fig. 4.11 and 4.13 were done for every year from 1979–1998 to get a better idea of how the monsoon onset is affected by the 12–24 and 30–60 day modes (individual years not shown). This analysis supports the hypothesis that these intraseasonal oscillations play a role in the onset. For a majority of the 20 years, these modes produced a noticeable signal in the SCS at the time of onset. However, there was some interannual variability in these modes, as there is in the onset of the monsoon itself. That issue will be discussed in section 4.4. Before the interannual variability can be addressed, generalizations of the relationship between the intraseasonal oscillations and the monsoon onset for the entire 20 year period should be made. This is done through the regression analysis described in Section 3.2.3.

One way to help understand what is happening during the monsoon onset is to

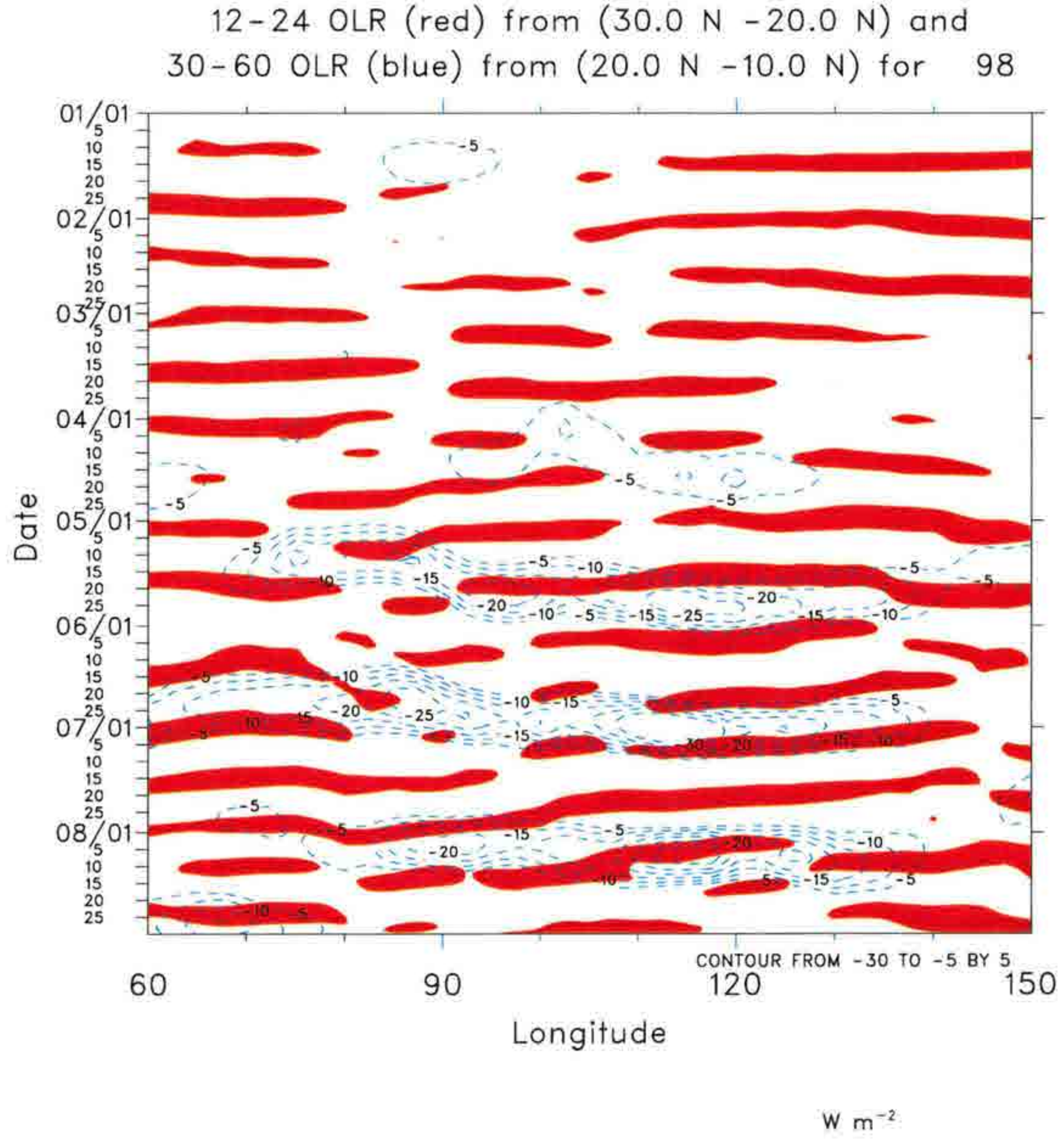

Figure 4.14: Hovmöller diagram of negative 12–24 day filtered OLR anomalies (red, solid) averaged between 20–30° N and negative 30–60 day filtered OLR anomalies (blue, dashed contour) averaged between 10–20° N for Jan. - Aug. 1998.

compare the onset period, May-June (MJ), with the entire monsoon season, May-August (MJJA). Regressions for both of these periods were computed for each of the base areas shown in Fig. 3.1. The standard deviations of OLR for MJ from 1979-1998 (Fig. 4.15) support the choice of base areas for analysis. These analysis boxes encompass the areas of highest variability over the SCS during the onset. The standard deviations for MJJA (not shown) are very similar in structure and magnitude. In general, for the SW, EQ and SC analysis areas, comparisons between the MJ and MJJA regressions yielded little difference in the structure of the OLR and circulations. Though the patterns were similar, the strength of the regressions tended to be slightly different. The regressed OLR and winds tended to be stronger for MJ than MJJA. This was especially noticeable in the 200 mb regressions. This strength discrepancy may be a result of the smaller sample size for the MJ regressions. However, this also may indicate that the intraseasonal modes are stronger during the SEAM onset than they are for the entire monsoon season. Wang and Wu (1997) showed that the magnitude of intraseasonal oscillations with a period of 20–70 days is largest in May over the SCS.

Though the strength of the regressions was the main difference between the MJ and MJJA regressions for most of the analysis boxes, the NE box showed both strength and structural differences between MJ and MJJA. Regressions of the other base areas did not show significant structural differences between MJ and MJJA. Figure 4.16 shows the MJ regression for the 12–24 day mode at 6 different lags. Figure 4.17 shows the MJJA regression for the same mode at the same lags. The most noticeable difference between these two 12–24 day regressions lies in the origin of the OLR anomalies. For the onset period, convection develops at lag -4 (Fig. 4.16a) around 25° N, 130° E in the middle of cyclonic circulation. As can be seen from subsequent lags, the convection and the cyclonic circulation propagate southwestward into the SCS. The area in which the convection originated and the direction it propagated is very similar to that seen for the 1998 monsoon (Fig. 4.11). By lag 0 (Fig. 4.16c), the entire SCS is dominated by negative OLR anomalies and cyclonic circulation.

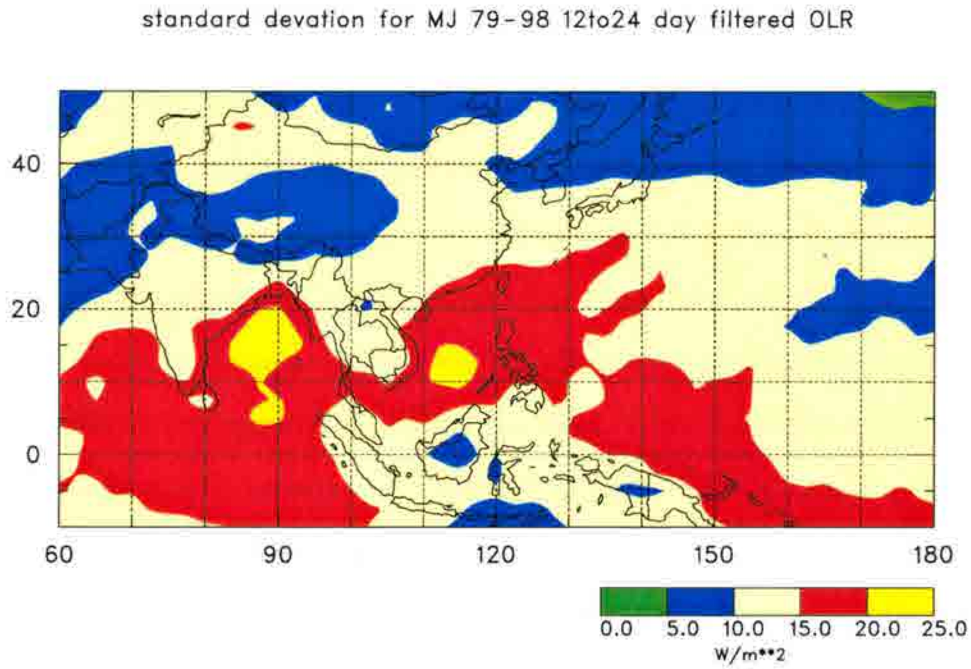

(a) 12–24 filtered OLR

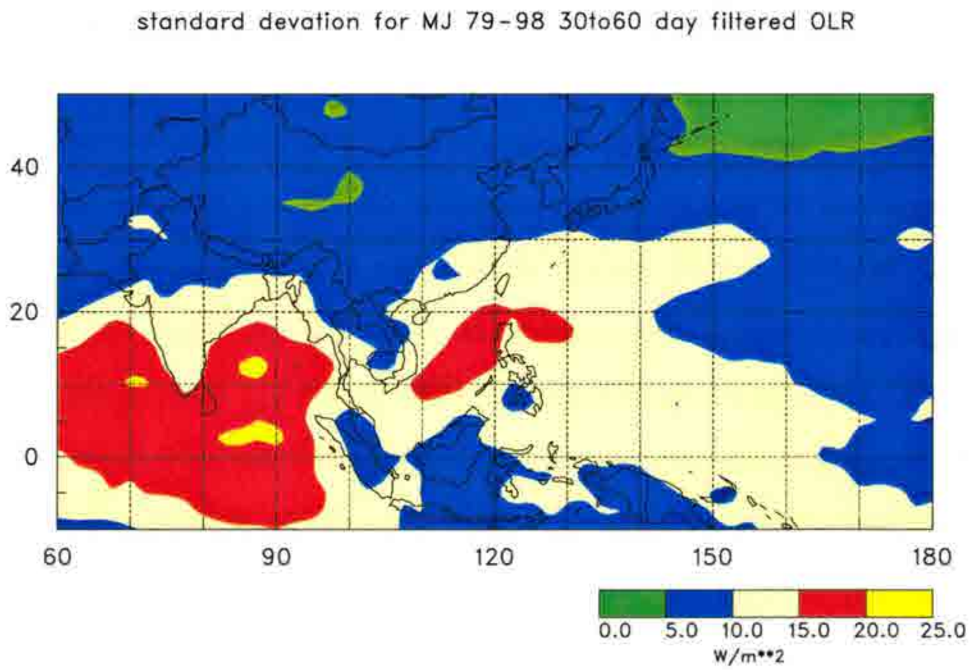

(b) 30–60 filtered OLR

Figure 4.15: Standard deviation of 12–24 day filtered OLR (a) and 30–60 day filtered OLR (b) for May-June 1979–1998.

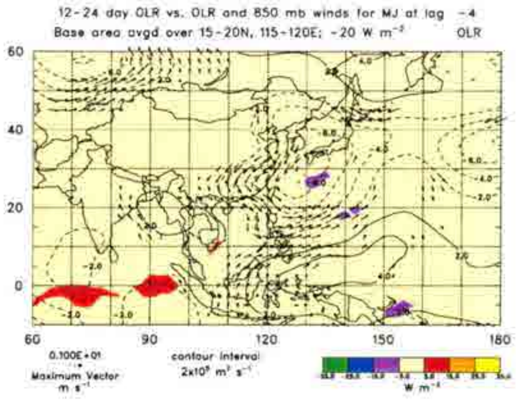

(a) lag -4

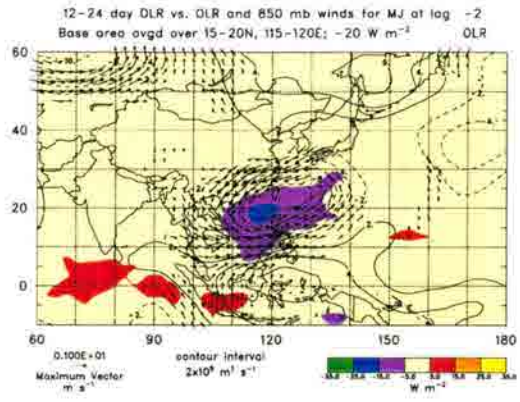

(b) lag -2

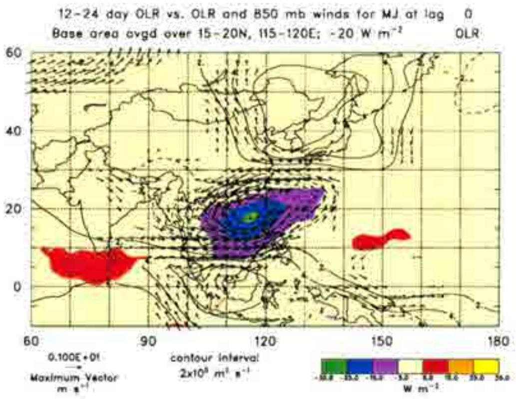

(c) lag 0

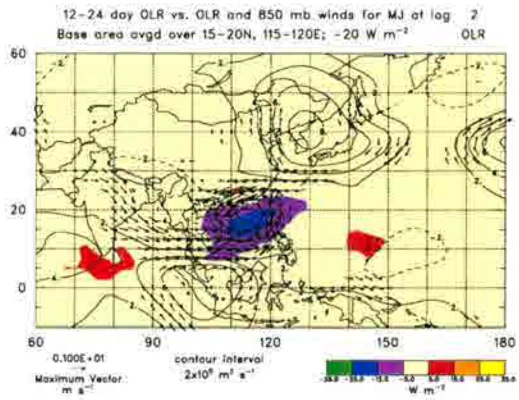

(d) lag 2

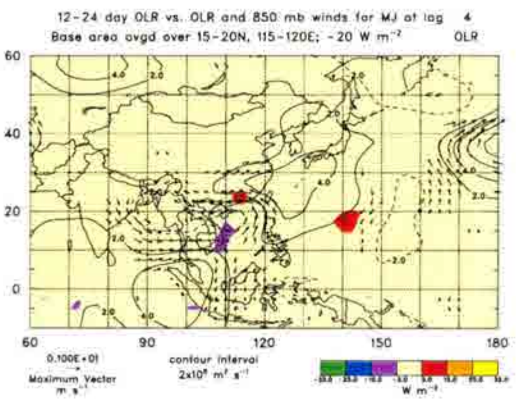

(e) lag 4

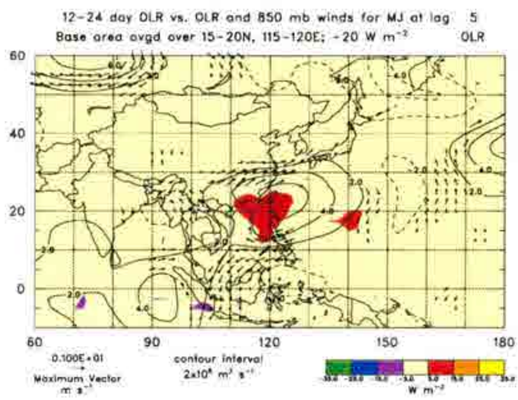

(f) lag 5

Figure 4.16: 12 to 24 day filtered OLR regressed against OLR (solid), 850 mb wind (vectors) and 850 mb streamfunction (contoured) for MJ in the NE base area. Only OLR and wind vectors which are statistically significant at 95% are plotted.

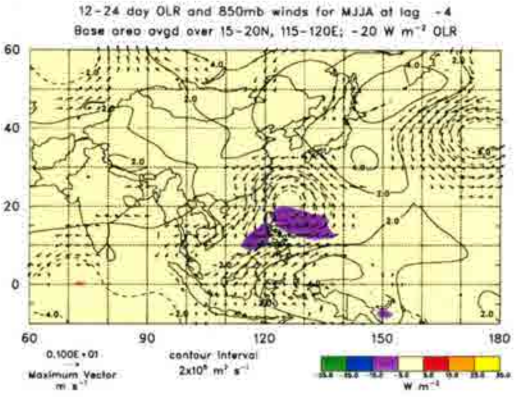

(a) lag -4

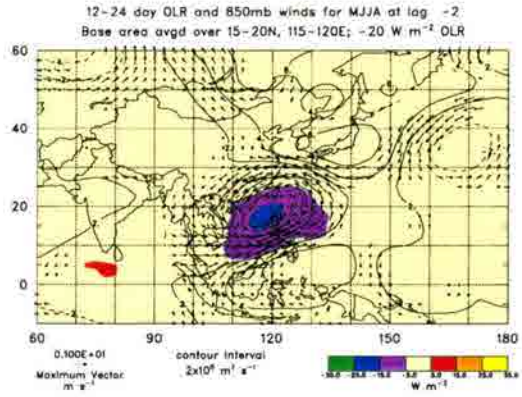

(b) lag -2

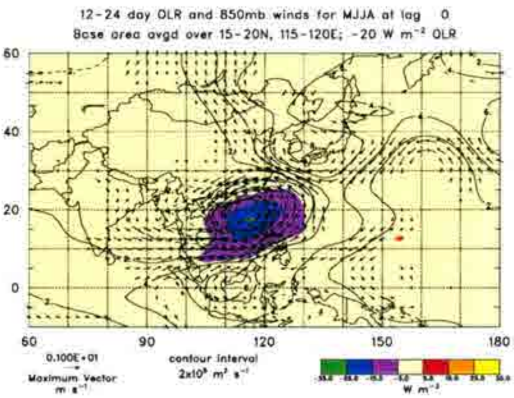

(c) lag 0

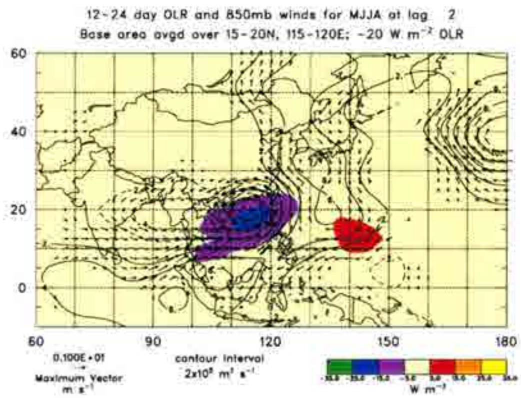

(d) lag 2

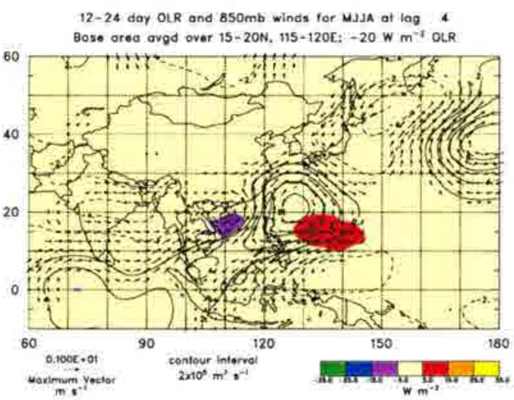

(e) lag 4

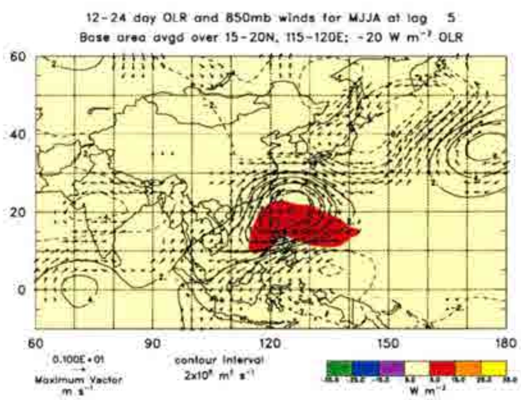

(f) lag 5

Figure 4.17: Same as Fig. 4.16 except for MJJA.

Notice a prominent anticyclonic circulation has developed to the north of the SCS, over Korea and northeastern China. As the convection continues to move slightly southwest and dissipate, this circulation propagates farther south toward the SCS. At lag +4 and lag +5 (Fig. 4.16e, f), positive OLR anomalies begin to develop near the SCS as the anticyclonic circulation continues to propagate south-southwest toward the SCS. Another feature to note is an area of clockwise circulation (positive streamfunction) that propagates westward, centered on the equator. At lag -4, it is centered near 135° E. By lag +5, it is centered about 90° E. This feature can also be seen in the MJJA regressions (Fig. 4.17), though it appears to move slightly faster.

Another feature that is similar between the two regressions is the southwestward propagation of the cyclonic and anticyclonic circulations into the SCS, even though the OLR anomalies have a different origin. In lag -4 for the MJJA regression (Fig. 4.17a) the convection is farther south and east of that in the MJ regression. It originates at about 10° N, 140° E at lag -5 (not shown). The convection orients itself similar to the MJ convection, but it propagates west-northwest into the SCS. Positive OLR anomalies behave the same way (Fig. 4.17d-f).

The features seen in the 12–24 day regressions are very similar to results presented by Fukutomi and Yasunari (1999). In a composite analysis of the summers from 1991–1994, they found OLR anomaly and circulation patterns in a 10–25 day period to have origin and propagation characterisics similar to these regressions. The similarity was especially evident in the MJJA regressions. Fukutomi and Yasunari (1999) described southwestward propagation of cyclonic and anticyclonic circulations and the development of associated OLR anomalies. They also emphesized the interaction between the midlatitudes and the tropics through a lower level wave train which develops from the SCS to the northern Pacific. This feature is also present in the streamfunction patterns in Fig. 4.17.

The 30–60 day regressions do not exhibit nearly as much difference between MJ and MJJA as the 12–24 day regressions do. The MJJA regression for the 30–60 day mode for the

NE box is shown in Figure 4.18. The origin and direction of propagation of convection of the MJJA regression is very similar to that of the 1998 analysis (Fig. 4.13). The 30–60 day regression exhibits signatures of the eastward-moving MJO and the northward-propagating monsoon trough (ITCZ). In the regression, there is a positive OLR anomaly and 850 mb anticyclonic circulation over the SCS at lag -15. Negative OLR anomalies develop over the southern part of India and just north of the equator between 120–140° E. As the positive OLR anomalies over the SCS dissipate at lag -10, the convection over India moves eastward and the convection near the equator moves northward and expands. By lag -5, the MJO (eastward moving) convection has reached Indochina and the ITCZ (northward moving) convection has made it to the SCS. Lag 0 shows convection at its maximum over the SCS. Westerly winds develop behind the MJO convection. At lag 5, the negative OLR anomalies over the SCS begin to dissipate, and positive OLR anomalies develop in the same locations as the negative anomalies at lag -10. The cycle continues on as the positive OLR anomalies gain strength at lag 10.

Why the 12–24 day regressed convection would differ so much between the onset and the whole monsoon period while the 12–24 day circulations remain fairly similar is difficult to understand. One possibility is that the nature of the 12–24 day convection during the onset is more influenced by midlatitudes than it is during the later part of the monsoon. The NE box lies between 15–20° N. This seems to be a sort of transition zone. Early in the season, that area is still affected by midlatitude fronts. This is also on the edge of the Meiyu-Baiu frontal zone. Later in the monsoon season, this frontal zone shifts northward, so the convection is more tropical in nature. Also, the tropical cyclone track develops in the western Pacific later in the monsoon season. That may influence the convection as well. The similarity of the structure of the MJ and MJJA regressions in the other base areas also supports this idea. None of the other areas are in as much of a transition zone as the NE box. The SW and EQ areas are influenced mostly by the tropics during both the onset and the entire monsoon season. The SC box is almost entirely influenced by the midlatitudes.

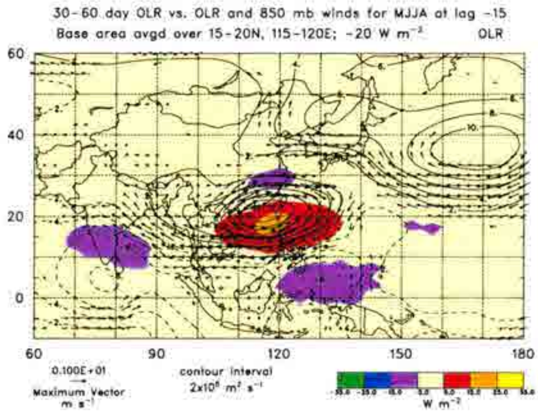

(a) lag -15

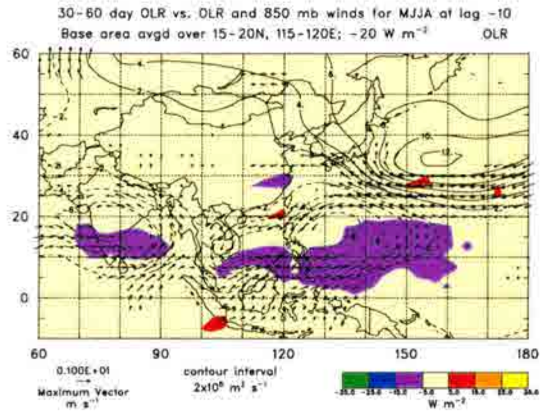

(b) lag -10

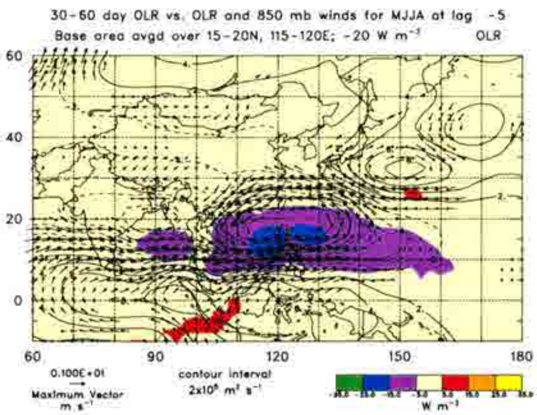

(c) lag -5

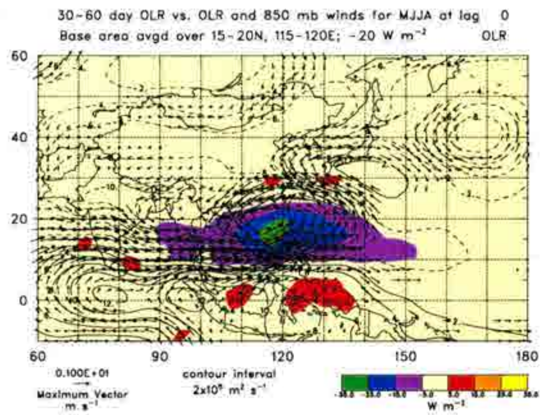

(d) lag 0

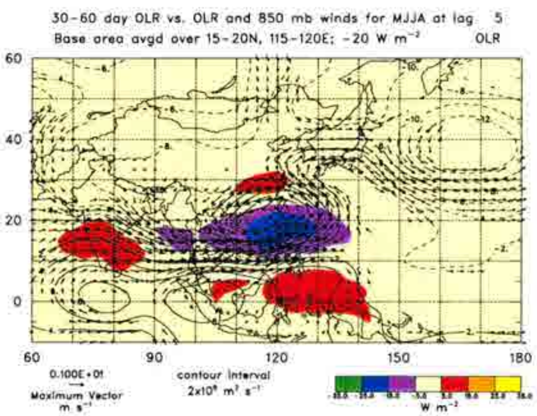

(e) lag 5

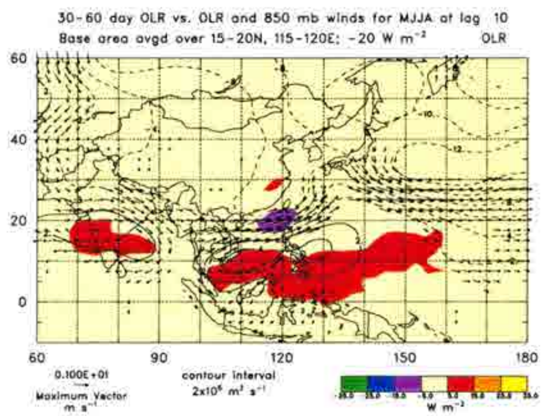

(f) lag 10

Figure 4.18: Same as Fig. 4.17 except for 30–60 day filtered OLR.

The similaritites and differences between the regressions for each of the base areas is also an important point to consider. A comparison between results from the different base areas helps to show the different types of influence over the SEAM before, during and after onset. Looking at the different base areas may also help identify from where the main forcing of the monsoon occurs. As one would expect, the regressions in each of the boxes show a predominence toward that area. This can be seen in comparing the 12–24 day regressions of OLR and 200 mb winds for the SC, NE and SW boxes in Figures 4.19, 4.20, and 4.21, respectively. The OLR patterns tend to be similar in orientation and propagation between the base areas but they have a slight bias toward the box over which the data were averaged. The OLR anomalies for the SW box are farthest south to start (Fig. 21a), while those for the SC box are farthest north (Fig. 19a). One difference in the propagation characteristics of the OLR anomalies is that the SC box develops more or less in situ. The other boxes show definite propagation. Another example of differing influence is seen in the comparison of the circulations for the boxes. The SC box shows very little structure along the equator, and significantly more at midlatitudes. An upper-level wavetrain can be seen across the entire domain at about 40° N. A similar feature was noted by Fukutomi and Yasunari (1999). However, there is not much to note along the equator for the SC box. The opposite is true for the SW box. A midlatitude wave train can be seen between 30–40° N (Fig. 4.21), but it is much weaker than that in the SC box and does not become clear until lag -6. A very prominent feature in the SW box, however, are westward moving disturbances along the equator. At lag -9 (Fig. 4.21a), there is an anticyclonic circulation centered at about 5° N, 145° E. By lag -3, this circulation is at 100° E and a cyclonic circulation has moved into the base domain. This equatorial disturbance is not seen in the SC regression. These westward-moving equatorial disturbances have also been observed in previous studies. Chen and Chen (1995) found the 12–24 day oscillation to exhibit a double-cell structure with one of the two cells centered near the equator (Fig. 2.6). Fukutomi and Yasunari (1999) also observed westward propagating wind anomalies in the off equatorial tropics and noted that these disturbances along with the aforementioned wave train are prominent features in the upper level circulation for this mode.

The NE box regression exhibits those features from both midlatitudes and along the equator. The midlatitude wave train can be seen at about 35° N. These circulations move eastward but are slightly south of that from the SC box. The westward moving equatorial disturbance also shows up the the NE regression. One feature in the NE box that is not seen in either the SC or SW boxes is a north-to-south movement of circulations. At lag -9 (Fig. 4.20a), the anticyclonic circulation centered at 30° N, 110° E is splitting apart from the portion of the circulation centered at 40° N, 145° E. The southern portion of the anticyclone moves south across China toward the SCS while the northern portion continues to move east. At lag -6, this anticyclonic circulation has completely separated into two smaller circulations with a cyclone now present between the two. A similar process occurs with the cyclonic circulation between lag -3 and lag 0. The equatorial disturbance can also be seen in the NE box regression. Positive streamfunctions in the equatorial western Pacific are clearly seen at lag -6 (Fig. 4.20b) similar to that in the SW box. This disturbance moves westward with its extent far enough north to affect the SCS. As in the SW box regression, it is followed by an area of negative streamfunctions by lag 0. The comparison of these regressions supports the idea that the NE box is a transition area between midlatitude and tropical influence on the SCS. The NE box regression is the only one that exhibits features from both midlatitudes and the tropics.

The circulation and convection patterns in the 12–24 day regressions and 200 mb winds are very similar to the patterns of the 12–24 day filtered OLR and 200 mb winds for 1998 (Fig. 4.12). Both show that the negative OLR anomalies occur ahead of the upper level troughs and positive OLR anomalies occur ahead of the upper level ridges. This is seen most clearly in the 12–24 day regressions for the NE box (Fig. 4.20) and the SC box (Fig. 4.19) and to a lesser extent for the SW box (Fig. 4.21). This is another example of the connection between the midlatitudes and the tropics. Previous studies (e.g.,

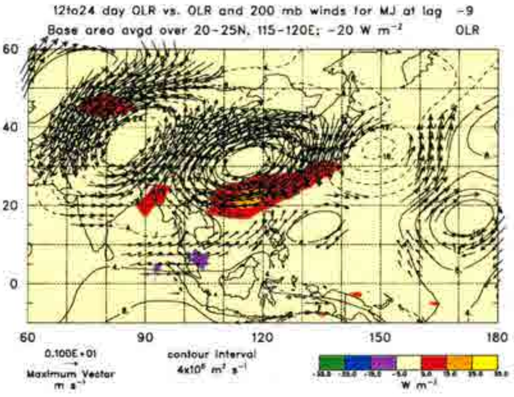

(a) lag -9

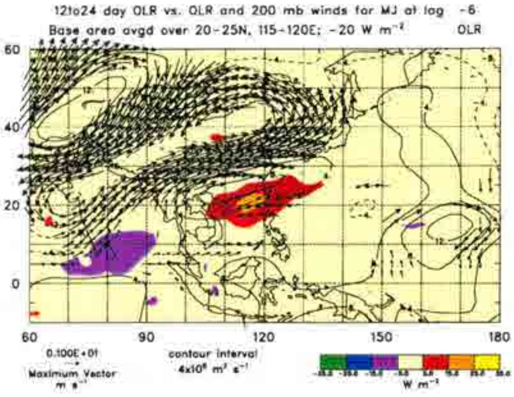

(b) lag -6

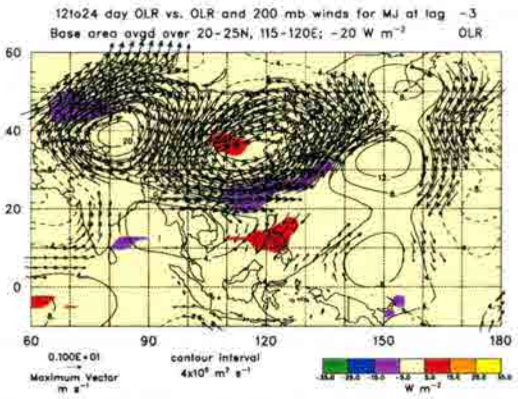

(c) lag -3

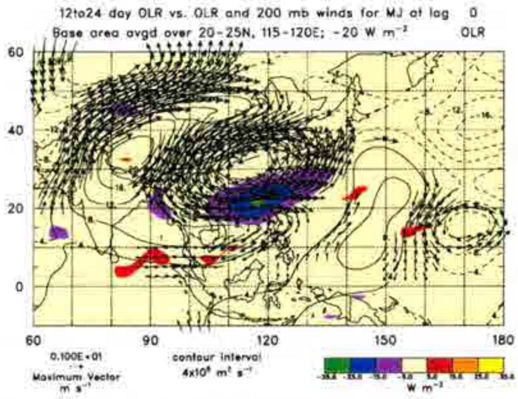

(d) lag 0

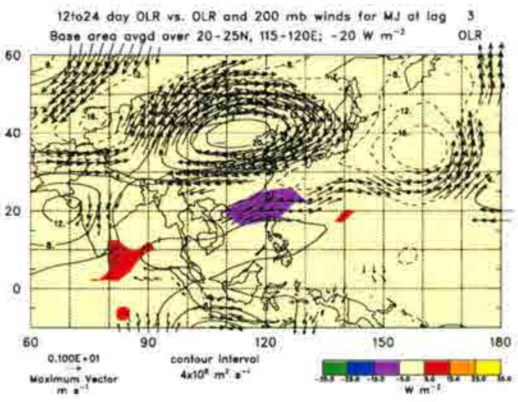

(e) lag 3

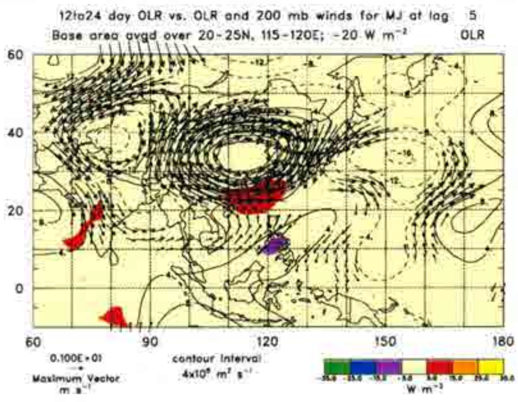

(f) lag 5

Figure 4.19: Same as Fig. 4.16 except for SC box at 200 mb.

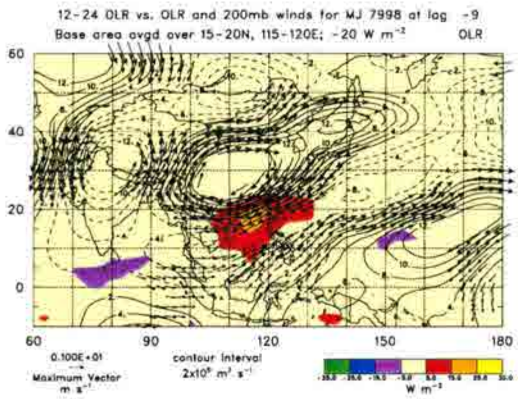

(a) lag -9

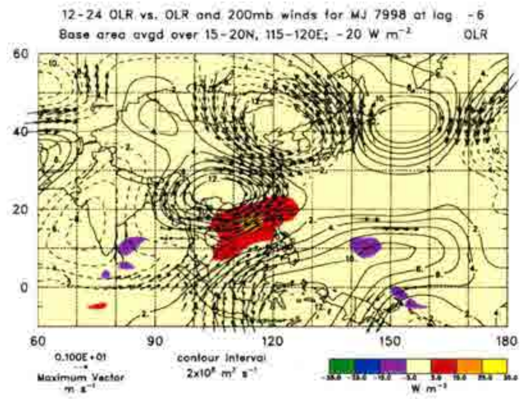

(b) lag -6

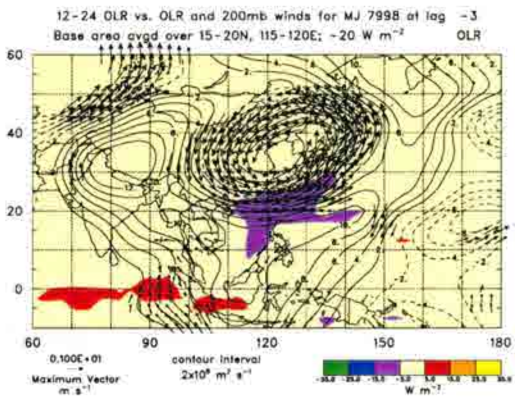

(c) lag -3

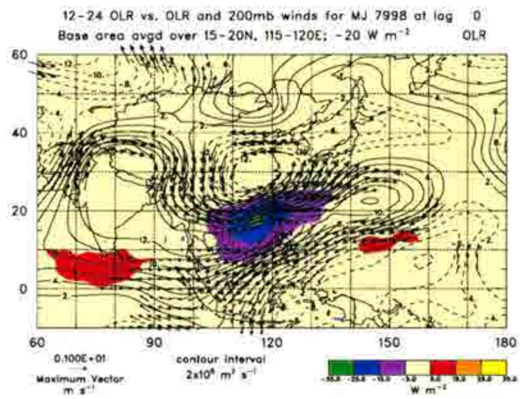

(d) lag 0

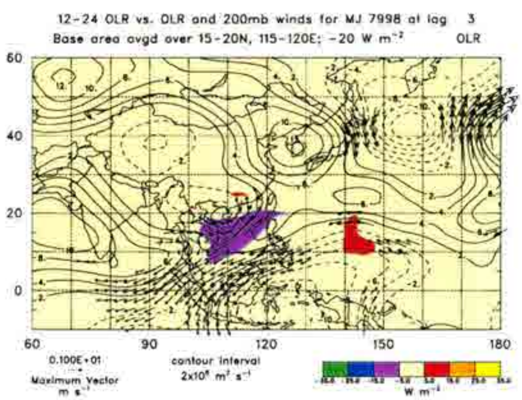

(e) lag 3

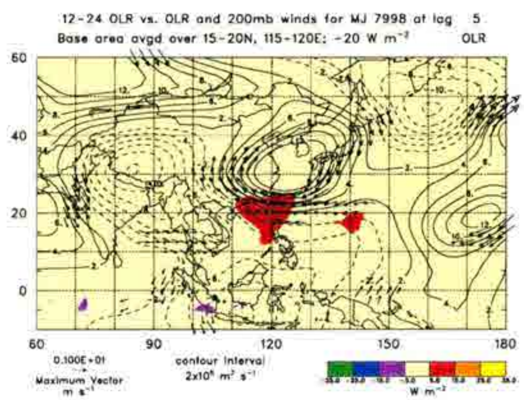

(f) lag 5

Figure 4.20: Same as Fig. 4.19 except for NE box.

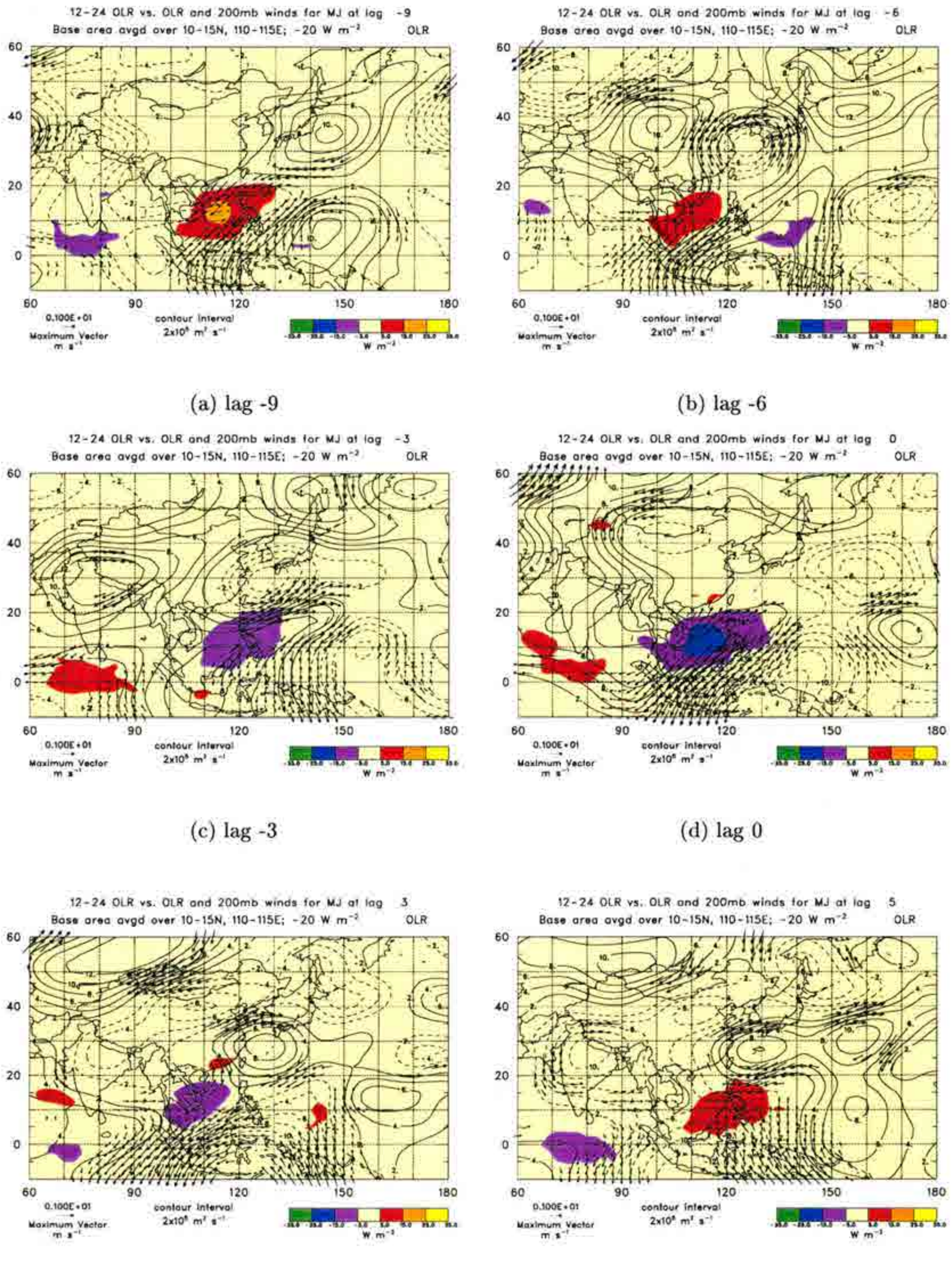

(a) lag -9

(b) lag -6

(c) lag -3

(d) lag 0

(e) lag 3

(f) lag 5

Figure 4.21: Same as Fig. 4.19 except for SW box.

Fukutomi and Yasunari 1998) suggest the convection over the SCS is a forcing mechanism for the generation of the upper level waves, specifically a Rossby wave train. However, in these regressions, the circulations are in place and moving toward the SCS before the OLR anomalies form. So, it does not appear that the upper level circulations are forced by the convection in this case, but rather the convection is forced by the midlatitude circulations.

A similar comparison between boxes can be made for the 30–60 day oscillations. There is not much difference between the the regressions for 30–60 day OLR and 850 mb winds between the NE box (Fig. 4.18) and the SW box (Fig. 4.22). They exhibit the same basic structure and features (described in detail in Section 4.3.1) with only a slight bias in the location of OLR anomalies and circulations toward the base area. Both the NE and SW boxes show eastward moving OLR anomalies like the MJO and northward moving band of OLR anomalies and corresponding trough/ridge like the ITCZ. However, there is a substantial difference between analysis from these boxes and the SC box (Fig. 4.23). In the SC box there is no definitive eastward propagating MJO-like disturbance, nor is there a clear ITCZ. Like the 12–24 day regressions, the OLR anomalies tend to develop over the analysis box without subsequent movement. At lag -15 (Fig. 4.23a), there is a band of positive OLR anomalies over the SCS, as there are at the same time for the NE and SW boxes. The positive OLR anomalies have dissipated by lag -10 and convection has developed to the east of the SCS. This convection remains fairly stationary in subsequent lags while more convection develops over the SCS and dissipates between lag 5 and lag 10. This is in contrast to the regressions in the NE and SW box which show more definite eastward and northward movement. The latter analysis areas exhibit signatures of the MJO and the ITCZ because they are in the regions these disturbances are more apt to affect (Wang and Rui 1990). The ITCZ convection tends to dissipate by about 20° N, and the convection associated with the MJO tends to remain south of 20° N for the NE and SW boxes as well. Because of a lack of influence from these disturbances over the SC box, it is not surprising that their signatures would not be present in the SC regression.

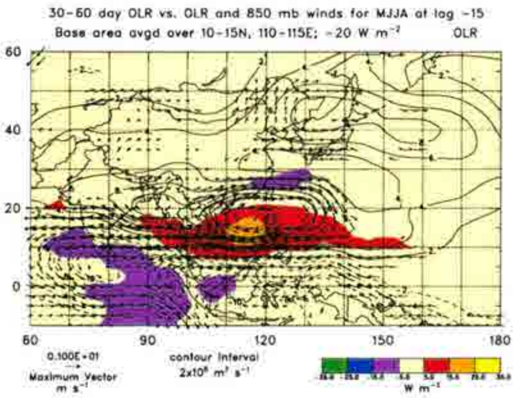

(a) lag -15

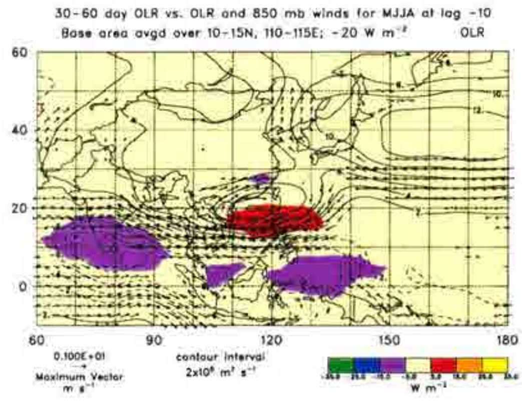

(b) lag -10

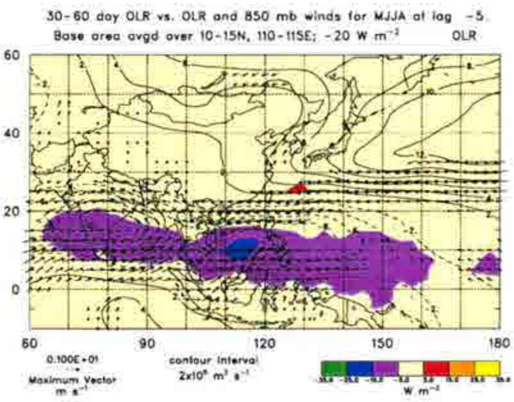

(c) lag -5

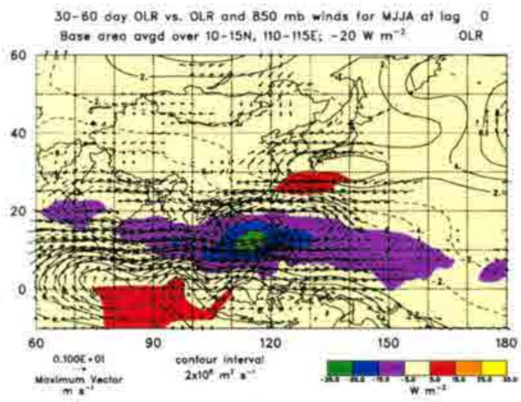

(d) lag 0

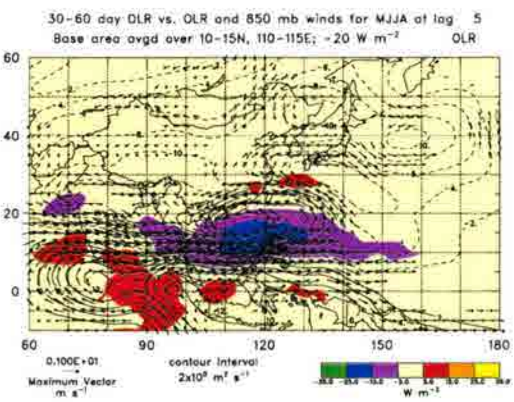

(e) lag 5

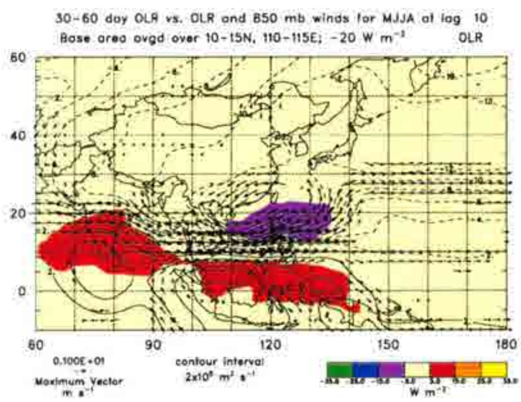

(f) lag 10

Figure 4.22: Same as Fig. 4.18 except for SW box.

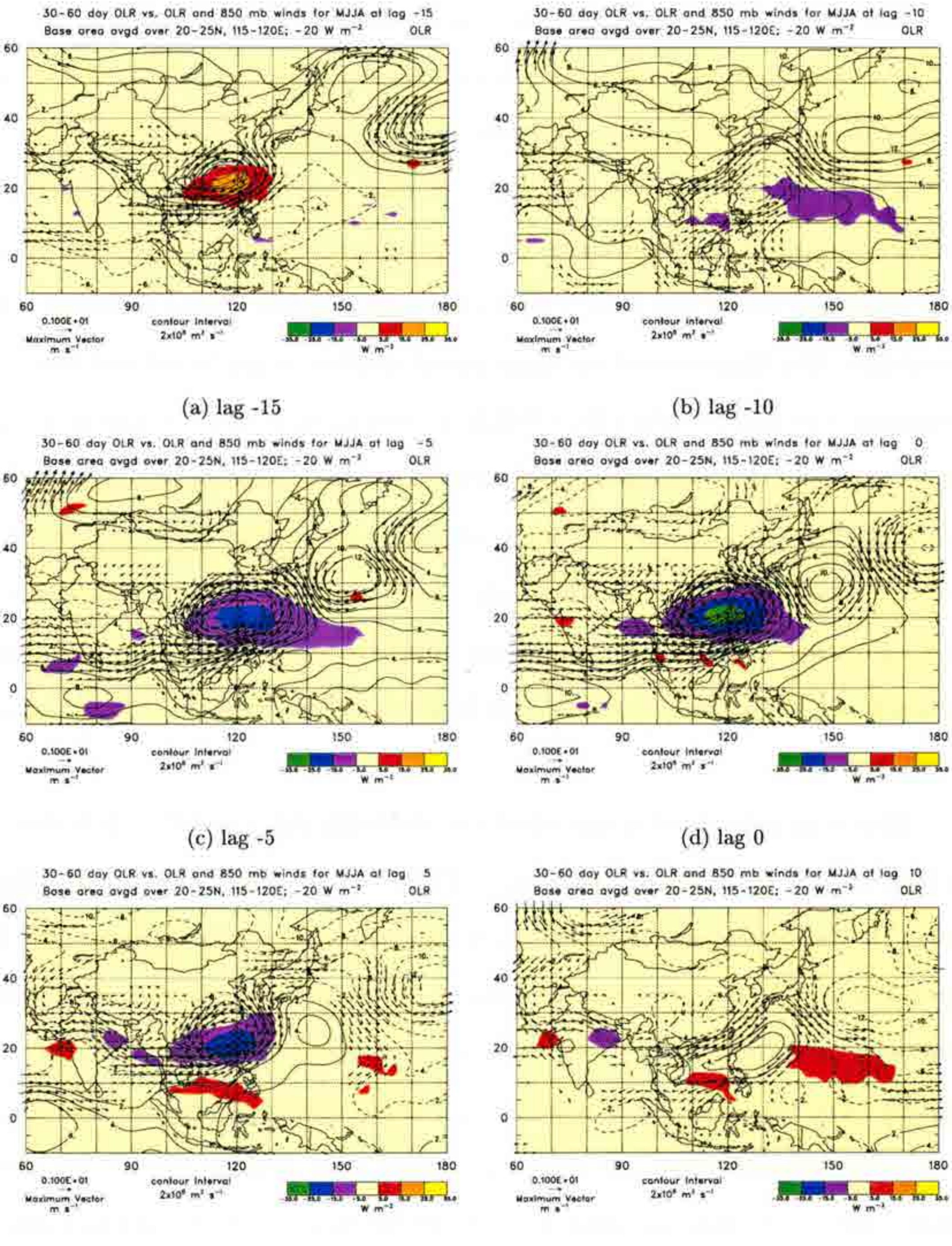

(a) lag -15

(b) lag -10

(c) lag -5

(d) lag 0

(e) lag 5

(f) lag 10

Figure 4.23: Same as Fig. 4.18 except for SC box.

4.3.3 Interaction of the intraseasonal modes

It is hard to gauge exactly how much influence the 12–24 day oscillations have on the 30–60 day oscillations or vice versa. Previous studies have suggested that the SEAM onset is a result of the phase-locking of the 12–24 and 30–60 day modes (e.g., Chen and Chen 1995). Judging from the nearly simultaneous arrival of these modes in the SCS during the 1998 onset one could argue that these modes must interact with one another. However, like many of the aspects of the SEAM, there tends to be interannual and spatial variability of these interactions. The interaction of the intraseasonal oscillations can be inferred through the comparison of a timeseries of the filtered OLR. Each of the timeseries is simply an average of the raw or filtered OLR over the NE or SW base area. Each figure consists of the unfiltered OLR (top), the 30–60 day filtered OLR (middle) and the squared 12–24 day filtered OLR with the 15 day running variance (bottom). The 15 day window for the running variance was an arbitrary choice made because it was within the period of oscillation and captured the trends of the data fairly well. Figure 4.24 shows the timeseries for 1980 averaged over the SW box.

This is an example of a year where the 30–60 day mode and the 12–24 day mode are both present during the monsoon onset. The 30–60 day OLR has a relative minimum around 16 May indicating a period of convection associated with that mode. The 12–24 day OLR and variance show a maximum during that same time, indicating that mode was active at the same time as the 30–60 day mode. A similar timeseries for 1998 over the NE box (Fig. 4.25) shows a year in which the 12–24 day and 30–60 day oscillations appear to be weakly present during the onset, but appear more strongly later in the monsoon season. There is no strong maximum in the 12–24 day variance associated with a minimum in the 30–60 day timeseries at the time of onset. In early July, however, there is a clear maximum in the 12–24 day timeseries associated with a minimum in the 30–60 day OLR. Some years, such as 1982, show no interaction of these modes since there are no strong 12–24 day maximums at the same time as a 30–60 day minimum (Fig. 4.26).

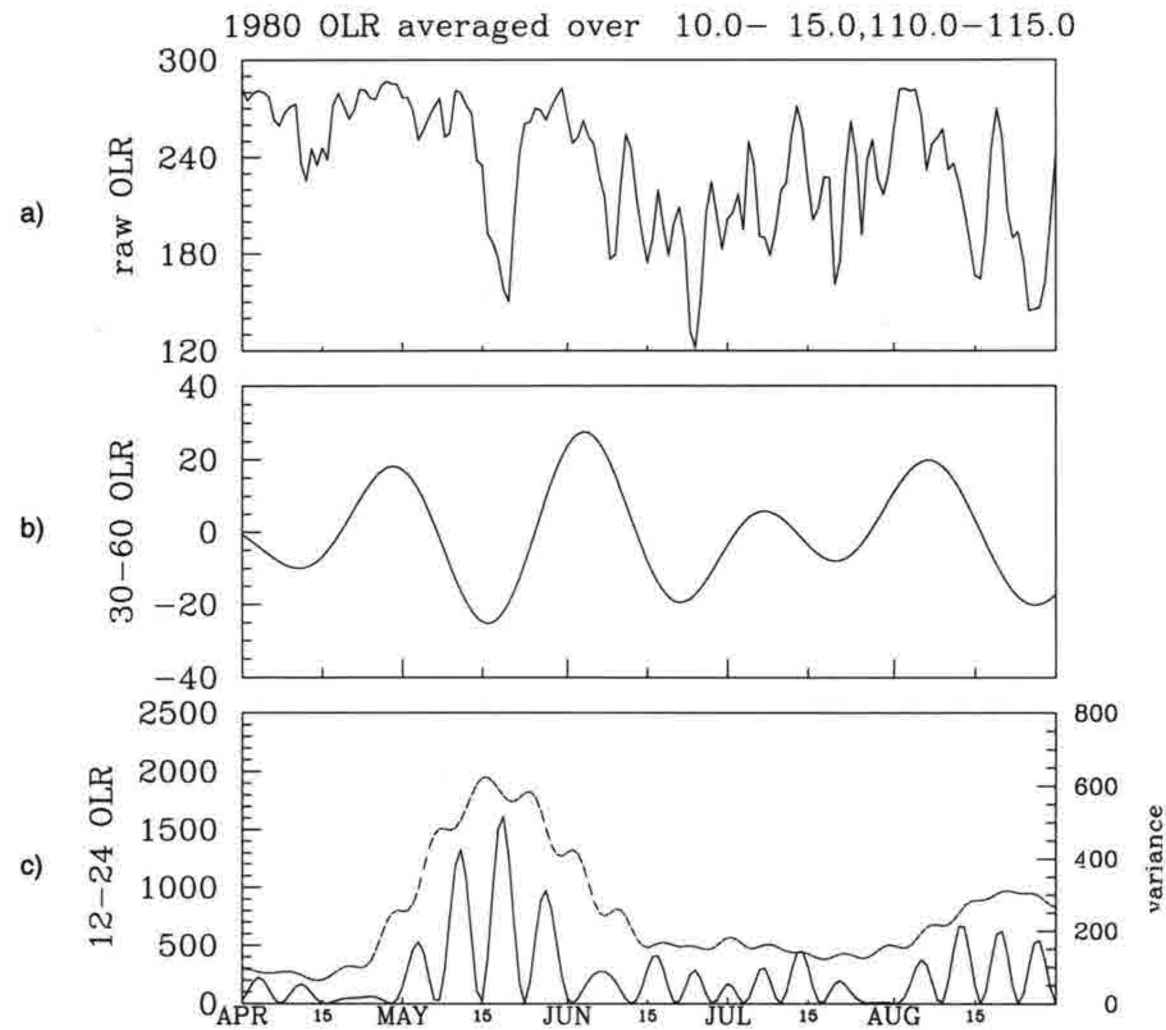

Figure 4.24: Timeseries of unfiltered OLR (a), 30–60 day filtered OLR (b) and squared 12–24 OLR (solid) with a 15 day running variance (dashed) (c) for the SW box during 1980. The OLR scale is on the left in W m^{-2} for (a) and (b) and W^2 m^{-4} for (c). The variance scale is on the right in units of W^2 m^{-4}.

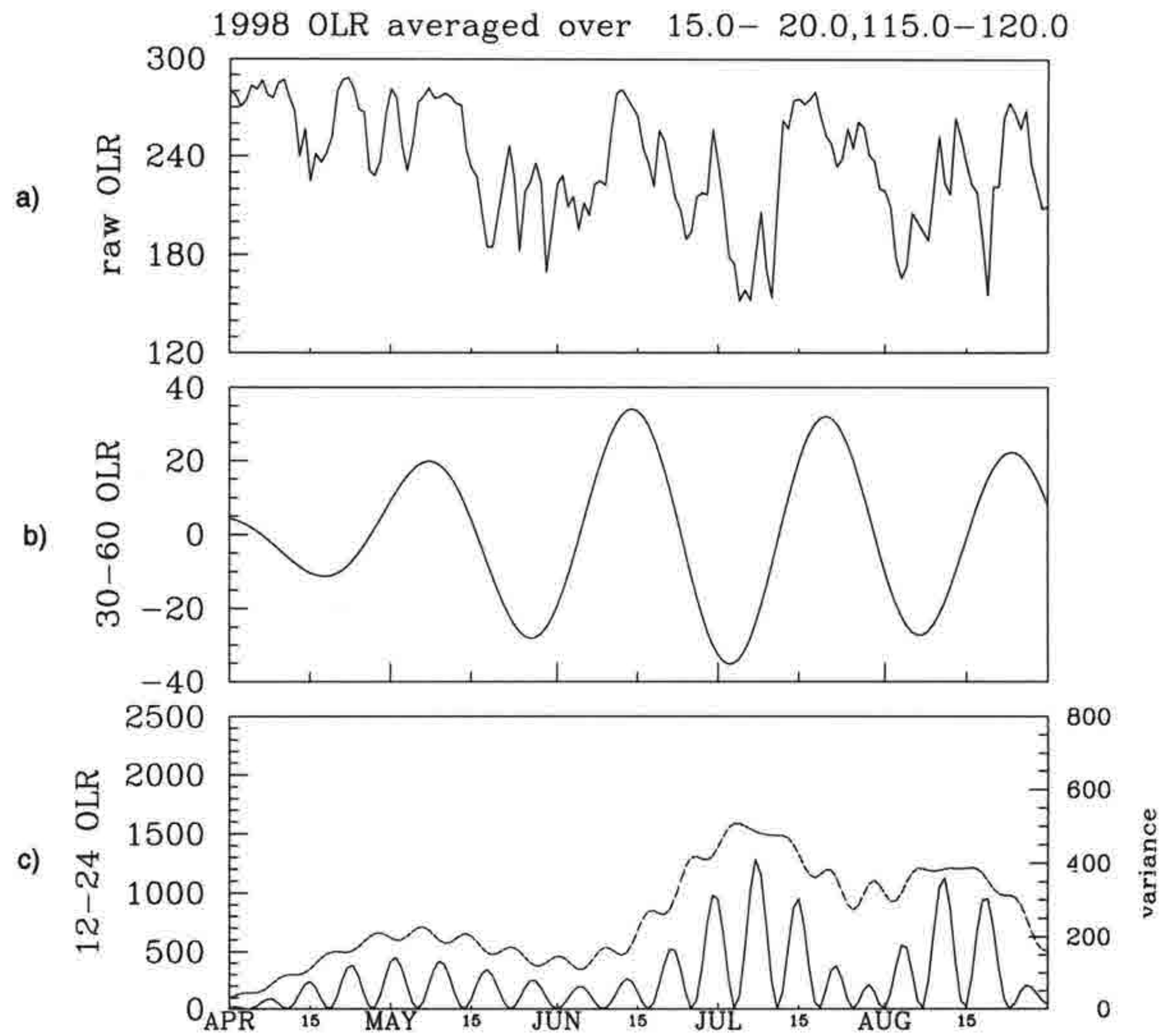

Figure 4.25: Same as Fig. 4.24 except for NE box during 1998.

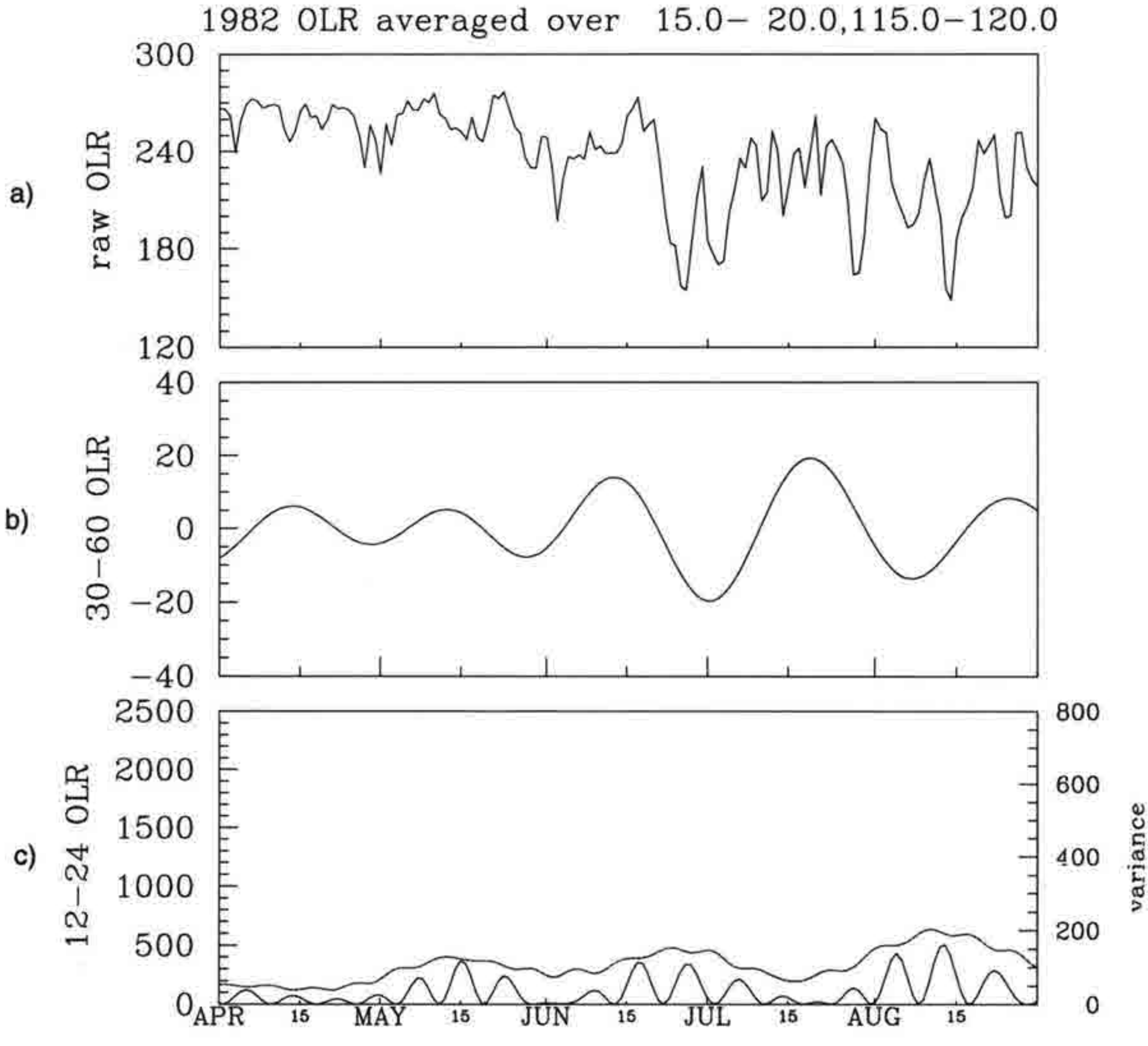

Figure 4.26: Same as Fig. 4.24 except for NE box during 1982.

4.4 Interannual variation of the SEAM onset

The interannual variability of the SEAM is an important aspect of the monsoon that must be addressed. So, this section seeks to answer the following question: How does the onset change from year to year, particularly in context of the 12–24 and 30–60 day modes? I will expand our knowledge of how the onset and these modes change each year and if these changes affect the timing of the onset.

4.4.1 Cataloging the 12–24 and 30–60 day oscillations

In order to help understand the interannual variability of the SEAM, it is necessary to get an idea of how both the intraseasonal oscillations and the onset timing vary. The strength or predominence of the 12–24 and 30–60 day oscillations varies quite a bit from year to year. This can be seen from a comparison of the spectral densities of OLR over the SCS. The spectra calculated at 10° N, 115° E for 1985, 1993, 1998 and the ensemble from 1979–1998 each display significant peaks over different periods (Fig. 4.27). In 1985, spectral peaks with periods of 4–5 days and 30–60 days are significant at the 95% level. There are statistically significant peaks centered around 20 days and 5 days, and a small peak beyond 30 days which does not eclipse the 95% level in 1993 while 1998 has prominent peaks at both 12–24 and 30–60 day periods. However, neither of those peaks in 1998 is statistically significant. The 1979–1998 ensemble spectrum also exhibits peaks with 12–24 and 30–60 day periods, but neither one is significant at the 95% confidence level. However, this does not necessarily indicate that these modes are not important. Clearly, there is a large amount of variablility in the spectra from year to year. The ensemble spectra tend to have "enhancements" instead of significant peaks even when there are significant peaks within these periods present in individual years. This may indicate that variability in these periods of oscillation are usually present but can be stronger in some years than others.

Interannual variations of onset timing were broken down into three categories: early, normal and late onset. The basis behind these choices was discussed in Section 4.1, and

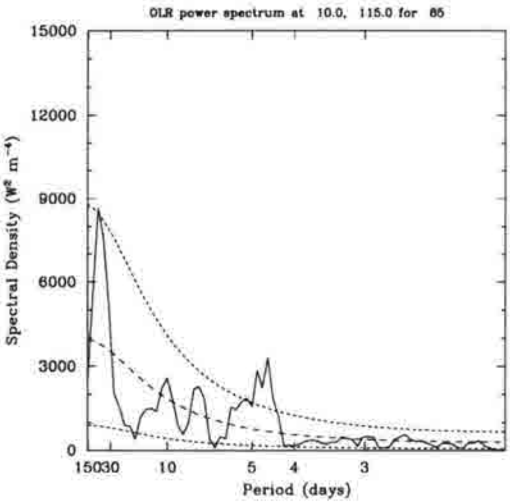

(a) 1985

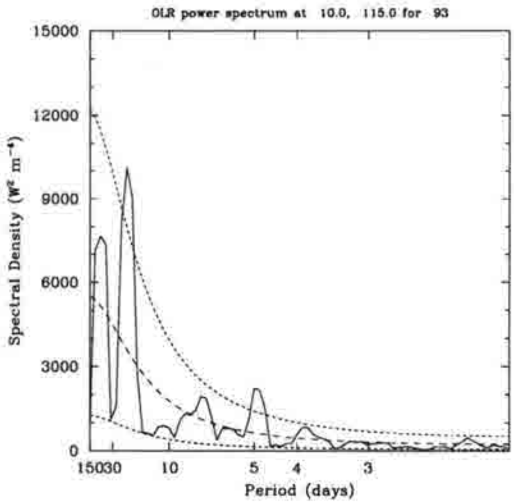

(b) 1993

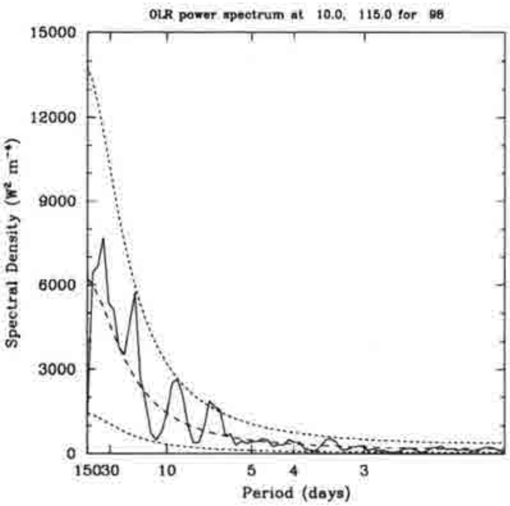

(c) 1998

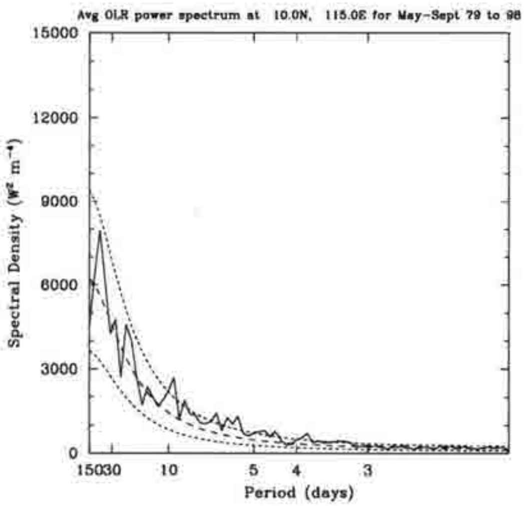

(d) 1979–1998 average

Figure 4.27: Spectral density estimates of OLR at 10° N, 115° E for 1985 (a), 1993 (b), 1998 (c) and the 1979–1998 ensemble (d). Lines are the same as Fig. 3.2

the selection of what constitutes an an early, normal or late onset year in this study are comparable to past works. In addition to catagorizing the monsoon onset timing, each year was placed into one of three categories which describe the intraseasonal oscillations. Each year can be described as having: 1) both the 12–24 and 30–60 day modes present at the time of onset, 2) having only the 30–60 day mode present at the onset or 3) having neither mode present at the onset. There were no years where only the 12–24 day oscillation was present at the onset. The placement of each year into one of these three categories was determined based on the timeseries analysis such as that in Fig. 4.24 and then compared to the animations of 12–24 day and 30–60 day filtered OLR and 850 mb winds such as that in Figs. 4.12 and 4.14. In general, the placement of the years into their categories yielded similar results from both methods.

The timeseries were calculated for each of the 5° x 5° boxes in the SCS between 10–20° N and 110–120° E. They were used to determine whether the 12–24 day and 30–60 day oscillations were present and prominent at the time of SEAM onset. For the oscillations to be considered present and prominent at the time of onset the 30–60 day OLR timeseries needs to have a relative OLR minimum (negative OLR anomaly) and there needs to be a relative maximum of the 12–24 OLR variance within ± 1 day of the previously determined onset date for that box. Upon inspection of all the timeseries plots, each year was labelled (rather subjectively) as "both modes", when both the 12–24 day oscillation and the 30–60 day oscillation were present at the onset, "30–60 only" when the 30–60 day oscillation was dominant at the onset, or "neither" when neither the 12–24 day or 30–60 day oscillations were predominant at the onset. The results are in Table 4.2. These categories are used for further analysis described in the next section.

As one would expect, the majority of years between 1979–1998 had normal onsets (Table 4.3). Perhaps more surprising is that only 1 year out of the 20 had an early onset, and there were twice as many late onset years in the southern SCS than the northern SCS. Having more late onsets in the southern SCS is somewhat contrary to traditional thinking

Table 4.2: Table of onset timing, intraseasonal oscillation and interannual variability categories for SEAM onset from 1979–1998. N indicates the northern SCS, S indicates southern and NS denotes both the northern and southern SCS.

Year	Early	Normal	Late	Both	30-60	Neither	El Niño	La Niña	Neutral
1979		NS		NS					NS
1980		NS		NS					NS
1981	N		S		NS				NS
1982		NS				NS	NS		
1983		N	S	NS			NS		
1984		NS				NS			NS
1985			NS			NS			NS
1986		NS			NS		NS		
1987			NS	NS			NS		
1988		NS		NS				NS	
1989		NS		NS				NS	
1990		NS			NS				NS
1991			NS	NS			NS		
1992		NS				NS	NS		
1993		N	S		NS				NS
1994		NS				NS	NS		
1995		NS		NS			NS	NS	
1996		NS		S	N			NS	
1997		NS		NS			NS		
1998		NS		NS			NS		

that the onset occurs first in the southern portion of the SCS and progresses northward (Fig. 2.3). More "normal" onsets in the northern SCS may indicate the presence of midlatitude influence which affects the northern part of the SCS and not the southern part. More than half of the years had both the 12–24 day and 30–60 day oscillations present at the onset, 25% had only the 30–60 day mode present and 25% of the years had neither of the modes present during the SEAM onset. There were no years when only the 12–24 day mode was present at the onset. These 20 years had a lot of ENSO activity as well. Selection of El Niño and La Niña years was based on the Southern Oscillation Index. Inspection of Niño 3.4 SST anomalies yielded similar results. Between 1979–1998, half of the years had an El Niño, while 20% were considered La Niña.

An interesting pattern to note in Table 4.2 is the quasi-biennial pattern of late onsets. From 1981–1993 every other year had a late onset with the pattern interrupted in 1989 and

Table 4.3: Percent of years from 1979–1998 which fall into each category.

	Early	Normal	Late	Both	30-60	Neither	El Niño	La Niña	Neutral
North	5%	80%	15%	50%	25%	25%	50%	20%	35%
South	0%	70%	30%	55%	20%	25%	50%	20%	35%

presumably again in 1995. These two years were active La Niña years. Many previous studies have observed a biennial pattern in sea surface temperatures (SSTs) and rainfall associated with the Indian and East Asian monsoons (e.g., Shen and Lau 1995; Meehl 1997). The biennial nature of the onset timing may indicate an interaction with the Tropospheric Biennial Oscillation (TBO). However, that will not be addressed in this study.

4.4.2 Intraseasonal oscillations and SEAM onset timing

Explanations of the interannual variability of the SEAM onset timing have been offered in terms of large-scale circulations and sea surface temperatures (SSTs) (e.g., Xie et al. 1998; Wang and Wu 1997). However, Wang and Wu (1997) found that the intraseasonal oscillations (ISOs) are notably variable from year to year in their amplitude, periodicity and phases. Similar results have been presented in this study, yet to this point there has been little explanation of the onset timing in terms of these ISOs. Given that the onset timing and the ISOs change from year to year, can the interannual variability of the onset timing be explained by the presence or lack of the 12–24 and 30–60 day oscillations?

Chen and Weng (1997) suggest that the interannual variation in the intensity and periodicity of the two intraseasonal modes causes the onset and the break dates of the SEAM to vary from one year to another. They found during summers with anomalously warm SSTs over the central-eastern equatorial Pacific, the SEAM onset is delayed by about 3 weeks and the occurrence frequency of the 12–24 day mode is reduced. According to Chen and Chen (1995), the presence of the 12–24 day mode is important since the onset is triggered by a phase-lock of the 12–24 day mode with a 30–60 day oscillation. Though it was not explicitly stated by Chen and Weng (1997), it is not unreasonable to assume that the reduction in 12–24 day occurrence frequency may result in a delayed onset of the SEAM. The following analysis will expand on this idea and ascertain if there is any connection between the occurrence of the 30–60 and 12–24 day oscillations and the onset timing.

One way to compare and contrast the onset timing of the different ISO categories is in timeseries of OLR and 850 mb zonal wind calculated for each of the categories found in Table 4.2. Timeseries were calculated by first taking the area average of the data for each year over the northern SCS (15–20° N, 110–120° E) and the southern SCS (10–15° N, 110-120° E) then taking the mean of the years included in the chosen category. These timeseries are basically composite timeseries of samples selected based on the various categories. From these timeseries, one can get a rough idea how the onset timing relates the the ISO categories. Tendencies for early, normal or late onset (relative to the 20 year mean) can be ascertained by analyzing these plots in the same way as was done to identify the monsoon onset in Section 4.1. Once a tendency for the timing has been identified, the timeseries of the ISO category can be compared with that of the timing category to see if they are similar. In this I am assuming that if those timeseries are similar then there may be a link between the ISO category and the onset timing. Figure 4.28 shows the OLR timeseries over these two areas for all 20 years, for years when both the 12–24 and 30–60 day oscillations were present at onset, years when the 30–60 day oscillation dominated and years when neither ISO mode was present at the onset. Figure 4.29 shows the same timeseries for the 850 mb zonal wind.

Years in which only the 30–60 day oscillation was present tended to have earlier onsets (by about a week) than other years (Fig. 4.28). This is especially true in the northern SCS. The 30–60 day OLR timeseries in the northern SCS (Fig. 4.28a) shows a rapid decrease in OLR below 240 W m^{-2} prior to 15 May. This is several days before any of the other categories display that signature of onset. The onsets are much closer to one another (around 15 May) in the southern SCS, but the years where the 30–60 day mode dominated was still earliest. Years where neither mode was present tended to have the latest onsets.

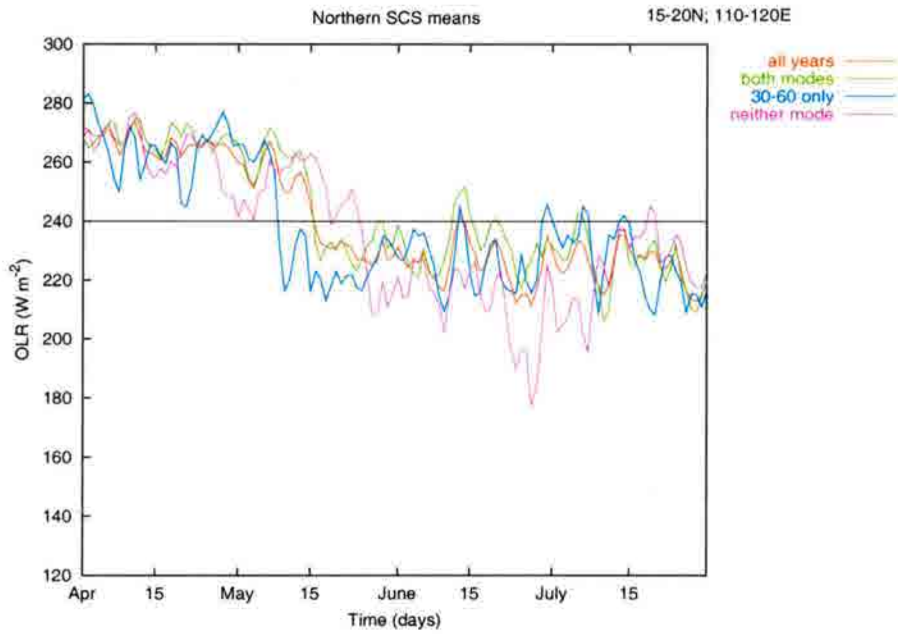

(a)

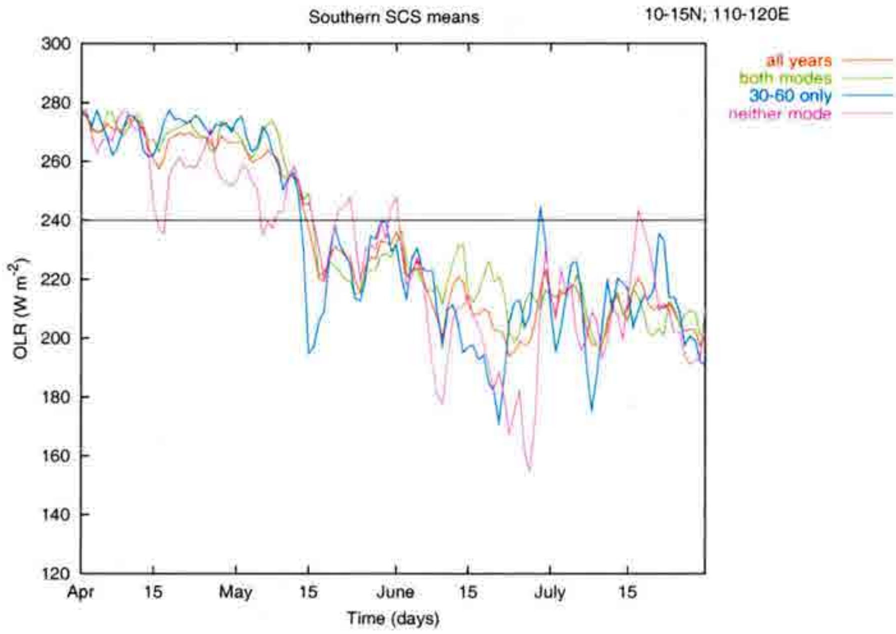

(b)

Figure 4.28: Timeseries of OLR for the intraseasonal oscillation categories in the northern SCS (a) and the southern SCS (b).

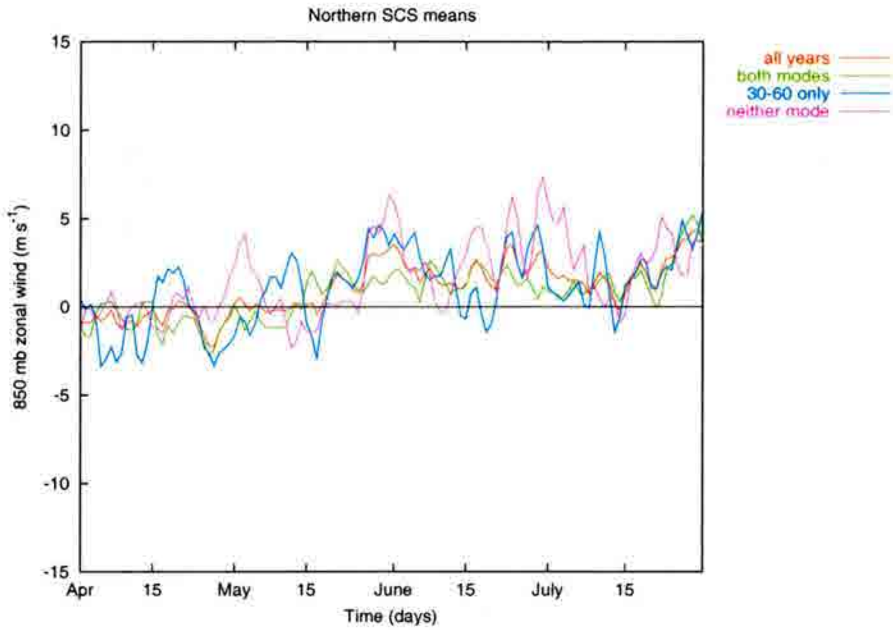

(a)

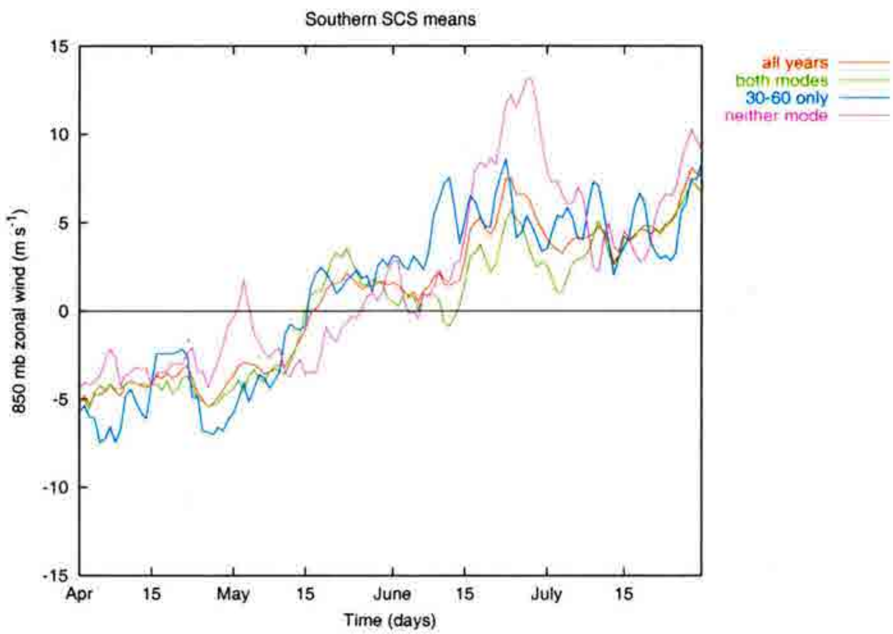

(b)

Figure 4.29: Same as Fig. 4.28 except for 850 mb zonal wind.

This is seen most clearly in the northern SCS OLR timeseries (Fig. 4.28b). The OLR did not drop below 240 W m^{-2} until late May, several days after the mean. A comparison between the OLR timeseries of years where neither mode was present and years which had late onsets shows for the northern SCS (Fig. 4.30a) that the late onset years have a slightly more delayed drop in OLR than the years where neither mode was present at onset. There is better agreement between the two timeseries in the southern SCS (Fig. 4.30b). These timeseries give an indication that there may be a connection between the late onset and the absence of the ISOs. Years where both the 12–24 and 30–60 day modes were present at the onset tended to be very close to the mean of all 20 years. The 850 mb zonal wind timeseries (Fig. 4.29) displayed similar tendencies as the OLR timeseries but not quite as clear. In the northern SCS, the years in which the 30–60 day oscillation dominated had switches from easterly to westerly winds early on but did not remain westerly whereas the in southern SCS the switch was not any earlier than the mean. Those years that had neither mode present at onset had the latest switches in both the northern and southern SCS. Years where both modes were present had changes from negative to positive zonal wind very close to the 20 year mean.

Another way to relate the ISO categories and the onset timing is in a regression analysis of each of the onset timing and oscillation categories. The regressions give an idea of the typical convection and circulation patterns associated with each of these categories. These regressions are calculated for both the 12–24 day and 30–60 day oscillation in the same way as those described in Section 4.3 except only the years which fall into the category are included in the calculation instead of all 20 years. In comparing and contrasting the regressions for each of the monsoon categories from Table 4.2 further insight into the connection between the onset timing and ISOs may be attained.

For the onset timing categories, one would expect the normal onset regression to be very similar to that of the full 20 year period since at least 70% of the years examined had normal onsets. Indeed this is the case. Figure 4.31 shows the lagged regression of

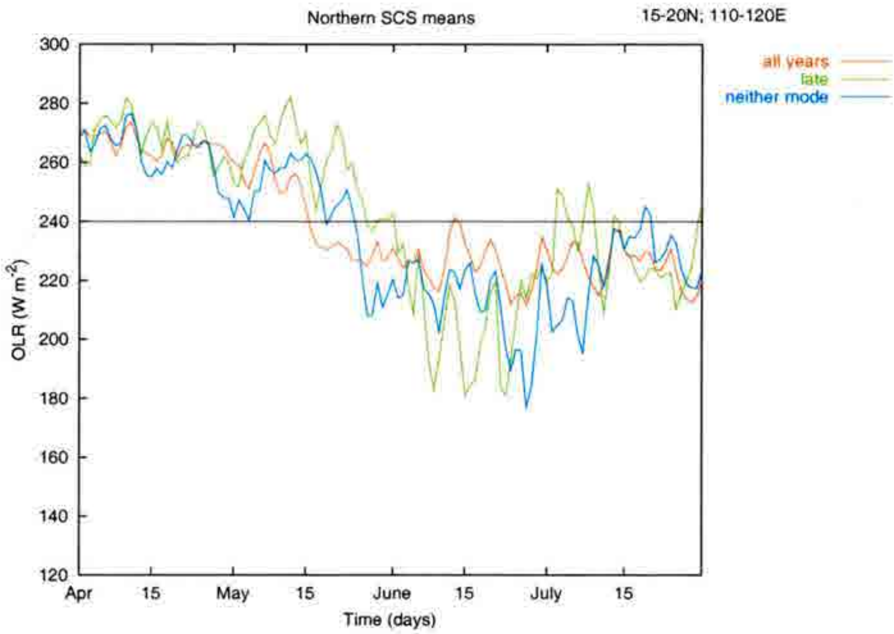

(a)

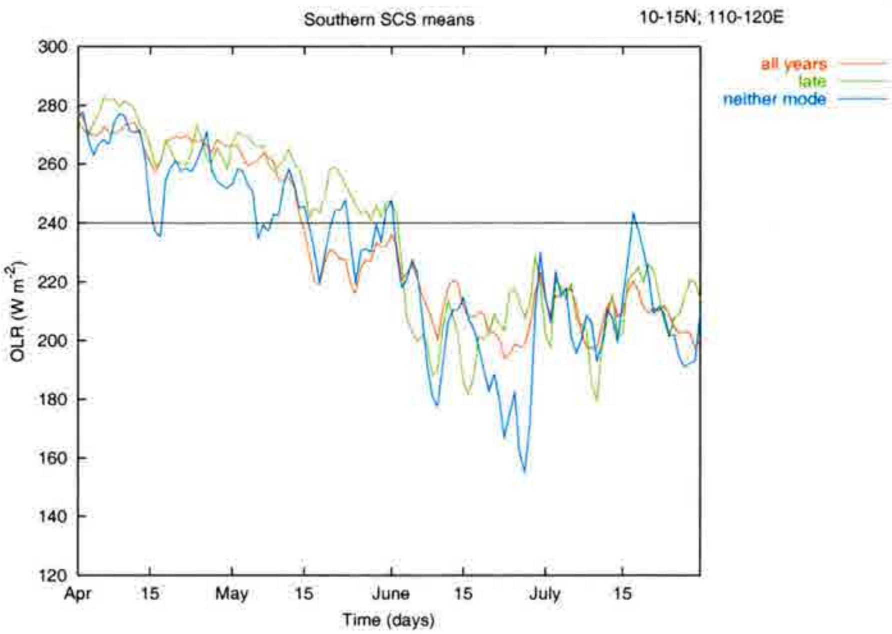

(b)

Figure 4.30: Same as Fig. 4.28 except for late onset years and years where neither ISO was present at onset.

the 12–24 day OLR and 850 mb wind over the NE box for the normal onset years. A comparison to Figs. 4.16 and 4.20 shows nearly identical features in the winds and OLR, respectively. OLR anomalies and circulations propagate west-southwest into the SCS and there is a westward-moving equatorial disturbance as previously described. The same 12–24 day regression for late onset years is shown in Figure 4.32. Notice it is very similar to the normal years' regression. This is not surprising. Chen and Weng (1997) found that the synoptic conditions over the SCS are the same in normal and late onset years. Given this, it is expected that the regressions are the same for the normal and late onset years since the regressions represent a specific event independent of the timing of that event. Though the orientation of the 12–24 day OLR anomalies is the same for these regressions, the OLR anomalies for the late onset regression tend to develop more in situ than the normal onset anomalies do. This may indicate that even though the structure of the anomalies is similar between late and normal onsets (perhaps due to similar synoptic conditions) the strength of the modes may differ. The lack of a definite propagation pattern in the regression for late onset years may indicate that the oscillation is weaker for late onset years than it is during normal onset years.

The 12–24 day regression for years in which both the 12–24 day and 30–60 day modes were present at the SEAM onset (Fig. 4.33) is also very similar to the regression for normal onset years. Again, this is to be expected since at least half of the years examined were years in which both ISO modes were present with the onset. There are many years in common between the normal onset years and years where both modes are present at the SEAM onset. This may be an indication that the phase-locking of the 12–24 day and 30–60 day as presented in Chen and Chen (1995) may be the normal SEAM onset trigger.

The 12–24 day regressions for years where only the 30–60 day mode was present and when neither mode was present at the onset paint a much different picture than the other regressions. As one might expect, the 12–24 day regressions do not display any of the "typical" features that have become recognizable with this mode in the years when

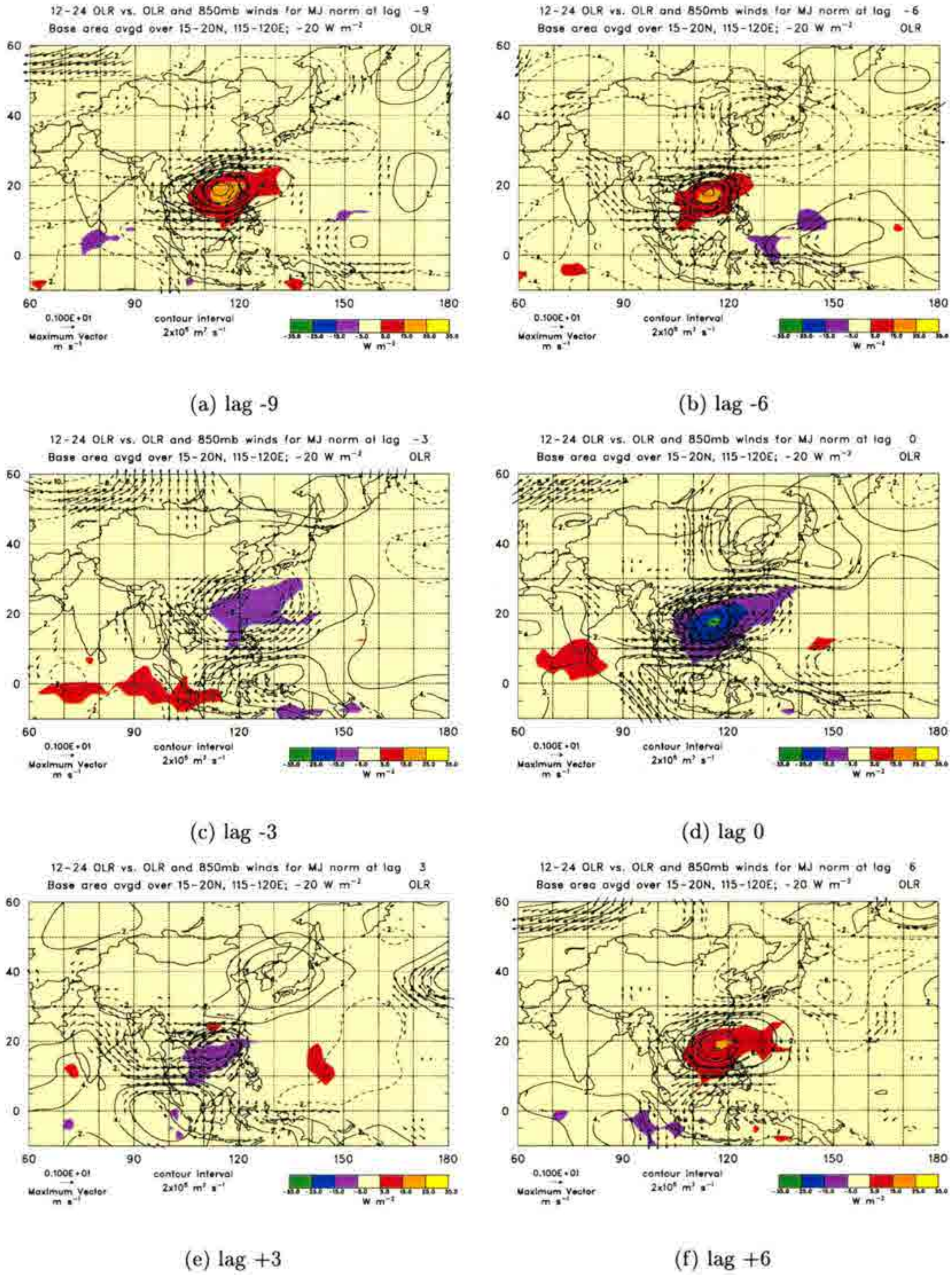

(a) lag -9

(b) lag -6

(c) lag -3

(d) lag 0

(e) lag +3

(f) lag +6

Figure 4.31: 12–24 day regression for normal onset years.

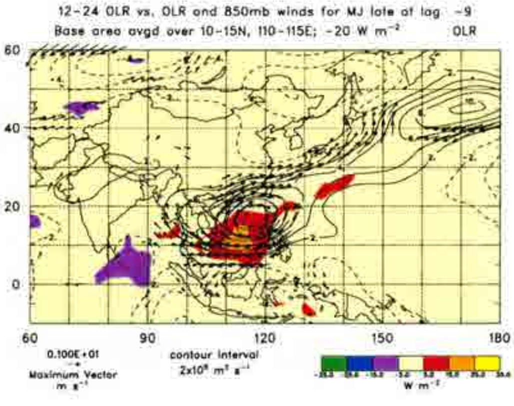

(a) lag -9

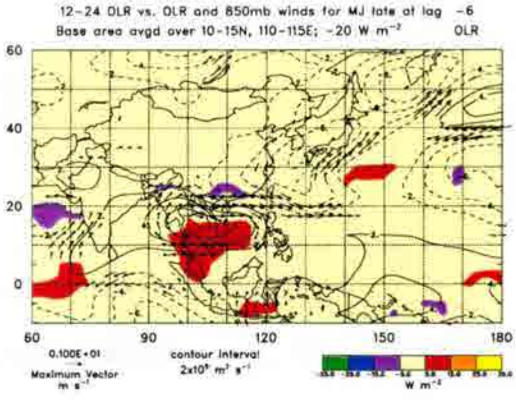

(b) lag -6

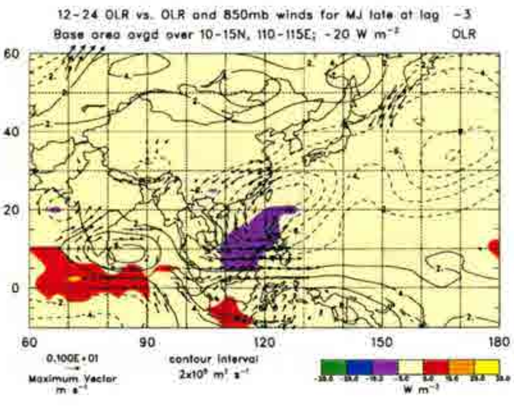

(c) lag -3

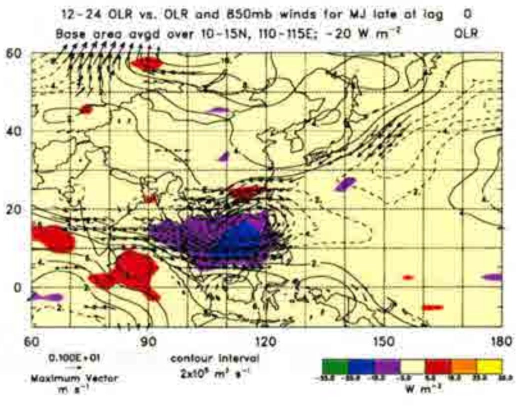

(d) lag 0

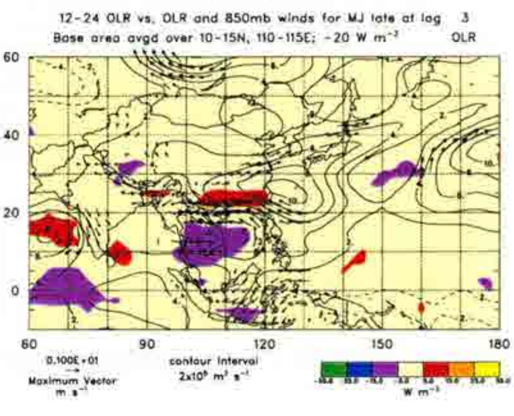

(e) lag +3

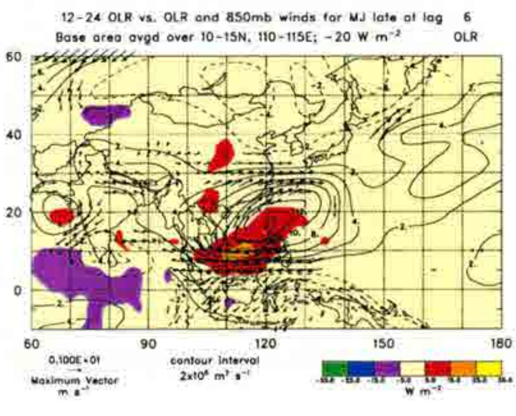

(f) lag +6

Figure 4.32: Same as Fig. 4.31 except for late onset in SW box.

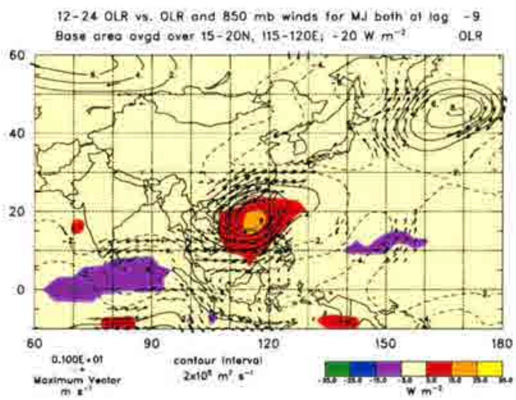

(a) lag -9

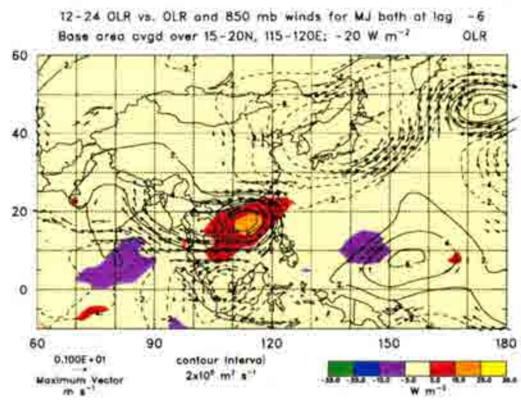

(b) lag -6

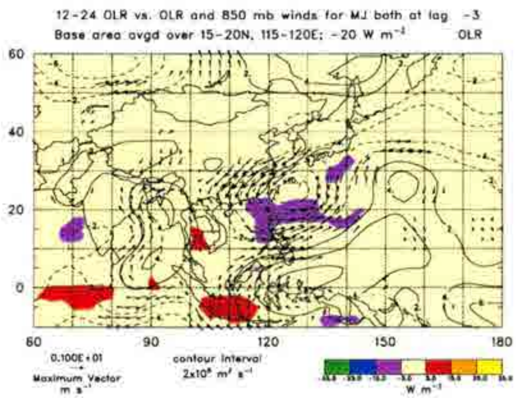

(c) lag -3

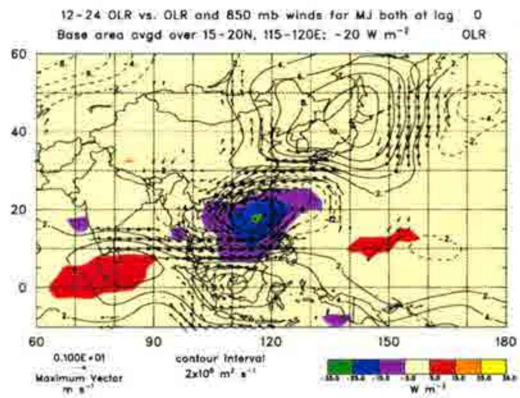

(d) lag 0

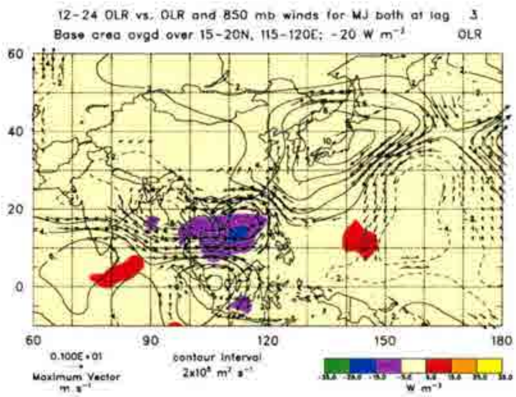

(e) lag +3

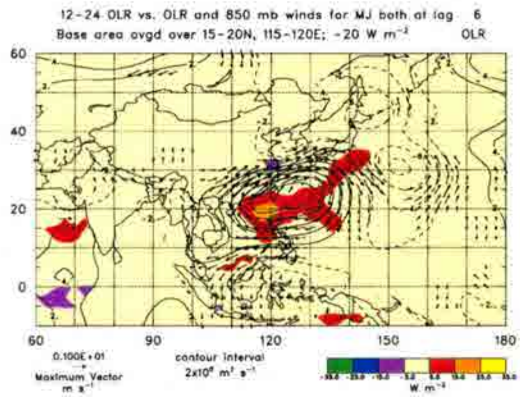

(f) lag +6

Figure 4.33: Same as Fig. 4.31 except for years with both modes present at onset.

only the 30–60 day oscillation was present at the SEAM onset (Fig. 4.34). There is no westward movement of disturbances at all. There is a slight south-to-north movement of OLR anomalies and corresponding streamfunctions. For instance, at lag -9 (Fig. 4.34a), there are positive OLR anomalies over the southern SCS along with a zonally elongated anticyclonic circulation. By lag -6 (Fig. 4.34b) both the OLR anomaly and the positive streamfunction have moved slightly north. This disturbance continues to move north and negative OLR anomalies form in the southern SCS with a cyclonic circulation at lag -3. At lag 0 the convection has moved slightly northward from its origin and the cycle continues. Positive OLR anomalies are over the southern SCS again by lag +6. Other features to note include eastward-moving circulations at midlatitudes and eastward-moving equatorial disturbances that form around 60° E and dissipate by the time they reach 90° E. These disturbances can be seen as positive OLR anomalies near the equator at lag -3 and negative OLR anomalies near the equator at lag +6.

The 12–24 day regression of the years where neither intraseasonal mode is prominent during the SEAM onset is suggestive of midlatitude frontal forcing at the onset. At lag -6 (Fig. 4.35b), positive OLR anomalies and an anticyclonic circulation are present over most of the SCS. A narrow band of convection has developed along 25° N between 110–130° E with westerly winds on its southern edge. This band of convection moves slightly southward into the northern SCS and the positive OLR anomalies have dissipated by lag -3. By lag 0 (Fig. 4.35d), the convection and cyclonic circulation have moved farther south and now encompass the entire SCS. This disturbance stalls out at about 15° N and has died out by lag +3. Positive OLR anomalies have formed on the southern coast of China and move south into the SCS by lag +6. Though no OLR anomalies are associated with them, alternating cyclonic and anticyclonic disturbances can be seen moving westward along the equator throughout this regression.

Like the regressions of the 12–24 day filtered OLR, the regressions of the 30–60 day filtered OLR for the years with normal onsets and years where both oscillations were present

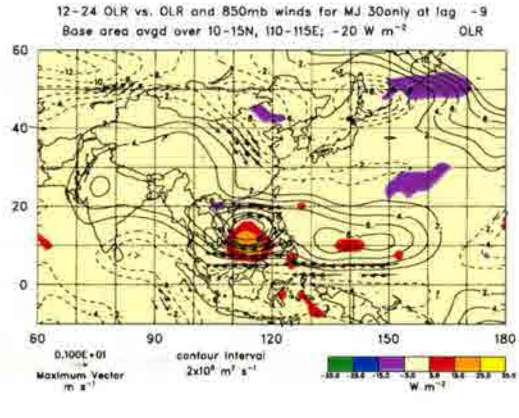

(a) lag -9

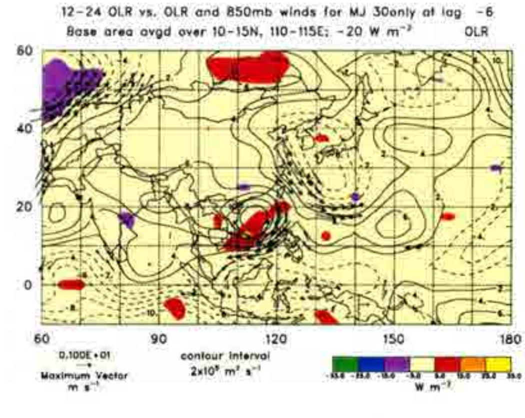

(b) lag -6

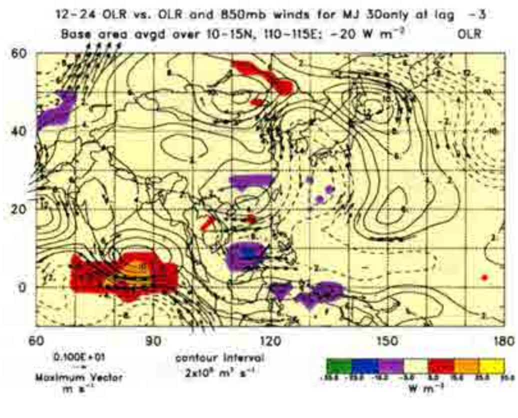

(c) lag -3

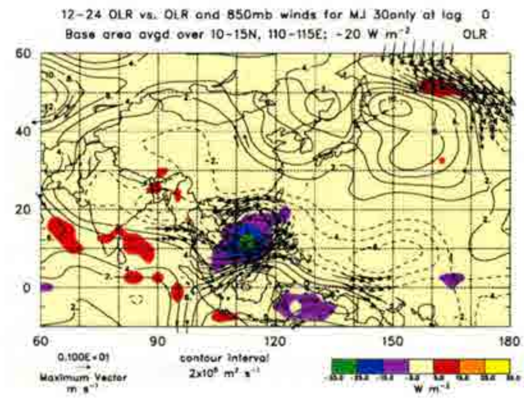

(d) lag 0

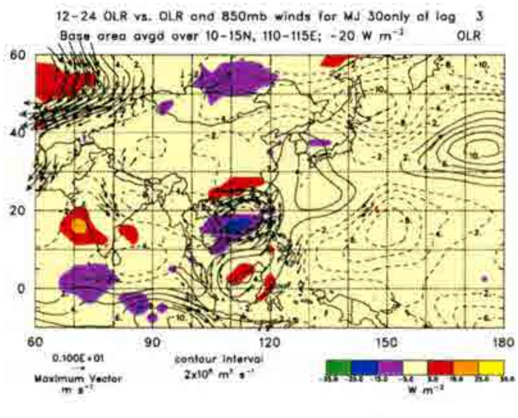

(e) lag +3

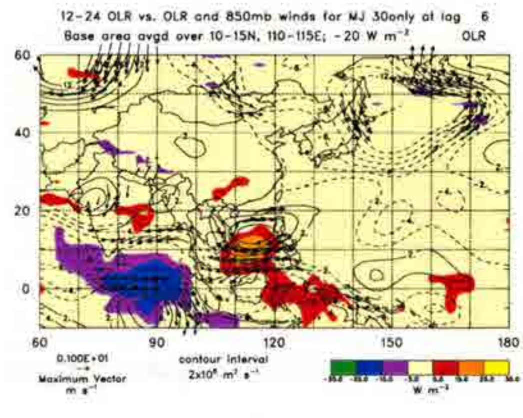

(f) lag +6

Figure 4.34: Same as Fig. 4.31 except for only 30–60 day mode present for SW box.

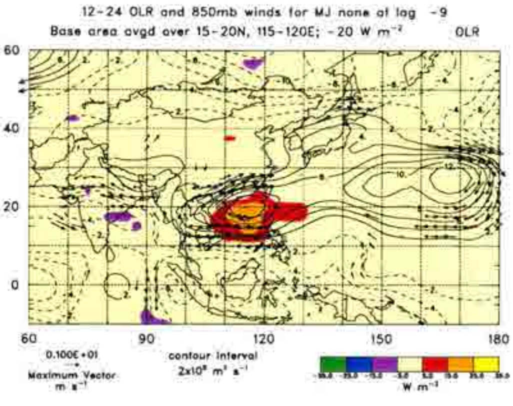

(a) lag -9

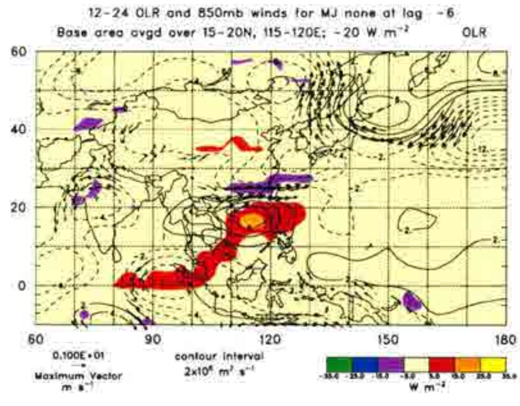

(b) lag -6

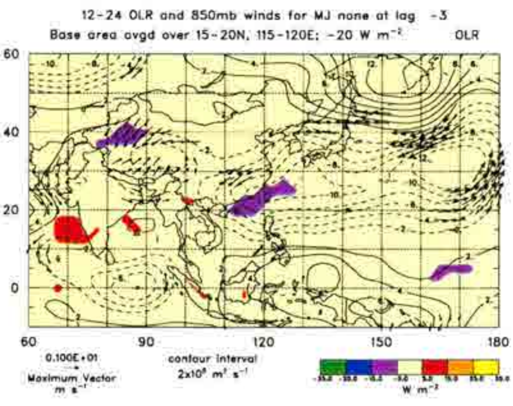

(c) lag -3

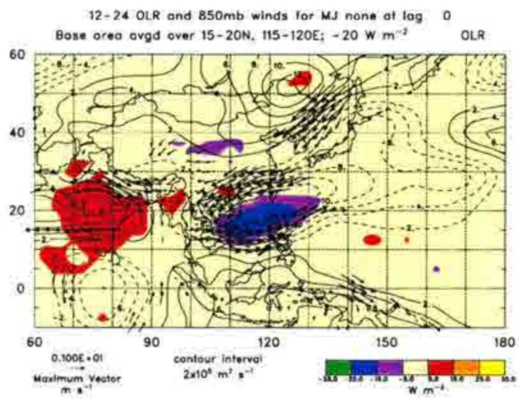

(d) lag 0

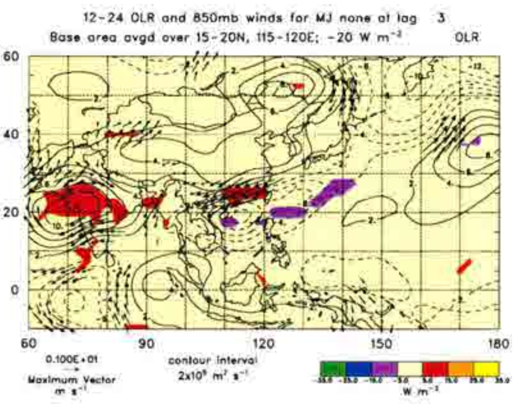

(e) lag +3

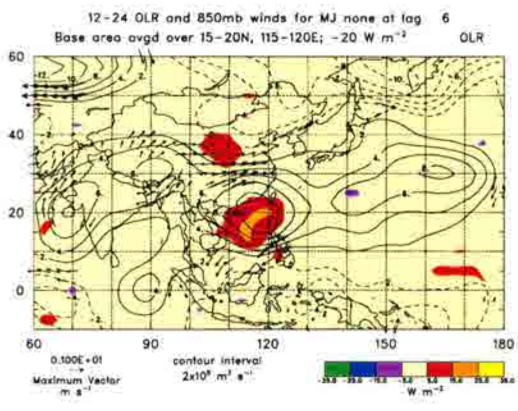

(f) lag +6

Figure 4.35: Same as Fig. 4.31 except for neither mode present at onset for NE box.

at onset (figures not shown) were very similar to the regressions for each other and the full 20 year dataset (Fig. 4.18). Additionally, the regression for years in which the only 30–60 day mode was present (figure not shown) was also very similar to that of the full 20 year regression. These results are to be expected. As with the 12–24 day regressions, the normal onset years and years with both modes present represent a majority of the 20 years analyzed. Thus, the regressions for those categories should be similar to the full 20 year regressions. Even though there are less years where only the 30–60 day oscillation was present at the onset, it is expected that it should display the same features since it is the dominant mode for those years. Each of these regressions exhibited the MJO and ITCZ convection signals as described in Section 4.3.

The two categories of 30–60 day regressions that were different in structure were the regressions of late onset years (Fig. 4.36) and years where neither the 12–24 day or 30–60 day mode were present at the SEAM onset (Fig. 4.37). For the late onset years, at lag -15 (Fig. 4.36a), as is typical, positive OLR anomalies are present over the SCS with anticyclonic circulation. By lag -10, these anomalies have weakened and a wave train is present stretching from the SCS northeastward into the northern west Pacific. There are also OLR anomalies associated with the wave train circulations. This is a feature that is not as obvious in 30–60 day regressions of other categories. By lag -5, a zonally oriented band of convection has developed at about 10° N stretching from India across the SCS and into the west Pacific. It does not propagate northward as is typical since it is in the same location at lag 0. This band dissipates through lag 5 and lag 10. For the regression of the years where neither mode was present at onset (Fig. 4.37), the OLR anomalies and circulations are not organized in the "typical" way aside from the OLR anomalies being zonally oriented over the SCS. Bands of OLR anomalies form in situ over the SCS, and do not propagate and the circulations tend to be stationary as well. Even though these regressions had different structures than the regressions of the other categories, they were not so different as to have completely unrecognizable features. They both still had bands of OLR anomalies that resembled the ITCZ. However, the MJO signal was not strong for either of these regressions. The absence of an MJO signal in only the regressions for the late onset years and years where neither intraseasonal mode was present may indicate that there is a connection between the lack of the MJO and delayed SEAM onsets.

Both the 12–24 day and 30–60 day regressions showed these modes to be weaker for late onset years than for normal onset years. Though not identical to the regressions for late onset years, the regressions for years where neither mode was present at the onset also displayed patterns that were different and weaker than the "normal" 12–24 and 30–60 day patterns. This further supports the idea that there is a connection between late onsets and the absence of the ISOs as first noticed in the timeseries analysis. This also points toward the idea that ISOs cannot be the sole forcing mechanism for the SEAM onset. The atmosphere must be in a proper state to sustain the convection initiated by the ISOs. If it is not, even the presence of the ISOs will not trigger the onset. The opposite is also true. Even if the atmosphere is in a state that would support the onset of the monsoon, without the ISOs present to trigger convection, the onset may not occur. Additionally, it is the variability of the ISOs that cause the broad range of onset times. Without the influence of the ISOs, there would likely be a lot less variability in the onset time, and the average onset would probably occur later. Webster (1987b) made a similar point with regard to the Indian monsoon onset.

4.4.3 Onset timing and ENSO

Chen and Weng (1997) suggest that it is the interannual variations of the intraseasonal oscillations that cause the interannual variations of the SEAM onset. If this is the case, then the causes of the interannual variations of the intraseasonal oscillations must be identified before the interannual variations of the monsoon onset can be understood. One possible cause for interannual variablity of the intraseasonal oscillations is the ENSO. Many studies have addressed a possible relationship with ENSO and the monsoon onset

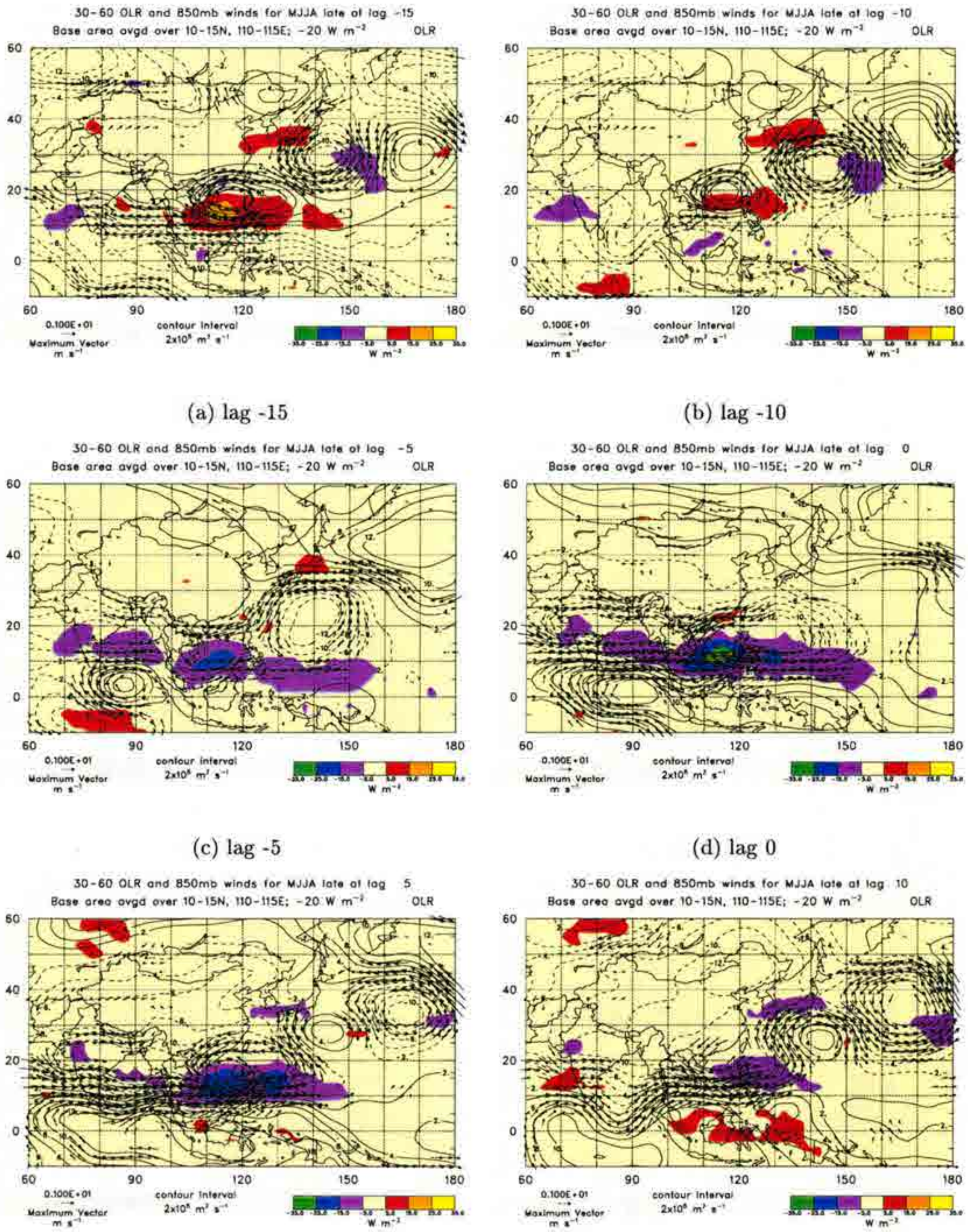

(a) lag -15

(b) lag -10

(c) lag -5

(d) lag 0

(e) lag 5

(f) lag 10

Figure 4.36: Same as Fig. 4.32 except for 30–60 day filtered OLR.

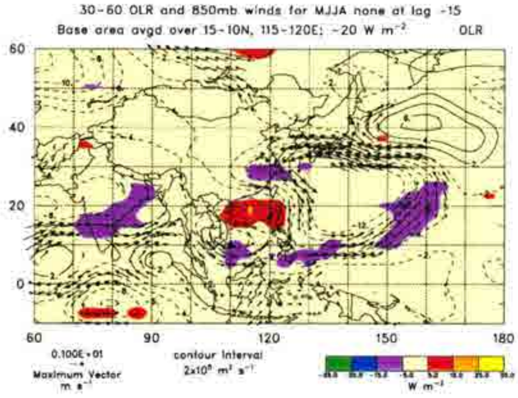

(a) lag -15

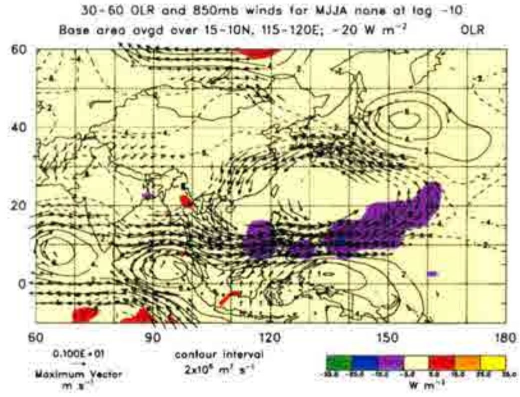

(b) lag -10

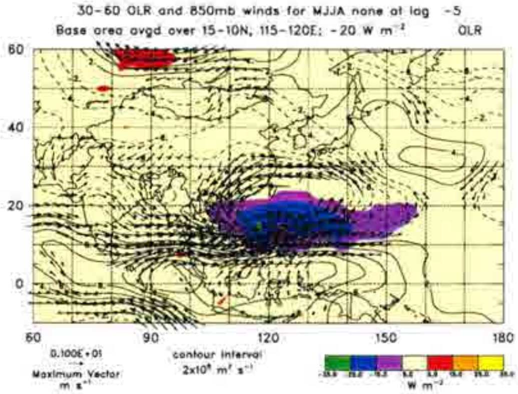

(c) lag -5

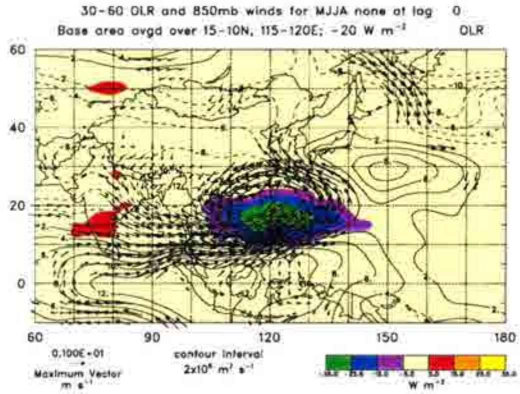

(d) lag 0

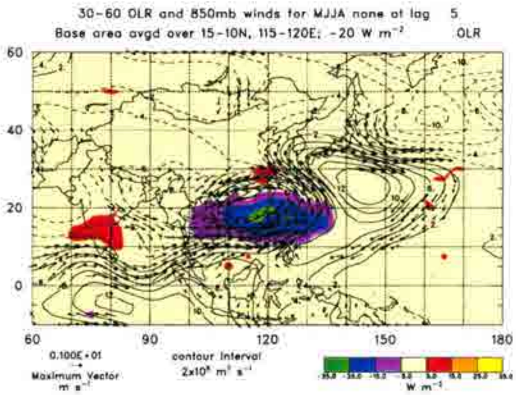

(e) lag 5

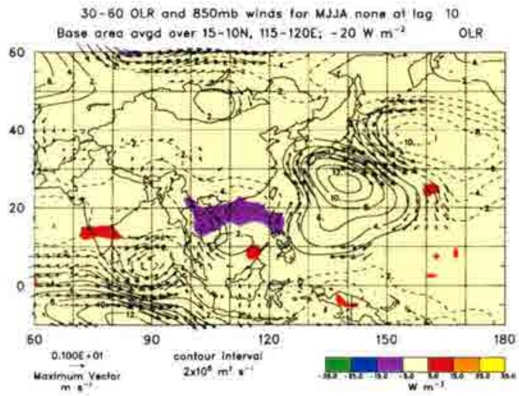

(f) lag 10

Figure 4.37: Same as Fig. 4.35 except for 30–60 day filtered OLR.

with many differing opinions. Xie et al. (1998) argue that the interannual variations of the SCS monsoon onset are closely related to ENSO events. They considered seven years to have delayed onsets between 1979–1995, and all seven were associated with El Niño events. During El Niño events, the Walker circulation is weak and SST anomalies over the western Pacific are negative. These features may act to enhance the western Pacific subtropical high (WPSH). The abnormal existence of the WPSH over the SCS is the direct cause for delayed onsets (Xie et al. 1998). However, Wang and Wu (1997) find no obvious and robust connection between the SEAM onset and ENSO based on their classification of normal and delayed onset years. The impact ENSO has on the behavior of ISOs is still not clear.

Timeseries and regression analyses like that described in Section 4.4.2 were performed for three ENSO categories: years with active El Niño, years with active La Niña, and neutral years. Unfortunately, these analyses did not really provide any insight to solving the debate of what influence ENSO has over the intraseasonal oscillations and onset timing of the SEAM.

The timeseries of OLR (Fig. 4.38) and 850 mb zonal wind (Fig. 4.39) for the ENSO categories do not reveal any obvious links between ENSO and the SEAM onset timing. In both the northern and southern SCS, the initiation of convection (inferred from OLR values < 240 W m^{-2}) occurred at roughly the same time for years with an El Niño, years with a La Niña and neutral years. La Niña years had the earliest initiation of convection and El Niño years had the latest inititation of convection, but they still occurred within a few days of one another. The shift from low-level easterlies to westerlies also occurred at roughly the same time for each ENSO category. Based on these timeseries, there does not appear to be a strong link between ENSO and the SEAM onset timing. If ENSO was a big factor in the onset timing I would expect there to be obvious differences between the timeseries.

In addition to the timeseries analysis, correlations and regressions between onset date and Niño 3.4 SST anomalies were computed. The results of this analysis showed a tendency for El Niño years to have onsets later than the mean onset date in both the

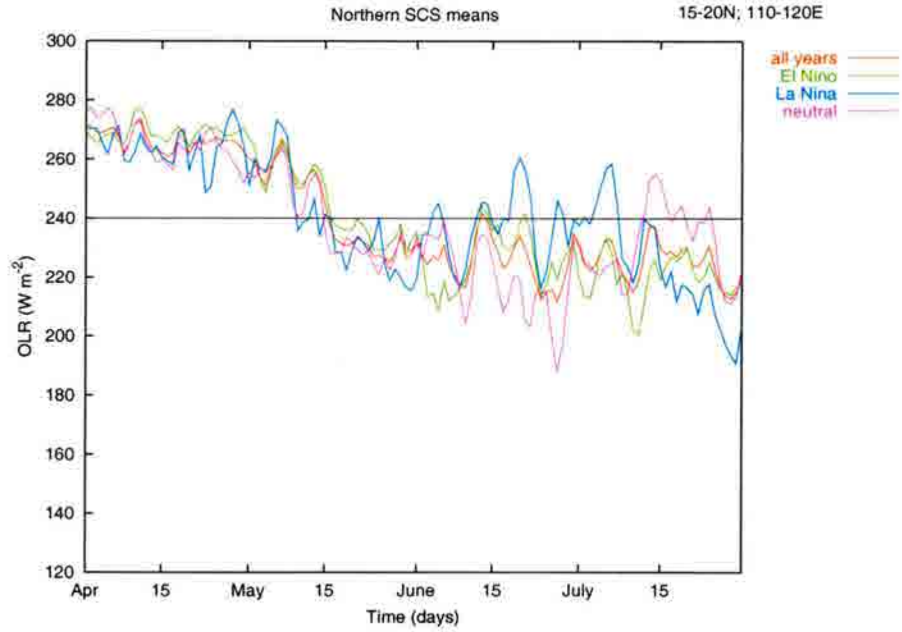

(a)

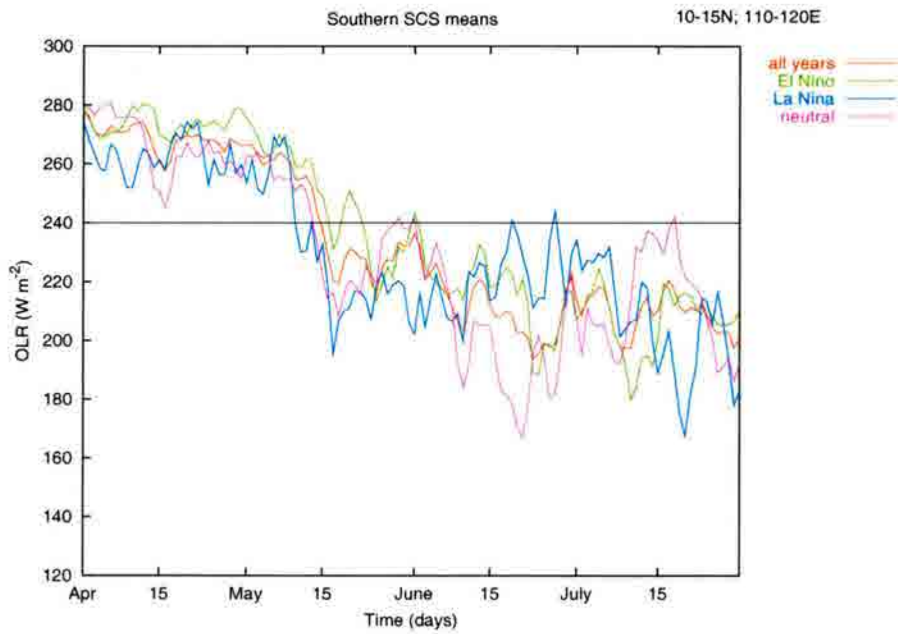

(b)

Figure 4.38: Timeseries of OLR for the ENSO categories in the northern SCS (a) and the southern SCS (b).

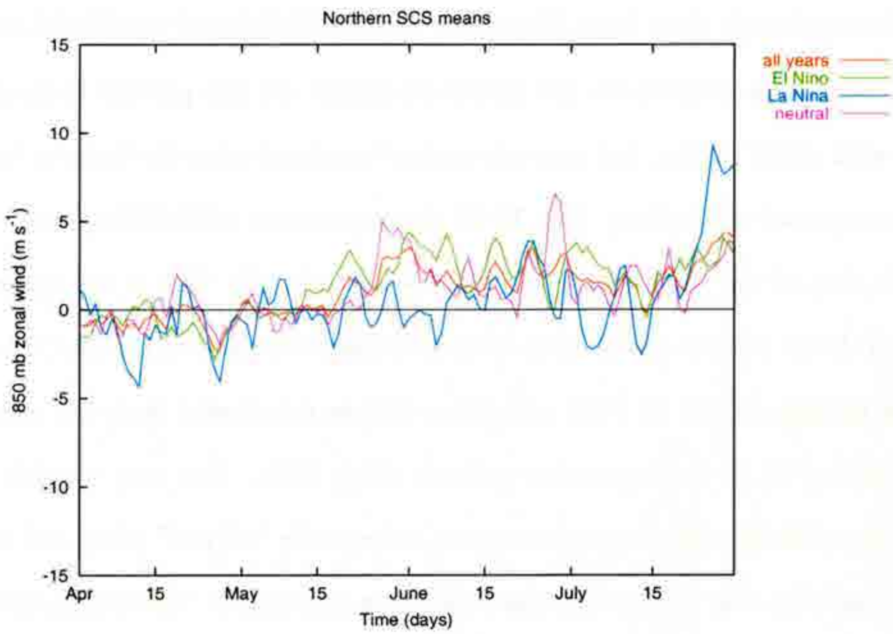

(a)

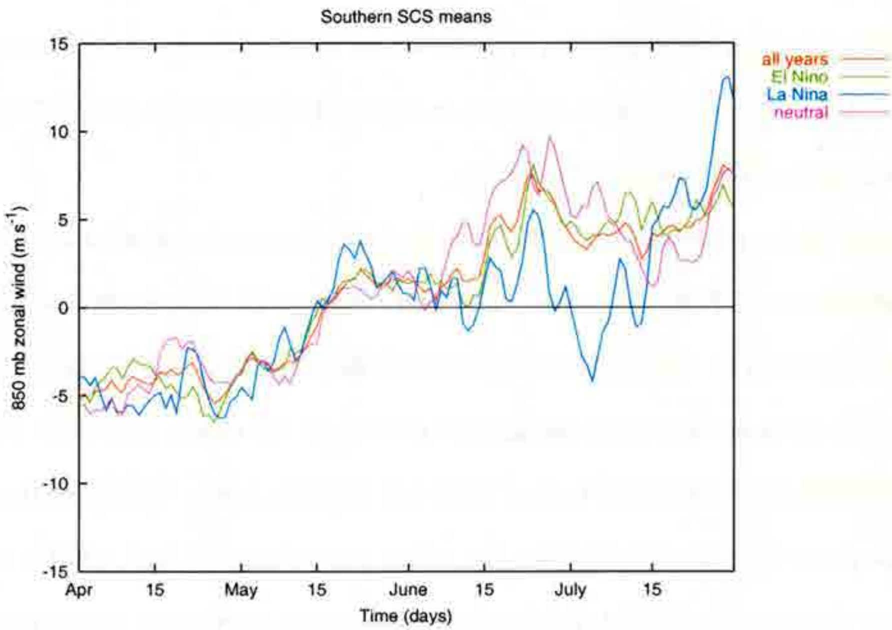

(b)

Figure 4.39: Same as Fig. 4.38 except for 850 mb zonal wind.

northern and southern SCS. However, none of the computed correlation coefficients were statistically significant at the 95% confidence level. This supports the results from the timeseries analysis that there is no strong link between ENSO and the SEAM onset timing.

The regression analysis for the ENSO categories did not provide much insight into any links with onset timing, but may say something about possible links to the behavior of the intraseasonal oscillations. The 12–24 day regressions of El Niño years were almost identical to that of the years with a normal onset (Fig. 4.31). This is not surprising given that 50% of the 20 years in the analysis were associated with El Niño events. The OLR and circulation patterns of the La Niña regressions (figure not shown) were not much different from the typical 12–24 day regression patterns (Fig. 4.31). The only notable differences were that the midlatitude influence was not as strong as in "normal" years and the origin of the OLR anomalies was farther east than the other regressions. The regression for neutral years (figure not shown) seemed to have a stronger midlatitude influence than the years with an ENSO event. The circulation and OLR anomaly patterns for the neutral years most closely resembled the regression of years where the intraseasonal oscillations were not active (Fig. 4.35). In neutral years, convection initiated along the coast of China and moved southward into the SCS in front-like fashion.

The 30–60 day regressions of ENSO categories had somewhat similar results as the 12–24 day regressions of ENSO categories. The years with an El Niño event had features that were almost identical to the regressions of the full 20 years (Fig. 4.18), normal onset years and years with both intraseasonal oscillations present at the onset. The OLR anomaly and circulation patterns displayed the typical MJO and ITCZ features. The 30–60 day regression of La Niña years differed slightly from the other regressions. It had a fairly stong ITCZ feature, but there was no MJO-type signal as west-to-east movement was suppressed. The movement of the OLR anomalies and the circulations were south-to-north. The regressions of neutral years also displayed the typical MJO and ITCZ features, although not quite as prominently as in the years with an El Niño event. The OLR anomaly pattern was very similar to that of the 20 year regression (Fig. 4.18) but the circulation pattern more closely resembled the years in which neither of the intraseasonal modes were present at the onset (Fig. 4.37).

In summary, from the timeseries and correlation/regression analysis, there appears to be no direct connection between onset timing and ENSO events. The regressions may provide some insight into the link between ENSO events and the behavior of the intraseasonal oscillations which may provide an indirect link between ENSO events and the onset timing. Regressions of years with an El Niño event were very similar to years where both intraseasonal modes were present at the onset. Neutral years appeared to be more similar to years where neither the 12–24 day or 30–60 day oscillation were present at the onset. Years with a La Niña event did not closely resemble any of the other regressions. The OLR and circulation patterns for the La Niña regressions were not so different from the other regressions as to be unrecognizable, however some of the typical features (namely midlatitude influence in the 12–24 day regressions and the MJO signal in the 30–60 day regression) were suppressed. It is difficult to make concrete conclusions based on this limited analysis. The 20 years that were analyzed were a particularly active period for ENSO. Ten of the 20 years had an El Niño event and 4 had a La Niña event. Becuase of this we may not have a clear picture of what a "normal" state is. Also the sample size of the La Niña years is much smaller than that of the other categories, so some of the differences between those years and the other may be accounted for by the noise from having less samples.

Chapter 5

CONCLUSIONS

5.1 Summary

The Southeast Asian monsoon (SEAM) is one part of the Asian monsoon system. It is a complicated component of the Asian monsoon system because it is influenced by both the tropics and midlatitudes. This complexity leads to many different hypotheses for the triggering and forcing mechanisms of the SEAM. Some of these ideas include Tibetan Plateau thermal forcing, midlatitude frontal systems and triggering by intraseasonal oscillations. This study investigates the role of intraseasonal oscillations in triggering the SEAM onset by studying the 1998 monsoon onset in detail and expanding the analysis to include the 20 years from 1979–1998.

The climatological onset date for the SEAM is mid-May and is one of the earliest of the entire Asian monsoon system. The onset for the 1998 SEAM was 20 May. Between 1979–1998, the onset dates over the South China Sea (SCS) ranged from as early as 10 May to as late as 15 June. The onset date was chosen to be the first day of sustained convection (based on analysis of outgoing longwave radiation (OLR)) and the commencement of a southerly and westerly component of the wind over the SCS. The SEAM onset was considered to be normal if it occurred between 11 May – 31 May. Onsets occurring prior to 11 May were considered an early onset and onsets after 31 May were considered a late onset.

Spectral analysis of OLR at each gridpoint in the SCS revealed intraseasonal oscillations with periods of 12–24 days and 30–60 days to be prominent during the monsoon season. The 12–24 day oscillation has been previously observed as a westward-moving disturbance with an equatorial and subtropical cell associated with it. The 30–60 day oscillation is comprised of a component which moves eastward from the equatorial Indian ocean and a northward-moving component from the equatorial region south of the SCS (Chen and Chen 1995). The SCS is an area of maximum variability for both of these oscillations during the monsoon onset period. Band-pass filtering of the OLR and winds at 850 and 200 mb was used to isolate these two oscillations.

During the 1998 monsoon, convection associated with the 12–24 day oscillation developed near Japan in a band situated from southwest to northeast. This convection propagated southwest into the northern SCS, arriving at the time of monsoon onset. This pattern of development and propagation of the 12–24 day convection represents the main influence this mode has on the 1998 SEAM onset. There is also a secondary contribution from convection propagating eastward from the Bay of Bengal (BOB). It is not clear what this 12–24 day mode represents physically. However, there appears to be a relationship between the upper level circulation and convection that may indicate there is midlatitude influence on the SCS in the form of Rossby waves.

The 30–60 day oscillation influences the SCS from two different sources. There is an area of convection and cyclonic circulation that develops near India and propagates eastward across the BOB and into the SCS. Because of its location and propagation characteristics this is likely a Madden-Julian oscillation (MJO) event. The MJO convection joins with a band of convection that originates near 10° N just east of the Philippines and moves northward into the SCS. This band of convection is the ITCZ or monsoon trough (e.g., Chen and Chen 1995). The MJO and the ITCZ join over the SCS at the monsoon onset. The nearly simultaneous arrival of the 12–24 day oscillation and the 30–60 day oscillation at the monsoon onset is evidence that these two modes together may have triggered the onset of the 1998 monsoon. Previous studies have also noted this behavior of ISOs at the time of SEAM onset (e.g., Chen and Chen 1995).

Lag regression analyses (following Kiladis and Weickman 1992) show the general pattern of convection and circulations of the 12–24 day and 30–60 day oscillations for the 20 years from 1979–1998. In general, the OLR anomalies and circulations during the onset period (May-June) for both modes had the same patterns as those observed for the 1998 monsoon. In addition to these patterns, westward-moving equatorial disturbances were observed in the 12–24 day regressions, but not much has been said about what these disturbances are. It was also observed for both modes that the OLR anomalies and circulations appeared to be stronger during the monsoon onset period compared to the entire monsoon season.

In addition to differences in the regressions between the monsoon onset period and the entire monsoon season, the regression results varied between the different base areas in and around the SCS. The differences between the results in the different areas show all of the different types of influence over the SEAM before, during and after the monsoon onset. The southernmost areas (south of 15° N) were influenced mainly by the tropics whereas the area from 20–25° N primarily displayed midlatitude influence. The area from 15–20° N was a transition zone between the two. The regressions with this base area exhibited features with both midlatitude and tropical origins and characteristics. In the 12–24 day regressions for this area, westward-moving equatorial disturbances were observed. The SCS was also influenced by disturbances propagating southwestward from near Japan. This pattern of the convection and circulation (especially at 200 mb) very closely resembled the patterns seen in the 1998 12–24 day filtered fields and is indicative of midlatitude Rossby wave forcing of the convection. Additional midlatitude influence was seen at both upper and lower levels in the form of a wave train which extended from the SCS into the northern Pacific. This wave train is an important link between the tropics and the midlatitudes. (Fukutomi and Yasunari 1999).

In the 20 years from 1979–1998, there was much interannual varibility in both the onset timing and the behavior of the intraseasonal oscillations. To better understand what role, if any, the intraseasonal oscillations have on the interannual variability of the monsoon onset each year was catagorized according to onset timing, presence of the intraseasonal oscillations and ENSO phase. Years where both the 12–24 and 30–60 day oscillations were present at the SEAM onset had normal onsets, and years where only the 30–60 day oscillation was present at the onset had the earliest onsets. Years where neither mode was present had the latest onsets. This result suggests that the intraseasonal oscillations are an important trigger for the SEAM onset. Once the atmosphere is "primed" to support a large outbreak of convection, the presence of the oscillations is needed trigger the onset. The absence of the intraseasonal oscillations may cause the onset to be delayed.

The 12–24 day oscillation exhibited the typical features for normal years and also years where both modes were present at the onset. In years with a late onset, the 12–24 day oscillation had the same structure as that of normal years, but it appeared to be weaker. The typical convection and circulations of the 12–24 day oscillation were completely absent during years when only the 30–60 day oscillation was present at the onset. In years where neither mode was present at the onset, the 12–24 day patterns had characteristics which resembled a midlatitude front. The 30–60 day oscillation exhibited the typical MJO and ITCZ patterns in years where both modes were present and years where only the 30–60 day mode was present at the SEAM onset. These features were also seen for years which had a normal onset. In years where the onset was delayed and years where neither mode was present at the onset, there was no MJO signal and only a slight trace of the ITCZ pattern. The results of these regressions also support the idea that the intraseasonal oscillations play an important role in the SEAM onset. The similarity of the regressions for normal onset years and years when both intraseasonal oscillations were present at the onset suggest the presence of these modes in the SCS is required for a normal onset. The absence of these modes will cause the onset to be delayed.

A direct link between the onset timing and ENSO events was not obvious from this study. However, ENSO events may affect the behavior of the intraseasonal oscillations. In years with an El Niño event, both the 12–24 and 30–60 day oscillations exhibited convection and circulation patterns that were consistent with both modes being present during the onset. Neutral years had patterns similar to years where neither oscillation was present at the onset. The 12–24 day oscillation and the 30–60 day oscillation during La Niña years did not resemble the convection and circulation pattern of any of the established categories. There was westward movement of disturbances in the 12–24 day period, but midlatitude influence was suppressed. The 30–60 day oscillation had the typical south-to-north movement of the ITCZ, but there was no MJO signal as east-west movement was suppressed.

5.2 Discussion

The goal of this study was to contribute toward a better understanding of the processes which may trigger the SEAM onset. Many possible triggering mechanisms have been proposed in previous studies and it seems to be a difficult task to separate all of the different possible forcing mechanisms. Indeed they may not be distinct and separate at all. It would be hard to argue that any one process in the atmosphere is completely segregated from any other process. Still, at some point the line must be drawn and distinctions must be made if any progress is to be made toward a better understanding of the SEAM.

Though not completely understood, intraseasonal oscillations seem to have a significant role in the triggering of the SEAM onset, even though they cannot be the sole forcing mechanism. The 12–24 day and 30–60 day oscillations are not just summertime phenomena. They occur year-round, though their exact period of oscillation, strength and location may vary a bit between seasons (Hartmann et al. 1992). So, why would these intraseasonal oscillations cause an outbreak of convection sufficient to trigger the monsoon onset in mid-May and not at some other time of the year? I think this is where the other aspects of the monsoon forcing, such as the heating of the Tibetan Plateau, or more directly the annual path of solar insolation, come into play. The atmosphere must be "primed" and ready to sustain the convection initiated by the intraseasonal oscillations. Conversely, it seems that even if the atmosphere is properly "primed", without the trigger that the intraseasonal oscillations provides, the onset will not occur. Webster (1987b) made a similar point with regard to the Indian monsoon onset noting that the two triggers for the Indian monsoon were the heating of the Tibetan Plateau and the MJO. He suggested it is the influences like the MJO that cause the range of onset times to be so broad, varying by 2–3 or even 4 weeks from year to year. If it weren't for the intraseasonal oscillations the window of onset times would be much narrower (Webster 1987b).

This idea can be extrapolated to the SEAM as well. Without the influence of the intraseasonal oscillations, I think there would be a lot less variability in onset time, and the onset would probably occur later on average. This is observed to a limited extent in the results of this study. The years where neither intraseasonal oscillation were present at the monsoon onset tended to be later than years where one or both of the oscillations were present. In particular, the absence of the MJO may be a cause for delayed onsets. The location of the MJO may also be an important factor in onset timing. During the boreal winter, the MJO track is located in the Southern Hemisphere. It moves northward as the seasons progress toward summer and doesn't reach latitudes that will affect the SCS until the summer. It was the first of these "summer" MJO tracks that coincided with the onset of the 1998 SEAM.

5.3 Future work

As may be the case in most research, it seems that this study raised more questions than it answered. There is a lot of future work to be done to understand how the intraseasonal oscillations relate to the SEAM onset.

The first step is to figure out what these oscillations are physically, particularly the 12–24 day oscillation. Though not completely understood, the eastward-moving 30–60 day mode is at least identifiable as the MJO. Further understanding of its role in the monsoon onset could be attained if the 12–24 day oscillation were identified in the same way. One step toward doing that would be to analyze the vertical structure of these modes.

This study did not have much insight as to the effects ENSO has on the SEAM onset timing and the intraseasonal oscillations, so those effects should be further studied. Also, the effects the Tropospheric Biennial Oscillation (TBO) (Chang and Li 2000) have on the SEAM onset need to be addressed. There was a bit of a biennial pattern of late onsets, so it is possible that there is a connection between the TBO and the SEAM. Another question to address is: how "normal" was the 20 years analyzed in this study? The 20 years between 1979–1998 was a very active ENSO period. Analysis of a larger dataset might provide more insight into the interactions of the intraseasonal oscillations and the SEAM onset and help better understand what causes the interannual variations of the intraseasonal oscillations. Understanding the interannual variations of the intraseasonal oscillations might help understand the interannual variations of the monsoon onset.

A final idea for future work would be to develop an index for determining the strength or activity of the intraseasonal oscillations. The method for doing that in this study was very subjective. With a more objective measure of the oscillations, further insight into connections with the onset timing or strength of the monsoon could be obtained.

REFERENCES

Chan, J.C.L., Y. Wang, and J. Xu, 2000: Dynamic and thermodynamic characteristics associated with the onset of the 1998 South China Sea summer monsoon. *J. Meteor. Soc. Japan*, **78**, 367–379.

Chang, C.-P., and G. T.-J. Chen, 1995: Tropical circulations associated with southwest monsoon onset and westerly surges over the South China Sea. *Mon. Wea. Rev.*, **123**, 3254–3267.

Chang, C.-P., and T. Li, 2000: A theory for the tropical tropospheric biennial oscillation. *J. Atmos. Sci.*, **57**, 2209–2224.

Chen, T.-C., and J.-M. Chen, 1995: An observational study of the South China Sea monsoon during the 1979 Summer: Onset and life cycle. *Mon. Wea. Rev.*, **123**, 2295–2318.

Chen, T.-C., S.-P. Weng, 1997: A further observational study of the South China Sea summer monsoon: Climatology and interannual variation. Tech. Report, Dept. of Geological and Atmospheric Sciences, Iowa State University, 41 pp.

Chen, T.-C., and S.-P. Weng, 1999: Interannual and intraseasonal variations in monsoon depressions and their westward-propagating predecessors. *Mon. Wea. Rev.*, **127**, 1005–1020.

Chen, T.-C., M.-C. Yen, and S.-P. Weng 2000: Interaction between the summer monsoons in east Asia and the South China Sea: Intraseasonal monsoon modes. *J. Atmos. Sci.*, **57**, 1373–1392.

Ciesielski, P. E., 1980: Variability within the ocean-atmospheric system over the north

Pacific. Environmental Research Papers No. 25, Colorado State University, Fort Collins, CO, 41pp.

Duchon, C. E., 1979: Lanczos filtering in one and two dimensions. *J. App. Met.*, **18,** 1016–1022.

Fukutomi, Y., and T. Yasunari, 1999: 10–25 day intraseasonal variations of convecton and circulation over east Asia and western north Pacific during early summer. *J. Meteor. Soc. Japan*, **77,** 753–769.

Gilman, D. L., F. J. Fuglister and J. M. Mitchell, Jr., 1963: On the power spectrum of "Red Noise". *J. Atmos. Sci.*, **20,** 182–184.

Haberman, R., *Elementary Applied Partial Differential Equations.*, 547 pp., Prentice-Hall, Inc., Englewood Cliffs, NJ, 1987.

Hartmann, D. L, M. L. Michelsen, and S. A. Klein, 1992: Seasonal variations of tropical intraseasonal oscillations: A 20–25 day oscillation in the Western Pacific. *J. Atmos. Sci.*, **49,** 1277–1289.

Johnson, R.H., and P.E. Ciesielski, 2001: The SCSMEX/GAME sounding network and the onset of the 1998 Asian Summer Monsoon. Proceedings of 4th International Conference on East Asia and Western Pacific Meteorology and Climate, 26-28 October 1999, Hangzhou, China (in press)

Kalnay, E., et al, 1996: The NCEP/NCAR 40-year reanalysis project. *Bull. Amer. Meteor. Soc.*, **77,** 473–471.

Kiladis, G. N., 1998: Observations of Rossby waves linked to convection over the eastern tropical Pacific. *J. Atmos. Sci.*, **55,** 321–339.

Kiladis, G. N., and K. M. Weickmann, 1992: Circulation anomalies associated with tropical convection during northern winter. *Mon. Wea. Rev.*, **120,** 1900–1923.

Lau, K.-M., and S. Yang, 1997: Climatology and interannual variability of the southeast Asian summer monsoon. *Adv. Atmos. Sci.*, **14,** 141–162.

Lau, K.-M., K.-M. Kim and S. Yang, 2000a: Dynamical and boundary forcing characteristics of regional components of the Asian summer monsoon. *J. Climate*, **13**, 2461–2482.

Lau, K.-M., Y. Ding, J.-T. Wang, R. Johnson, T. Keenan, R. Cifelli, J. Gerlach, O. Thiele, T. Rickenbach, S.-C. Tsay, P.-H., Lin, 2000b: A report of the field operations and early results of the South China Sea monsoon experiment (SCSMEX). *Bull. Amer. Meteor. Soc.*, **81**, 1261–1270.

Li, C., and M. Yanai, 1996: The onset and interannual variability of the Asian summer monsoon in relation to land-sea thermal contrast. *J. Climate*, **9**, 358–375.

Li, C., and X. Qu, 1999: Atmospheric circulation evolutions associated with summer monsoon onset in the South China Sea. *Chinese J. of Atmos. Sci.*, **23**, 311–325.

Li, C., and J. Wu, 2000: On the onset of the South China Sea summer monsoon in 1998., *Adv. Atmos. Sci.*, **17**, 193–204.

Liebmann, B. and C. A. Smith, 1996: Description of a complete (interpolated) outgoing longwave radiation dataset. *Bull. Amer. Meteor. Soc.*, **77**, 1275–1277.

Livezey, R. E. and W. Y. Chen, 1983: Statistical field significance and its determination by Monte Carlo techniques. *Mon. Wea. Rev.*, **111**, 46–59.

Lu, M.-M. and Y.-L. Chen, 2000: Large-scale features associated with extremely early or late onset of the South China Sea summer monsoon. *submitted to TAO.*

Madden, R. A. and P. R. Julian, 1971: Description of a 40–50 day oscillation in the zonal wind in the tropical Pacific. *J. Atmos. Sci.*, **28**, 702–708.

Madden, R. A., 1986: Seasonal variations of the 40–50 day oscillation in the tropics. *J. Atmos. Sci.*, **43**, 3138–3158.

Meehl, G. A., 1997: The south Asian monsoon and the tropospheric biennial oscillation. *J. Climate*, **10**, 1921–1943.

Nitta, T., 1987: Convective activities in the tropical western Pacific and their impact on the northern hemisphere summer circulation. *J. Meteor. Soc. Japan*, **65**, 373–390.

Ramage, C., *Monsoon Meteorology.* Internationsl Geophysics Series, Vol. 15, 296 pp., Academic Press, San Diego, CA., 1971.

Shen, S., and K.-M. Lau, 1995: Biennial oscillation associated with the east Asian summer monsoon and tropical sea surface temperatures. *J. Meteor. Soc. Japan*, **73,** 105–124.

Tao, S., and L. Chen, 1987: A review of recent research on the East Asian summer monsoon in China, in *Monsoon Meteorology.* ed. by C.-P. Chang and K.N. Krishnamurti, 544 pp., Oxford University Press, New York, NY.

Ueda, H., and T. Yasunari, 1998: Role of warming over the Tibetan plateau in early onset of the summer monsoon over the Bay of Bengal and South China Sea. *J. Meteor. Soc. Japan*, **76,** 1–12.

Wang, B., and H. Rui, 1990: Synoptic climatology of transient tropical intraseasonal convection anomalies. *Meteor. Atmos. Phys.*, **44,** 43–61.

Wang, B., and R. Wu, 1997: Peculiar temporal structure of the South China Sea summer monsoon. *Adv. Atmos. Sci.*, **14,** 177–194.

Wang, B., and Z. Fan, 1999: Choice of south Asian summer monsoon indices. *Bull. Amer. Met. Soc.*, **80,** 629–638.

Webster, P. J., 1987a: The elementary monsoon, in *Monsoons.* ed. by Fein and Stephens, John Wiley & Sons, Inc., New York, NY, 3–32.

Webster, P. J., 1987b: The variable and interactive monsoon, in *Monsoons.* ed. by Fein and Stephens, John Wiley & Sons, Inc., New York, NY, 296–330.

Webster, P. J., and S. Yang, 1992: Monsoon and ENSO: Selectively interactive systems. *Quart. J. Roy. Meteor. Soc.*, **118,** 877–926.

Wilks, Daniel S., *Statistical Methods in the Atmosphseric Sciences.* International Geophysics Series, Vol. 59, 467 pp., Academic Press, San Diego, CA, 1995.

Wu, G., and Y. Zhang, 1998: Tibetan plateau forcing and the timing of the monsoon onset over south Asia and the South China Sea. *Mon. Wea. Rev.*, **126,** 913–927.

Xie, A., Y.-S. Chung, X. Liu, and Q. Ye, 1998: The interannual variations of the summer monsoon onset over the South China Sea. *Theor. Appl. Climatol.*, **59,** 201–213.